7-10-2013

Orbital-scale fluctuations in continental weathering flux and continental ice-volume during greenhouse and icehouse climate intervals : evidence from oxygen and neodymium isotopes

Bethany Theiling

Bethany Purdin Theiling
Candidate

Earth and Planetary Sciences
Department

This dissertation is approved, and it is acceptable in quality and form for publication:

Approved by the Dissertation Committee:

Maya Elrick, Chairperson

Yemane Asmerom

Viorel Atudorei

Peter Fawcett

Gerilynn Soreghan

Gary Weissmann

ORBITAL-SCALE FLUCTUATIONS IN CONTINENTAL WEATHERING FLUX AND CONTINENTAL ICE-VOLUME DURING GREENHOUSE AND ICEHOUSE CLIMATE INTERVALS: EVIDENCE FROM OXYGEN AND NEODYMIUM ISOTOPES

BY

BETHANY PURDIN THEILING

B.A., Anthropology, Florida State University, 2003
M.S., Geology, The University of Georgia, 2005

DISSERTATION

Submitted in Partial Fulfillment of the
Requirements for the Degree of

Doctor of Philosophy

Earth and Planetary Sciences

The University of New Mexico
Albuquerque, New Mexico

May 2013

DEDICATION

I would like to dedicate this work to my husband, Mark Theiling, and my father, John Purdin.

To my father, thank you for opening my eyes to the wonders of the world we live in. You taught me to question, to explore, and to love every moment of it. You are a shining example of what it is to be an excellent teacher and mentor.

To Mark, thank you for showing me the world has more to offer than I ever dreamed. You taught me to love the journey, not just the destination. You are my inspiration.

On my grey days, you both helped lift the fog to show me how colorful the world really was.

ACKNOWLEDGEMENTS

This work was supported by NSF proposal EAR-0920830 and RAC funding from the University of New Mexico. Many thanks to Dani Gutierrez, Viorel Atudorei, Victor Polyak, Stephanie Yurchyk, Andrew Yuhas, and Zach Wallace for their assistance in the lab and in conducting fieldwork. I would also like to thank two anonymous reviewers for their insightful comments and suggestions regarding Chapter 1 during the journal submission process.

10^4-10^5 YEAR FLUCTUATIONS IN CONTINENTAL WEATHERING FLUX AND CONTINENTAL ICE-VOLUME DURING GLOBAL GREENHOUSE CLIMATE INTERVALS: EVIDENCE FROM OXYGEN AND NEODYMIUM ISOTOPES WITHIN THE CONTEXT OF CYCLOSTRATIGRAPHY

by

Bethany Purdin Theiling

B.A., ANTHROPOLOGY, FLORIDA STATE UNIVERSITY, 2003
M.S., GEOLOGY, THE UNIVERSITY OF GEORGIA, 2005
PH.D., EARTH AND PLANETARY SCIENCES, THE UNIVERSITY OF NEW MEXICO

ABSTRACT

Rapid changes in global and local climate and weather, noticeable over our lifetimes, have spurred heated public and political debate over the cause of these climatic changes, whether or not we can reverse, stop or slow down this process, and how to create adequate models that can predict Earth's changing climate. To create the most accurate models of future climate, many researchers look to past greenhouse intervals for insight; intervals of time identified by high modeled atmospheric CO_2, a lack of glacial deposits, and geologic evidence of globally high sea-levels—all of which suggest little to no glacial ice and a relatively monotonous climate. However, recent stratigraphic and geochemical evidence from the Cretaceous 'supergreenhouse' interval document compelling evidence to support dynamic greenhouse climates.

The goals of the studies hereafter described are to document and describe orbital-scale (10^4-10^5 yr) climate fluctuations recorded by $\delta^{18}O$ as a proxy for glacio-eustasy and sea surface temperature and ε_{Nd} as a proxy for continental weathering and wet/warm or dry/cool climate during two global greenhouse intervals: the Late Silurian and Late Devonian.

The first study (Chapter 1) explores whether glacio-eustasy was the driver for orbital-scale shallowing-upward cycles developed in Late Silurian and early Late Devonian tropical and subtropical greenhouse climates. Two intra-cycle $\delta^{18}O_{conodont\ apatite}$ trends were observed: asymmetric trends demonstrating progressive $\delta^{18}O$ increases coincident with facies shallowing, or symmetric trends demonstrating initially decreasing, then increasing $\delta^{18}O$ values. These isotopic trends and intra-cycle magnitudes support the hypothesis that these cycles developed in response to glacio-eustasy during glacial stages, implying that Late Silurian and Late Devonian greenhouse climates were more dynamic than traditionally assumed.

Relationships between orbital-scale continental weathering flux and glacial-interglacial marine cycles was first assessed comparing intra-cycle ε_{Nd} and $\delta^{18}O$ values from Middle Pennsylvanian icehouse cycles (Chapter 2). Observed conodont $\delta^{18}O$ trends support previous interpretations that sampled cycles were generated by glacio-eustasy (30-50 m magnitudes) combined with <1° sea surface temperature changes. ε_{Nd} trends typically demonstrate lower ε_{Nd} values during interglacial intervals and higher ε_{Nd} during glacial intervals, supporting claims that increases in precipitation and/or air temperatures during interglacial intervals result in increased continental weathering rates and/or increased flux to marine basins.

Using this initial continental weathering flux study and Pleistocene Nd-isotope studies as a model, we tested the phase-relationships of continental weathering flux and sea-level change in Upper Silurian and Upper Devonian greenhouse cycles (Chapter 3). Upper Silurian ε_{Nd} demonstrates relatively uniform intra-cycle values, due to averaging out of far-field source variations in continental weathering flux, relatively uniform Late

Silurian sub-tropical climate, and/or subdued continental weathering and flux due to the absence of upland and inland vascular land plants. Upper Devonian ε_{Nd} demonstrate greater intra-cycle variation in ε_{Nd}, which may be due to enhanced chemical weathering as a result of upland and inland colonization of land plants with large root systems and an intensified hydrologic cycle due to evapotranspiration. Observed ε_{Nd} trends support the hypothesis that these greenhouse cycles record increases and decreases in continental weathering due to increases and decreases in precipitation and/or air temperature. ε_{Nd} and $^{147}Sm/^{144}Nd$ values for Upper Silurian and Upper Devonian cycles support previous claims of far-field transport of Caledonian Mountain Belt material via trans-Laurentian fluvial systems.

TABLE OF CONTENTS

LIST OF FIGURES

LIST OF TABLES

CHAPTER 1
OXYGEN ISOTOPIC EVIDENCE FOR ORBITAL-SCALE GLACIAL ICE-VOLUME CHANGES DURING MIDDLE PALEOZOIC (SILURIAN AND DEVONIAN) GREENHOUSE TIME INTERVALS

Bethany P. Theiling, Maya Elrick

ABSTRACT

Observations of rising pCO_2, sea levels, and global temperatures motivates a more comprehensive understanding of greenhouse climate analogues throughout Earth's history. This study explores whether glacio-eustasy was the driver for orbital-scale (10^4-10^5 yr) shallowing-deepening marine cycles developed in Late Silurian and early Late Devonian greenhouse climates. $\delta^{18}O_{conodont\ apatite}$ values from 14 Upper Silurian and Upper Devonian cycles record two intracycle trends: progressive $\delta^{18}O$ increases coincident with facies shallowing, or initially decreasing, then increasing $\delta^{18}O$ values; average intracycle magnitudes are 1.5‰. These isotopic trends support the hypothesis that these cycles developed in response to glacio-eustasy, sea surface temperature changes, and potentially local increases in subtropical evaporation rates during glacial stages. These data suggest that glacial ice existed and fluctuated on orbital timescales during Late Silurian and early Late Devonian greenhouses, adding to an increasing body of evidence that illustrate greenhouse climates were not as uniformly warm and stable as previously thought.

INTRODUCTION

The past 100+ years of observations describing increasing pCO_2, rising sea-levels, retreating continental glaciers and sea ice, increasing global temperatures, and perturbations in regional global climate stimulate detailed characterization of global greenhouse climates. The Cretaceous 'supergreenhouse' is often considered the closest

analogue to Earth's next greenhouse interval, typified by significantly higher pCO_2 than present and a comparable continental configuration to the modern. Nevertheless, while Cretaceous sea surface temperatures (SST) calculated using a variety of methods exceed ~35°C for tropical (Forster et al., 2007; Bornemann et al. 2008) and ~20°C for polar latitudes (Herman and Spicer, 1996), an increasing body of work communicates compelling stratigraphic and $\delta^{18}O$ evidence for glacio-eustatic fluctuations occurring on orbital (10^4-10^5 yr) timescales (e.g. Miller et al., 1999; Gale et al., 2002; Bornemann et al., 2008). Such data suggest that the Cretaceous was not as uniformly warm and ice free as previously thought.

Although modeled atmospheric paleo-pCO_2 illustrates higher than present concentrations for other Phanerozoic greenhouse intervals (Cambrian-Early Ordovician, Late Silurian-Late Devonian and the Late Permian-Jurassic) (Berner, 2001), a growing body of research documents significant $\delta^{18}O$ changes associated with eustatic sea-level fluctuations and glacial dropstones (Stoll and Schrag 2000; Bornemann et al. 2008). These findings imply that some greenhouse time intervals accommodate continental ice, in direct opposition to traditional greenhouse climate models. If greenhouse intervals can include both high-latitude glacial ice and very warm tropical SST, climate prediction models must reflect the large pole-to-equator temperature gradients and address the feedback mechanisms required to create such atmospheric and oceanic conditions.

The focus of this study is to test the hypothesis that continental ice was present and growing and melting over orbital timescales during portions of two Paleozoic greenhouse time intervals—the Late Silurian and early Late Devonian. We utilize marine conodont

apatite from two different successions of subtropical, shallow-water platform carbonates for $\delta^{18}O$ analyses.

GEOLOGIC SETTING

Upper Silurian

Traditionally, the Silurian has been interpreted as a greenhouse interval based on a wide latitudinal distribution of reefs (Copper, 2002), shallow-water carbonates (Lubeseder, 2008) and tropical and temperate biota (Copper and Scotese, 2003), a lack of glacial deposits (Lehnert et al., 2006), globally high sea levels, and low $\delta^{18}O$ (Veizer et al., 1999). However, recent data from Upper Silurian marine deposits record a range of geochemical and stratigraphic evidence indicating dynamic climatic/paleoceanographic conditions, including large positive $\delta^{13}C$ excursions (Joachimski et al., 2002; Munnecke et al. 2003; Saltzman, 2005), My-scale $\delta^{13}C$ and $\delta^{18}O$ fluctuations (Samtleben, 2000; Munnecke et al., 2003), and the occurrence of repeated orbital-scale upward-shallowing marine sedimentary cycles (or parasequences) (Calder and Gibling, 1994; Brett et al., 1998; Cotter, 1998; Dorning and Harvey, 1999; Al-Shaieb et al., 2001; Bourque, 2001; Anderson and Goodwin, 2003; Skompski et al., 2008; Cramer, 2009).

Sampled Upper Silurian cycles (Pridolian-Ludlovian) of the Haragan-Henryhouse Formation (HHF) were deposited on a tectonically quiescent, southeastward-dipping carbonate ramp ~20-30°S of the paleo-equator (Al-Shaieb et al., 2001; Cocks and Torsvik, 2002) (Figure 1). Observed HHF subtidal cycles are characterized by thinly bedded shale and nodular argillaceous skeletal mudstone/wackestone (substorm wave base) overlain by medium-bedded skeletal wackestone-packstone (near fairweather wave base) which show no evidence of subaerial exposure (Figure 2).

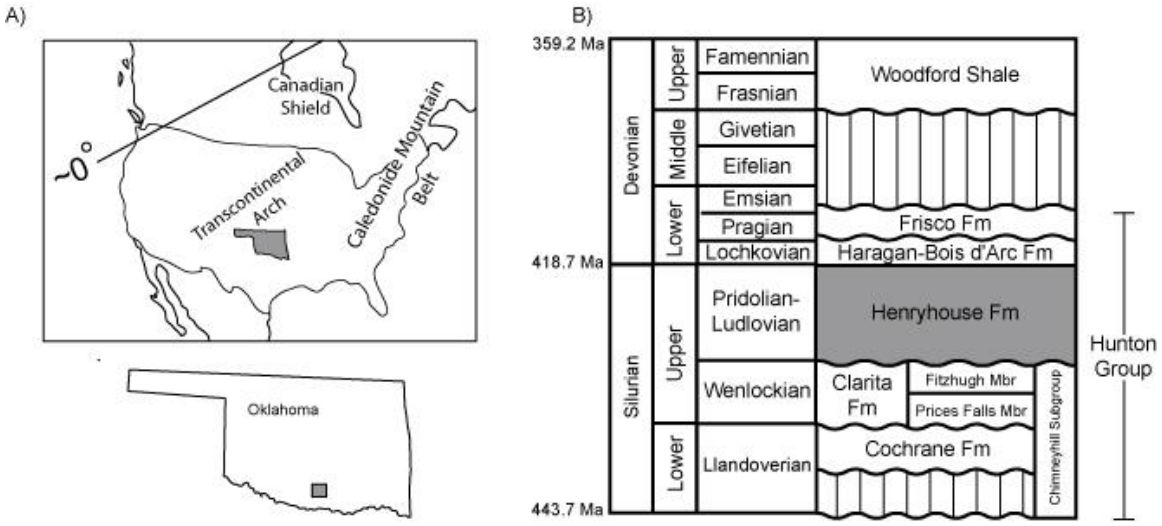

Figure 1. A) Late Silurian paleogeographic reconstruction of North America with major uplifts and orogenic fronts labeled in comparision to the estimated paleoequator. Gray shaded area indicates position of Oklahoma (United States), inset outlines the Arbuckle Mountains study area located on I-35. B) Silurian-Devonian chronostratigraphy of the study area (modified from Barrick, 1990). Abbreviations: Lst = Limestone, Fm = Formation, Mbr = Member. Wavy horizontal lines indicate disconformities. Vertical lines = unconformity. Ages for Silurian and Devonian periods from Gradstein et al. (2004).

Upper Silurian (Priodolian-Ludlovian) conodont samples were collected from the *Oulodus elegans detorta* conodont Zone (Barrick, 1975) (Figure 1), and are primarily *Belodella* elements, though sample 6.0 was a mixture of *Belodella* (coniform) and *Icriodus* (platform). Age control is based on conodont and graptolite biostratigraphy (Barrick et al., 1990). Coeval Upper Silurian cycles are found worldwide (e.g. Cotter, 1998; Dorning and Harvey, 1999; Samtleben et al., 2000); those with adequate biostratigraphic time control reveal cycle durations of between ~20-120 ky (Jeppsson, 1997; Crick et al., 2001; Cramer et al, 2009), suggesting orbital climate influences during this time.

Upper Devonian

Evidence for Early through early Late Devonian greenhouse climates is based on similar characteristics as that for the Silurian. Similar to the Silurian, the Late Devonian also records large, positive $\delta^{13}C$ excursions (Joachimski and Buggisch, 1993; Joachimski

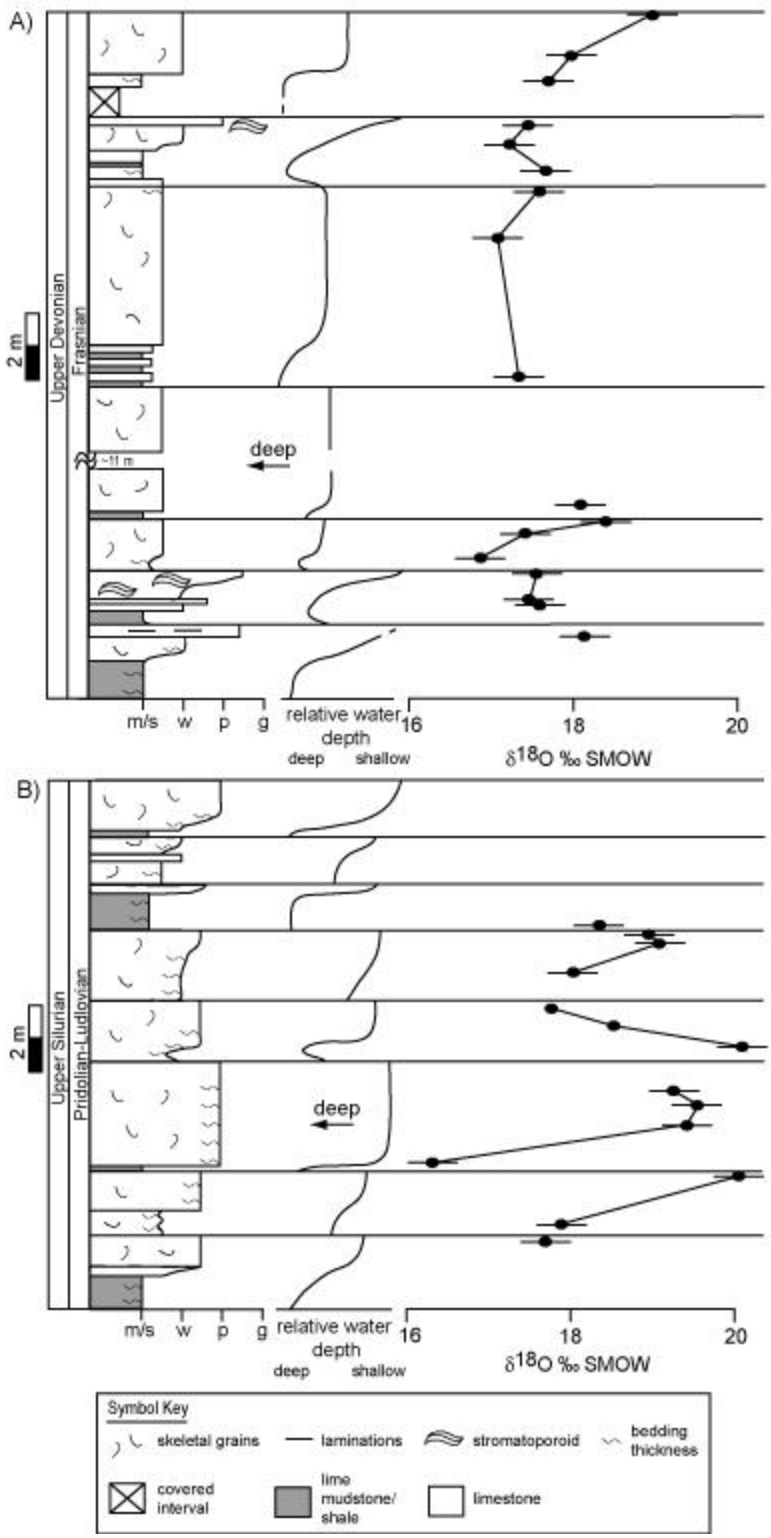

Figure 2. Cyclostratigraphy and associated $\delta^{18}O$ trends. A) Upper Devonian (Frasnian; *hassi* conodont Zone) cycles from Devil's Gate Formation, central Nevada (~10 km northwest of Eureka, Nevada). B) Upper Silurian (Pridolian-Ludlovian*; Kockelella crassa-Ozarkodina snajdri* conodont Zone) cycles from the Henryhouse Formation, central Oklahoma Arbuckle Mountains (~10 km south of Davis, Oklahoma). Long horizontal lines indicate cycle boundaries. m/s=lime-mudstone/shale, w=wackstone, p=packstone, g=grainstone

et al., 2002; Saltzman, 2005; van Geldern et al., 2006), My-scale $\delta^{18}O$ fluctuations (Joachmiski et al., 2009), and common orbital-scale upward-shallowing cycles (LaMaskin and Elrick, 1997; Gong et al., 2001; Yiming et al., 2001; Chen and Tucker, 2003; Ma et al., 2008; Zamanzadeh 2009; Whalen and Day, 2010).

Sampled Upper Devonian (Frasnian) cycles were deposited along a westward-deepening carbonate ramp ~10-20°S of the paleo-equator (Stampfli and Borel, 2002). Sampled subtidal cycles are characterized by thin, interbedded limestone and shale (rhythmites) or thin-bedded skeletal mudstone-wackestone (below storm wave base) overlain by medium- to thick-bedded skeletal mudstone-packstone, some of which contain in-growth-position *Amphipora*-type and/or lenticular stromatoporoids (near fair-weather wave base likely within photic zone) (Figure 2).

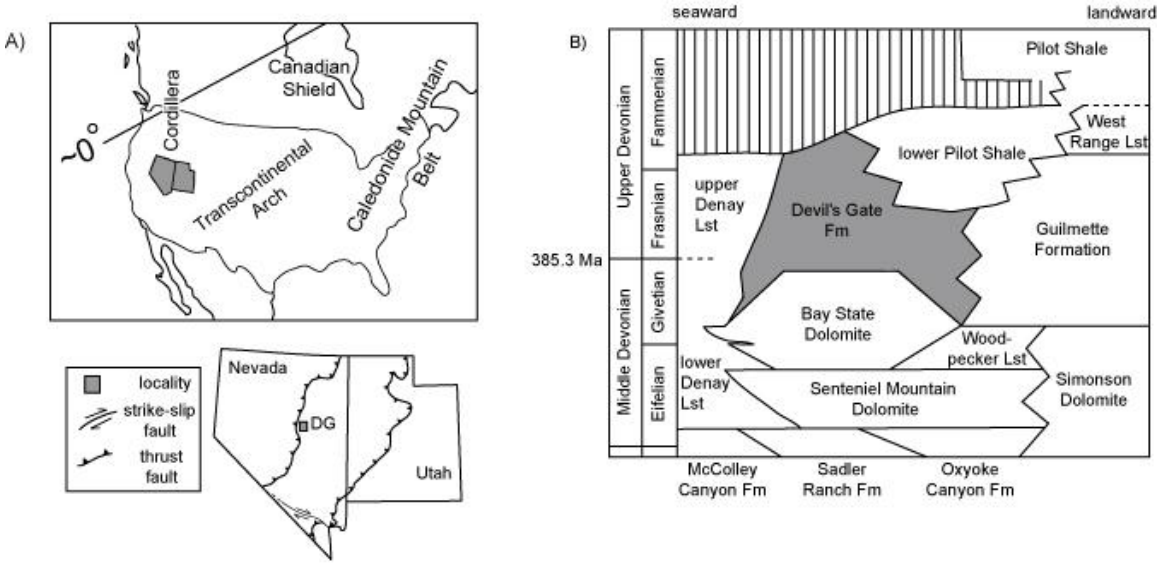

Figure 3. A) Late Devonian paleogeographic reconstruction of North America with major uplifts and orogenic front labeled in comparison to the estimated paleoequator. Grady shaded area indicates the positions of Nevada and Utah (United States). Inset outlines Nevada and Utah, showing locations of major faults and the Devil's Gate Pass study area (gray square)(modified from Sandberg et al., 2003). B) Middle-Late Devonian chronostratigraphy of the study area (modified from Johnson and Murphy, 1984; LaMaskin and Elrick, 1997). Abbreviations:Lst = Limestone, Fm = Formation. Vertical lines = unconformity. Age of Middle-Upper Devonian boundary from Gradstein et al. (2004).

Upper Devonian (Frasnian) conodont samples were collected from the *hassi* conodont Zone of the Devil's Gate Formation (Figure 3), and are primarily *Polygnathus* taxa. Age control is based on conodont biostratigraphy (e.g. Sandberg and Ziegler, 1996; Morrow and Sandberg, 2003). Coeval Upper Devonian cycles east of the study area record ~30-165 ky durations (LaMaskin and Elrick, 1997) and in other global localities record ~20 ky durations (Chen and Tucker, 2003).

Determining the magnitude of water-depth change responsible for cycle development in these and other ancient cyclic deposits is difficult, particularly because depth-diagnostic facies are lacking. However, interpretations from previous studies of meter-scale cycles from various Paleozoic successions composed of similar facies changes and from epicontinental seaway settings suggest magnitudes of less than 10-20 meters for sampled Upper Silurian and Upper Devonian cycles (e.g., Osleger, 1991; Immenhauser and Scott, 2002; Immenhauser, 2009).

METHODS AND RESULTS

Isotopic ratios were determined by reducing Ag_3PO_4 in a continuous flow TC-EA connected to a Finnigan Mat 253 mass spectrometer using a method modified from O'Neil et al. (1994) and Bassett et al. (2007). $\delta^{18}O$ data are reported in ‰ with respect to SMOW (Table 1). Reproducibility of $\delta^{18}O$ measurements was determined by replicate analyses of internal standards and uncertainty is ±0.3‰ (1σ).

$\delta^{18}O$ analyses from sampled Upper Silurian and Upper Devonian cycles yield two major trends. Three of four sampled Silurian cycles and two of five sampled Devonian cycles demonstrate a progressive increase in $\delta^{18}O$ in-phase with shallowing-upward facies trends (asymmetric cycles; Figure 1). The range in magnitude of intracycle

isotopic change for these cycles is 1.0-3.2‰, analogous to magnitudes recorded across Pleistocene glacial-interglacial cycles (e.g., Shackleton et al., 1988; Lisiecki and Raymo, 2005). Three of five sampled Upper Devonian cycles demonstrate an initially decreasing, then increasing $\delta^{18}O$ into the cycle cap (Fig.1). The total magnitude of intracycle isotopic change for these symmetric $\delta^{18}O$ trends is <0.5‰. One Silurian cycle records progressively decreasing $\delta^{18}O$ trends.

distance from stratigraphic base (m)	$\delta^{18}O$ (‰)
Upper Silurian	
2.1	17.6
2.5	17.9
4.1	19.4
4.3	16.3
5.4	19.4
6.0	19.5
6.4	19.4
7.7	20.1
8.3	18.7
8.8	18.2
9.9	18.6
10.7	19.4
11.1	19.1
11.3	19.1
Upper Devonian	
1.9	17.7
2.9	17.1
3.0	16.9
3.8	17.0
4.3	16.3
5.0	16.9
5.5	17.9
5.9	17.6
21.3	17.3
25.5	17.1
26.9	17.6
27.5	17.7
28.3	17.2
28.9	17.4
30.2	17.7
31.0	18.0
32.2	19.0

Table 1. Table of conodont $\delta^{18}O$ values with stratigraphic depth (m) separated into Upper Silurian and Upper Devonian ages.

DISCUSSION

Those Silurian and Devonian cycles that display $\delta^{18}O$ trends coincident with water-depth changes support the hypothesis that these cycles were generated by orbital-scale climate changes--namely glacio-eustasy combined with SST changes. We preclude tectonic origins for cycle development because while some type of recurrent, high-frequency subsidence/uplift has been argued for particular cycles deposited in tectonically active regions (Cisne, 1986), there are no realistic explanations as to why tectonically induced water-depth changes would control systematic $\delta^{18}O$ trends similar to those observed in this study.

Measured asymmetric $\delta^{18}O$ trends could be generated by thermo-eustasy, groundwater storage/release, or glacio-eustasy. Orbital-scale SST changes driving thermo-eustasy (thermal expansion/contraction of seawater) could explain the observed relationships between isotopic and intracycle facies trends under ice-free conditions; however, calculated estimates on the magnitude of sea-level change caused by 4-14°C shift (Silurian) or 0.5-7°C shift (Devonian) in SST (Kolodny et al., 1983; Pucéat et al., 2011) are <5 m (Schulz and Schäfer-Neth, 1998), assuming $\delta^{18}O_{seawater}$ of -1‰. Such small thermo-eustatic magnitudes are insufficient to explain the observed range of water-depth changes estimated by facies changes.

Periodic and climatically-controlled storage and release of groundwater may explain $\delta^{18}O$ shifts and associated sea-level fluctuations (Hay and Leslie, 1990; Faure et al., 2002), in which increased groundwater storage of low $\delta^{18}O$ meteoric waters lowers global sea-level and locally increases surface seawater $\delta^{18}O$ values, and release of groundwater raises sea levels and decreases $\delta^{18}O$. While this model is attractive to explain greenhouse

cycles, we cannot use this mechanism to explain observed cyclic facies and $\delta^{18}O$ changes without a process-oriented model to rationalize cyclic groundwater storage.

Therefore, we suggest that the growth and melting of continental and alpine glaciers combined with SST variations generated observed $\delta^{18}O$ and sea-level changes (Figure 2). In the following discussion, we estimate the potential magnitudes of paleoclimate and sea-level changes necessary to create the observed isotopic shifts. Because independent temperature proxies are limited for pre-Cretaceous marine deposits, it is difficult to estimate the relative effects of ice-volume versus SST changes. Under Neogene icehouse conditions, ~70% of observed $\delta^{18}O$ values are due to ice-volume and ~30% are due to SST effects (Fairbanks and Matthews, 1978). Applying this 70:30 proportionality to these greenhouse data results in glacio-eustatic sea-level fluctuations of ~65-200 m for Upper Silurian cycles and 8-80 m for Upper Devonian cycles with coeval SST fluctuations of <4°C and <2°C, respectively. Such large magnitudes of eustatic change are unreasonable because subaerial exposure features are not observed in these subtidal cycles and observed facies changes suggest <10-20 m of sea-level change. Assuming a smaller ice-volume contribution (e.g., 30:70; Pekar et al., 2005) results in smaller glacio-eustatic estimates (~20-90 m for Silurian cycles, ~10-35 m for Devonian cycles) but unrealistic SST changes for subtropical paleolatitudes (up to 10°C for Silurian cycles, and ~5°C for Devonian cycles). These results suggest that an additional mechanism influenced the observed intracycle isotopic trends.

Glacial intervals (low sea level) are typified by globally higher $\delta^{18}O_{seawater}$ values, drier/windier subtropical climates (e.g., van Zeist, 1967; Janecek and Rea, 1983; Rea, 1994), and associated increased evaporation rates. These increased evaporation rates,

particularly in subtropical paleolatitudes, may have further enriched local surface $\delta^{18}O_{seawater}$ values, resulting in accentuated glacial-interglacial isotopic shifts. While these local evaporation effects may explain increased intracycle isotopic shifts, the contribution of evaporation to the $\delta^{18}O$ values must have been small because the diversity and abundance of typically open-marine fauna is similar throughout Silurian and Devonian cycle development. In addition, the measured isotopic values lie within the range of conodont $\delta^{18}O$ previously reported in coeval Silurian and Devonian successions (Joachimski et al., 2004; Žigaité et al., 2010). Most importantly, while local orbital-scale evaporation variations may explain some of the observed greenhouse $\delta^{18}O$ isotopic shifts, only glacio-eustasy can account for the observed intracycle water-depth changes.

If our glacio-eustatic hypothesis is correct, then symmetric (decreasing, then increasing upward) $\delta^{18}O$ trends within asymmetric (shallowing-upward) cycles chronicle a more complete record of the glacial-interglacial climate transition, where decreasing and low $\delta^{18}O$ values represent the transition into maximum interglacial intervals and $\delta^{18}O$ increases record the transition into full glacial intervals, while asymmetric cycles with asymmetric $\delta^{18}O$ trends record only the interglacial to glacial portion of the climatic transition. We suggest that asymmetric cycles with symmetric $\delta^{18}O$ trends are generated as a result of the interplay between sedimentation rate, subsidence and eustasy; i.e., sedimentation outpaced accommodation gains and peak interglacial conditions (sea-level highstand) occurred just below the subtidal cycle caps (Jervey, 1988).

CONCLUSIONS

Intracycle $\delta^{18}O$ trends support the hypothesis that glacio-eustasy, combined with some SST and local seawater evaporation changes, generated these Upper Silurian and

Upper Devonian cycles. These results combined with previous studies suggest very warm subtropical SSTs for the Late Silurian and early Late Devonian, but imply that polar/high latitudes provided suitable climates for some glacial ice growth during particular orbital configurations. Furthermore, these data suggest that pole-to-equator temperature gradients may have been steeper than previously assumed for portions of some greenhouse time intervals and that significant ocean-atmosphere feedbacks should be included in greenhouse climate models. In order to revise the current paradigm for greenhouse (ice-free) and icehouse (large ice sheets) time intervals, we emphasize the significance of glacial ice as a driver for orbital-scale sea-level change during both greenhouse and icehouse intervals and suggest that orbital cyclicity in portions of some greenhouse climates permit the growth of polar and alpine glaciers.

CHAPTER 2

INCREASED CONTINENTAL WEATHERING FLUX DURING ORBITAL-SCALE SEA-LEVEL HIGHSTANDS: EVIDENCE FROM ND AND O ISOTOPE TRENDS IN MIDDLE PENNSYLVANIAN CYCLIC CARBONATES

Theiling, Bethany P., Elrick, Maya, and Asmerom, Yemane

Abstract

Despite the common occurrence of orbital-scale (10^4-10^5 yr) sedimentary cycles in a wide range of Proterozoic through Neogene marine and non-marine depositional systems, understanding the effects and phase relationships of orbital-scale climate drivers on time-equivalent marine and non-marine deposits is difficult mainly due to correlation limitations between the geographically isolated deposition settings. Results from this study assess the relationships between orbital-scale continental weathering flux and glacial-interglacial marine cycles using Nd isotopes (from whole rock limestones) and $\delta^{18}O$ values (from conodont apatite) from Middle Pennsylvanian cyclic marine carbonates in the U.S. Southwest.

Conodont $\delta^{18}O$ trends from 2 of 4 sampled glacial-interglacial carbonate cycles support previous interpretations that observed water-depth changes were controlled by glacio-eustasy (30-50 m magnitudes) combined with <1° seawater temperature changes. Two additional sampled cycles show initially increasing, then decreasing $\delta^{18}O$ trends. Based on these results, we suggest that $\delta^{18}O$ better defines a eustatic sea-level curve, rather than a facies-derived curve.

ε_{Nd} trends in 5 of 8 sampled cycles are higher during regressive intervals (early glacial phase) and lower during sea-level highstands (interglacial phase), supporting the

hypothesis that increases in precipitation and/or air temperatures during interglacial intervals result in increased continental weathering rates and/or increased flux of weathered solutes to the Middle Pennsylvanian marine basin. This hypothesis is in contrast to traditional sequence stratigraphic interpretations (increased siliciclastic shedding into marine basins during falling sea level/lowstands) and suggests that climatically-controlled precipitation and/or air temperature fluctuations influenced continental weathering flux more than sea level-controlled shoreline or baseline position in this paleotropical location. These results highlight the use of combined ε_{Nd} and $\delta^{18}O$ analysis as a tool for evaluating the response of marine and coeval non-marine systems to orbital-scale climate changes, particularly in deep-time depositional systems.

Keywords: cycles, orbital-scale, neodymium, oxygen, sea-level, glacioeustasy, glacio-eustasy, continental weathering, $\delta^{18}O$, ε_{Nd}, glacial-interglacial

Introduction

Sedimentary cycles (or parasequences) recording orbitally-driven climate changes are documented in a wide range of Precambrian through Phanerozoic marine and continental deposits including shelf, slope, and open-ocean marine environments and fluvial, lacustrine, and paleosol deposits (e.g. Anderson, 1982; Arthur et al., 1986; Goldhammer et al., 1987; Olsen & Kent, 1996; Gale et al., 2002; Laurin et al., 2005; Culver et al., 2011). The widespread occurrence of such cycles across a range of geologic time periods and settings suggests that orbitally-forced climate changes are a major driver of sedimentation patterns at 10^4-10^5 yr timescales.

Despite the common occurrence of orbital cycles in the sedimentary record, it has been difficult to assess the effects and phase relationships of orbital forcing on time-

equivalent marine and non-marine deposits, particularly in deep-time systems (pre-Cenozoic). These difficulties are due mainly to limitations related to correlating between marine and geographically isolated non-marine successions at the orbital and sub-orbital timescales using conventional correlation tools such as biostratigraphy, magnetostratigraphy, carbon-isotope stratigraphy, and/or tephrachronology (e.g., Shishkin and Ochev, 1993; Lozovsky and Yarshenko, 1994; Arens and Jahren, 2000; Mundil et al., 2003; Jahren et al., 2001). An additional complexity is that many deep-time marine successions lack coeval continental deposits due to erosion, nondeposition, and/or later deformation. Understanding the flux and timing of continental material (solid and dissolved load) to adjacent marine basins in the context of orbitally-driven climate changes has important implications for evaluating global oceanic elemental and nutrient budgets, biologic productivity, carbon cycling, and pCO_2, with its associated climatic effects.

Some previous attempts to understand the effects of and relationships between orbital-scale climate change and deep-time marine and coeval continental deposits were conducted on interbedded marine and non-marine facies (Soreghan, 1994; Miller et al., 1996; Rankey, 1997). Continental climate interpretations were based on the nature and occurrence of climatically sensitive non-marine facies (i.e., eolian, paleosols, fluvial deposits), whereas sea-level interpretations tracking glacial-interglacial climate phases and glacio-eustasy were made from interbedded cyclic marine deposits. Soreghan (1994) and Rankey (1997) interpreted wetter Pennsylvanian continental climates during interglacial phases (sea-level highstands) with drier conditions during glacial phases (sea-level lowstands). In contrast, Miller et al. (1996), working on Permian deposits, report

wetter or more seasonally variable conditions during glacial phases (sea-level lowstands). These opposing interpretations are due in part to the fact that the analyzed successions contained interbedded continental and marine deposits which are not strictly time-equivalent and therefore cannot track coeval climatic responses to orbital forcing.

Alternative approaches to evaluating the effects of orbital climate change in marine and coeval non-marine systems include combined analysis of geochemical proxies for sea surface temperature (SST) and glacio-eustasy ($\delta^{18}O$ values) and continental weathering flux (Os, Sr, and/or Nd isotopes) that occur in marine strata. The use of these proxies within fully marine successions removes potential effects of miscorrelation between marine and non-marine strata and does not require the presence of coeval non-marine successions. Although Sr isotopes have been utilized in a variety of studies to track changes in mantle versus continental flux, the $>10^6$ yr oceanic residence time for Sr precludes its use in orbital-scale paleoclimate studies. The short oceanic residence time of Nd (10^2 yr) however, implies that Nd-isotopic ratios will be incorporated into marine sedimentary deposits before homogenization by oceanic mixing. In addition, REE are immobile (insoluble) and therefore, relatively unsusceptible to diagenesis (McLennan, 1989; Banner, 2004). Therefore, Nd isotopes can be utilized for regional-scale continental weathering flux studies to evaluate orbital- and suborbital-scale climate changes across varying climate zones/belts.

Recent advances in multi-collector inductively coupled mass spectrometry (MC-ICPMS) have made possible the rapid high-precision isotopic analysis of small quantities of Nd, opening the use of Nd isotopic data for high-resolution chemostratigraphic reconstruction in carbonates. The objectives of this study are to describe and interpret

changes in $\delta^{18}O$ values from conodont apatite and Nd-isotopes from cyclic whole rock limestones to assess the effects and timing relationships between orbitally driven glacial-interglacial marine cycles and continental weathering flux (a term we use to refer to continental weathering rates and/or transport to a basin).

Geologic Background

The Pennsylvanian Earth system was dominated by the early formation of the Pangaean supercontinent, the large Panthalassic ocean, and by major fluctuations in continental ice-volume centered in high-latitude Gondwana (Caputo and Crowell, 1985; Veevers and Powell, 1987; Frakes and Francis, 1988; Crowell, 1999; Scotese, 2001; Isbell et al., 2003; Fielding et al., 2008). Growth and melting of glaciers caused sea-level fluctuations of >50 m (e.g. Heckel, 1977; Goldhammer and Elmore, 1984; Soreghan, 1994; Joachimski et al., 2006; Rygel et al., 2008; Elrick et al., 2009) which generated orbital-scale cycles (Heckel 1977, 1994, 1997; Soreghan and Giles, 1999) and million year (My)-scale depositional sequences (Algeo et al., 1991; Soreghan, 1994; Wiberg and Smith, 1994; Scott and Elrick, 2004, Elrick and Scott, 2010).

During the Pennsylvanian, New Mexico was located approximately 5-10° south of the paleoequator (Scotese and Golonka, 1992). Tectonic subsidence rates related to Ancestral Rocky Mountain deformation were minimal during the Early and Middle Pennsylvanian and highest during the Late Pennsylvanian (Virgilian or Gzhelian) (Dickinson and Lawton, 2003).

The Middle Pennsylvanian (Desmoinesian or Moscovian) Gray Mesa Formation accumulated in the Lucero Basin of central New Mexico (Figure 4; Kelley and Wood, 1946; Martin, 1971; Kues and Giles, 2004) and is comprised of nearly 300 m of cyclic,

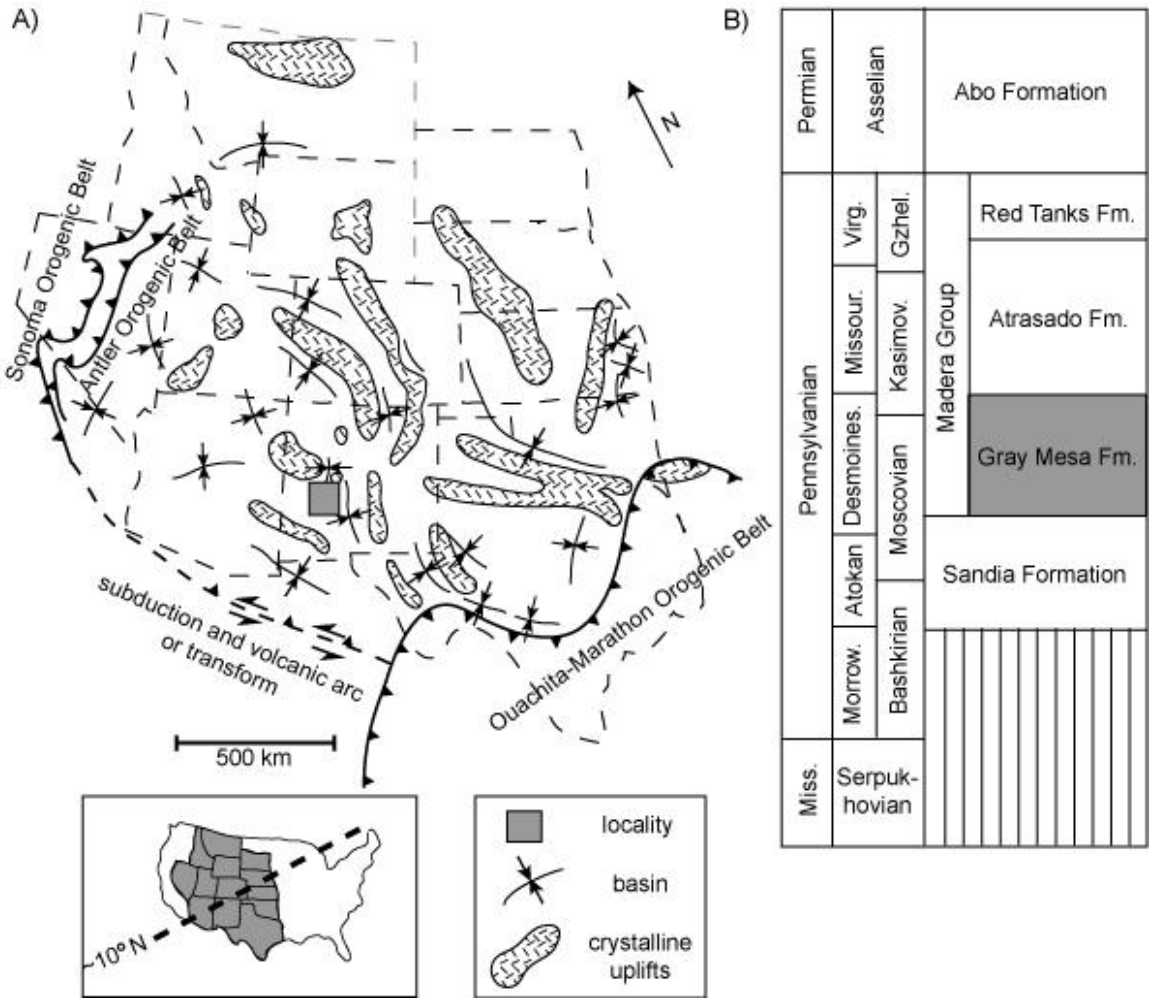

Figure 4. A) Paleogeographic reconstruction of the western United States showing locations of Precambrian crystalline uplifts, basins, and major faults, with inset showing estimated Pennsylvanian paleolatitude for study area (modified from Kluth and Coney, 1981). Gray shaded square outlines the Lucero Basin and Mesa Sarca study area. B) Pennsylvanian chronostratigraphy of the study area. Abbreviations: Virg. = Virgilian, Missour. = Missourian, Desmoines. = Desmoinesian, Morrow. = Morrowian, Kasimov. = Kasimovian, Gzhel. = Gzhelian.

mixed carbonate-siliciclastic marine deposits (Martin, 1971, Scott and Elrick, 2004; Elrick and Scott, 2010). The Lucero Basin was surrounded by relatively low-relief Precambrian crystalline uplifts (~1.4-1.65 Ga; Karlstrom et al., 2004) associated with formation of the Ancestral Rocky Mountains (Figure 4; Kluth and Coney, 1981; Ye et al., 1996). Within the Lucero Basin, northward increases in both siliciclastic sediment abundance and grain size suggest sourcing from the nearby Penasco Uplift to the northeast (Martin, 1971; Scott and Elrick, 2004). Age control for the Grey Mesa

Formation is based on limited fusulinid and conodont biostratigraphy (Kelly and Wood, 1946; Wengerd, 1956; Martin, 1971).

At the Mesa Sarca study area (Figure 4), the Gray Mesa Formation is composed of ~75 orbital-scale upward-shallowing subtidal cycles (or parasequences) (Scott and Elrick, 2004). Subtidal cycles provide a more continuous record of deposition relative to peritidal cycles because of relatively uninterrupted deposition in subtidal marine environments. Typical Gray Mesa subtidal cycles (1.5-5 m) are characterized by thinly bedded, argillaceous, skeletal mudstone/wackestone or covered intervals at cycle bases (deeper subtidal facies), thin- to medium-bedded, bioturbated skeletal wackestone/packstone in the middle of cycles (shallow subtidal facies), with medium- to thick-bedded, skeletal wackestone/packstone and rare grainstone cycle caps (shallowest subtidal facies). Approximately 40% of cycle caps display evidence of subaerial exposure, including meteoric $\delta^{13}C$ signatures, calcretes, and regolith breccias (Figure 5; Scott and Elrick, 2004; Elrick and Scott, 2010).

Previous studies of Gray Mesa cycles in the study area document orbital-scale sea-level fluctuations and systematic up-cycle increases in whole rock $\delta^{13}C$ and conodont $\delta^{18}O$, which together indicate high-amplitude (>50 m) glacio-eustasy was responsible for cycle development and subaerial exposure during sea-level fall/lowstands (Scott and Elrick, 2004; Elrick and Scott, 2010).

Methodology

This study focuses on samples collected from 8 successive, subtidal cycles in the lower 35 m of the Gray Mesa Formation (highstand systems tract of Sequence 1; Scott and Elrick, 2004).

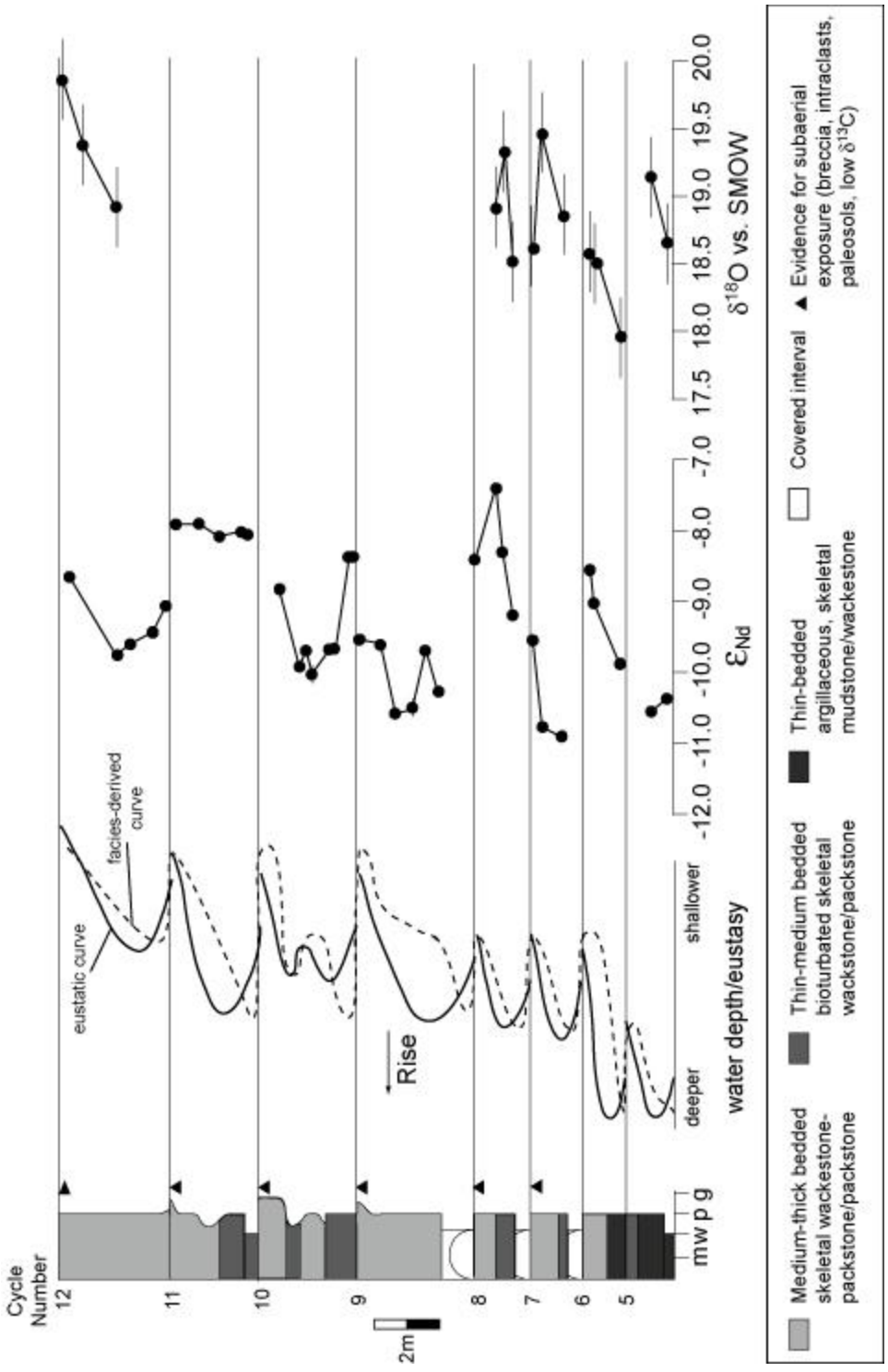

Figure 5. Cyclostratigraphy of the targeted lower Gray Mesa Formation versus relative water depths (dashed line) determined from facies analysis and eustatic sea-level (solid line) estimated from the combined effects of sedimentation, subsidence, and sea-level change, $\delta^{18}O_{apatite,}$ and ε_{Nd} trends. Cycle numbers are based on previous work by Scott and Elrick (2004). $\delta^{18}O$ data from cycle 12 is taken from Elrick and Scott (2010). Error bars for ε_{Nd} are smaller than the size of the data point, when not shown suggesting that small isotopic variations recorded in cycle 10 are significant.

Oxygen Isotopes

Analyses of conodont $\delta^{18}O$ were used to verify that Gray Mesa cycles sampled for Nd isotopes formed in response to orbital-scale glacio-eustasy. Oxygen isotopes from marine calcite are a well-established tool for determination of seawater temperature changes and ice-volume effects (e.g. Epstein et al., 1953; Emiliani, 1955, Shackleton and Opdyke, 1973; Veizer et al., 1999). $\delta^{18}O$ from conodont apatite is considered more reliable for pre-Mesozoic studies than calcite because it is less susceptible to diagenetic alteration (Bryant et al., 1996; Iacumin et al., 1996; Wenzel et al., 2000; Joachimski et al., 2004). Conodont apatite has been shown to precipitate in equilibrium with ambient seawater when compared to coeval fish teeth (Amzy et al., 1998). In addition, conodont $\delta^{18}O$ values demonstrate smaller isotopic variability than coeval calcite (Wenzel et al., 2000).

Samples for conodont analyses were collected at 0.1-0.5 m intervals depending on observed facies changes, with individual samples weighing between 10-25 kg. Conodonts were extracted from whole rock limestones using conventional separation techniques of Sweet and Harris (1988).

Oxygen isotopic analyses were performed on ~500 μg of Ag_3PO_4 crystals, formed from the conversion of conodont apatite using a method modified from O'Neil et al. (1994) and Bassett et al. (2007). Isotopic ratios were determined by reducing Ag_3PO_4 in a continuous flow TC-EA and analyzed on a Finnigan Mat 253 mass spectrometer at the University of New Mexico Stable Isotope Laboratory. Oxygen isotope data are reported in ‰ with respect to SMOW (Table 2). Reproducibility of $\delta^{18}O$ measurements was

determined by replicate analyses of internal standards and with an uncertainty of ±0.3‰ (1σ).

Cycle #	Sample[a]	$^{143}Nd/^{144}Nd$	Apparent ε_{Nd}[b]	Sm (ppm)	Nd (ppm)	ε_{Nd} @ 300My[c]	$\delta^{18}O$ vs. SMOW
5	MS 15.25	0.51193889	-13.64	0.471	2.572	-10.37	18.66
	MS 15.75	0.51191552	-14.09	0.541	3.150	-10.56	19.15
6	MS 16.7	0.51193550	-13.70	0.273	1.723	-9.86	17.97
	MS 17.5	0.51196700	-13.09	0.702	4.732	-9.01	18.51
	MS 17.65	0.51203105	-11.84	2.543	13.910	-8.56	18.58
7	MS 18.5	0.51189999	-14.40	0.495	2.853	-10.90	18.85
	MS 19.1	0.51187610	-14.86	0.273	1.847	-10.77	19.47
	MS 19.5	0.51194919	-13.44	0.958	6.092	-9.56	18.60
8	MS 20.0	0.51197513	-12.93	2.075	12.740	-9.19	18.52
	MS 20.3	0.51201953	-12.06	0.635	3.916	-8.30	19.33
	MS 20.5	0.51206820	-11.12	1.000	6.106	-7.39	18.92
	MS 21.2	0.51201256	-12.20	0.008	0.050	-8.39	
9	MS 22.3	0.51194099	-13.60	0.728	4.028	-10.27	
	MS 22.7	0.51194725	-13.47	1.138	7.067	-9.69	
	MS 23.1	0.51192636	-13.88	0.119	0.667	-10.50	
	MS 23.6	0.51191119	-14.18	0.298	1.770	-10.56	
	MS 24.1	0.51196090	-13.21	0.208	1.231	-9.61	
	MS 24.7	0.51196808	-13.07	0.135	0.786	-9.53	
10	MS 24.9	0.51200185	-12.41	1.419	9.469	-8.36	
	MS 25.1	0.51200074	-12.43	1.051	7.055	-8.36	
	MS 25.5	0.51194909	-13.44	0.503	3.124	-9.65	
	MS 25.7	0.51194280	-13.56	0.337	2.136	-9.70	
	MS 26.0	0.51189839	-14.43	0.239	1.630	-10.31	
	MS 26.2	0.51191768	-14.05	0.138	0.913	-10.04	
	MS 26.4	0.51193553	-13.70	0.616	4.055	-9.71	
	MS 26.6	0.51192514	-13.91	0.202	1.327	-9.92	
	MS 27.2	0.51198182	-12.80	0.229	1.493	-8.84	
11	MS 28.2	0.51201351	-12.18	0.781	5.360	-8.04	
	MS 28.4	0.51202656	-11.93	1.119	7.221	-8.00	
	MS 29.1	0.51201110	-12.23	0.723	4.975	-8.08	
	MS 29.7	0.51202369	-11.98	0.434	2.934	-7.89	
	MS 30.4	0.51201959	-12.06	0.576	3.972	-7.90	
12	MS 30.5	0.51194642	-13.49	0.656	4.909	-9.07	
	MS 31.1	0.51193722	-13.67	0.898	6.314	-9.45	
	MS 31.8	0.51193345	-13.74	0.121	0.835	-9.58	
	MS 32.2	0.51190907	-14.22	0.483	3.666	-9.75	
	MS 33.7	0.51195786	-13.27	0.826	6.589	-8.65	

[a]Sample numbers represent distance (m) above underlying sequence boundary, identified by Scott and Elrick (2003).

[b]Value of ε_{Nd} at present day.

[c]ε_{Nd} during estimated time of depositon (300 My), where $^{147}Sm/^{144}Nd$ = Sm(ppm)/Nd(ppm)*

Natural abundance of $^{147}Sm/^{144}Nd$*Atomic weight of Nd/Sm, then $^{143}Nd/^{144}Nd_{(t=300\ My)} = {}^{143}Nd/^{144}Nd_{measured}$-(et-1)* $^{147}Sm/^{144}Nd$,

$\varepsilon_{Nd}(t=300\ My) = (^{143}Nd/^{144}Nd_{(t=300\ My)}/^{143}Nd/^{144}Nd_{CHUR(t=300\ My)}-1)*10000$

Table 2. 143Nd/144Nd, apparent εNd (value at present), Sm and Nd concentrations (ppm), εNd (t=300 My), and δ18O data for sampled intervals. t=300 My is assumed as an approximate age for deposition of Gray Mesa cycles to determine εNd at the time of deposition.

Neodymium Isotopes

^{143}Nd is the decay product of ^{147}Sm ($t_{1/2}$ = 106 Ga). Variations in $^{143}Nd/^{144}Nd$ are typically expressed by ε_{Nd} values, defined as ($^{143}Nd/^{144}Nd_{sample}/^{143}Nd/^{144}Nd_{CHUR}$ -

1)*10,000, where CHUR is the $^{143}Nd/^{144}Nd$ ratio of the chondritic undifferentiated reservoir at the time of interest. Because Nd has a larger ionic radius than Sm, Nd is considered 'more incompatible' than Sm. More incompatible elements will be preferentially partitioned into the crust during mantle melting and differentiation. Consequently, the continental crust has a lower Sm/Nd ratio than the depleted mantle (as sampled by mid-ocean ridge basalts [MORB]) and as a result, a less radiogenic Nd-isotopic composition (typically ε_{Nd} = -20 for crust with a mean age of 2 Ga; Goldstein and Jacobsen, 1987) compared to MORB (typically > +8; Shirey, 1991). The short oceanic residence time of Nd ($<10^2$ yr) however, implies that Nd-isotopic ratios will be incorporated into marine sedimentary deposits before homogenization by oceanic mixing (oceanic mixing time ~1000 yrs). In addition, REE are immobile (insoluble) and therefore, relatively unsusceptible to diagenesis (McLennan, 1989; Banner, 2004). Therefore, Nd isotopes can be utilized for regional-scale continental weathering flux studies to evaluate orbital- and suborbital-scale climate changes across varying climate zones/belts. Because the seawater REE budget is dominated by continental input (Goldstein and Jacobsen, 1987), ε_{Nd} in marine deposits can serve as a proxy for changes in the regional continental weathering flux, and can be used to track paleo-ocean circulation (e.g. Martin and Macdougall, 1995; Reynolds et al., 1999; Thomas, 2004; Piotrowski et al., 2005; Puceat et al., 2005; Scher and Martin, 2006; Via and Thomas, 2006; MacLeod et al., 2008) and emergence/flooding of continental landmass (Fanton et al., 2002).

Nd-isotopic analyses were performed on powdered whole-rock limestones collected at a 0.1-1 m sampling resolution. Approximately 500 mg of powder was drilled from

each sample using a diamond-bit Dremel© in order to avoid stylolites, intraclasts, large skeletal grains, and veins. The powder was dissolved in 6N HCl. The soluble and insoluble fractions were then centrifuged and the supernate was separated into two Teflon© beakers, one to be used to analyze concentrations of Sm and Nd for calculation of $^{147}Sm/^{144}Nd$, and one to be used for REE and Sm-Nd column separation for analysis of $^{143}Nd/^{144}Nd$.

For this initial effort, we used a small aliquot of the supernate to determine the Sm/Nd ratio of the samples to calculate initial $^{143}Nd/^{144}Nd$ ratios. The Sm/Nd fraction was dried down, dissolved in 200 μL 7N HNO_3, capped, and left overnight. The sample was then dissolved in 50 mL of 10 ppb In + 3% HNO_3, and was analyzed on a Thermo X-series II inductively coupled plasma quadrupole mass spectrometer (ICPQMS) at the University of New Mexico Radiogenic Isotope Laboratory. The initial $^{143}Nd/^{144}Nd$ values were calculated using an age of 300 Ma (approximate depositional age of Gray Mesa Formation; Table 2). We have verified this initial method using a total spiking method, whereby a calibrated spike with known $^{147}Sm/^{150}Nd$ was added to sample supernate to determine sample $^{147}Sm/^{144}Nd$.

The supernate used for analysis of $^{143}Nd/^{144}Nd$ was dried down and dissolved sequentially in 7N HNO_3 and 15N HNO_3, drying after each acid addition. The sample was then dissolved in 4 mL 1N HNO_3, centrifuged, and the supernate was added to 250μL cation exchange columns filled with TRU-SP resin, cleaned, and conditioned with 1N HNO_3. REE were collected using a modified method of Asmerom (1999). REE fractions were dried down and dissolved in 200 μL 0.18N HCl and were added to REE exchange columns cleaned and conditioned with 0.18N HCl. Nd was separated and

collected using a modified method of Asmerom (1999). The sample solution was dried and dissolved in 1 mL 3% HNO_3 for analysis on a Thermo Neptune multi-collector inductively coupled plasma mass spectrometer (MC-ICPMS) at the University of New Mexico Radiogenic Isotope Laboratory.). Reproducibility of ε_{Nd} was determined using replicate analyses and is reported for each sample, ranging between 0.05 and 0.26 ε-units and averaging 0.11 ε-units (2σ) (Table 2, Figure 5). Error bars of less than 0.20 ε-units are smaller than data points and therefore not shown in Figure 5. The La Jolla Nd isotopic standard was run with each batch, obtaining a mean value of $^{143}Nd/^{144}Nd$ ratio of 0.511825± 4 (2σ), which is within the accepted range of values for the standard (Pier et al., 1989).

Results

$\delta^{18}O$ values range between 18.0-19.5‰. The change in $\delta^{18}O$ values across individual sampled cycles ranges between 0.5‰ and 0.9‰ (Table 2, Figure 5). Cycles 5, 6, and 12 show progressive up-cycle increases in $\delta^{18}O$. Data for cycle 12 comes from Scott and Elrick (2004). Cycles 7 and 8 show initially increasing, then decreasing $\delta^{18}O$ trends.

ε_{Nd} values (t=300 My; estimated age of Grey Mesa cycles) range between -10.9 and -7.4 (Table 2, Figure 5). The change in ε_{Nd} values across individual sampled cycles ranges between 0.2-2.0 ε-units. Five of the eight sampled cycles are characterized by initially decreasing, then increasing ε_{Nd} values. Because only 2 samples were recovered for cycle 5, no trend is specified. Cycle 6 shows progressively decreasing ε_{Nd} values. Cycle 8 shows initially increasing, then decreasing ε_{Nd} values.

$\delta^{18}O$ vs. ε_{Nd} do not covary (Figure 6). Systems in which the supply of continental weathering flux co-varies with $\delta^{18}O$ suggest that both isotopic systems were influenced

by the same process on the same spatial or temporal scale, namely global glacial-interglacial climate changes (Vance et al., 2009). That $\delta^{18}O$ vs. ε_{Nd} do not covary suggests that these proxies were influenced by either different processes or that they are affected on a different spatial scale (e.g. global vs. regional changes).

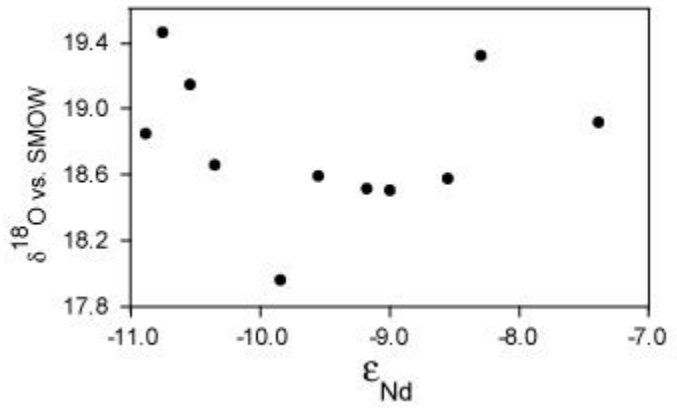

Figure 6. ε_{Nd} vs. $\delta^{18}O$ for sampled Gray Mesa cycles. The lack of co-variance suggests that continental weathering flux (ε_{Nd}) is locally-derived. Co-variance of ε_{Nd} and $\delta^{18}O$ would suggest that changes in continental weathering flux were influenced by either the same process (i.e. glacio-eustasy and SST change) or that changes in continental weathering flux occurred on the same spatial scale (i.e. global vs. regional).

Discussion

$\delta^{18}O$ trends

The systematic up-cycle increase in $\delta^{18}O$ values in 3 of 5 cycles supports the expected relationship between sea level and glacial growth and melting recorded in the Pleistocene-Holocene (e.g., Shackleton et al., 1988; Zachos et al., 2001; Lisiecki and Raymo, 2005; Raymo et al., 2006; Massari et al., 2007) and previous interpretations that these Pennsylvanian cycles were generated by glacio-eustatic sea-level change combined with some SST change (Joachimski et al., 2006; Elrick and Scott, 2010) (Figure 5). Without the aid of independent temperature proxies such as foraminiferal Mg/Ca ratios, we cannot separate the effects of changes in glacial ice volume versus seawater temperature.

If the measured isotopic shifts were due *entirely* to SST change, then the estimated temperature change across individual cycles would range between 2-4°C, applying the phosphate-water fractionation and temperature equations from Kolodny et al. (1983) and Pucéat et al. (2010). This range of temperature change would produce only a <0.5 m thermo-eustatic sea-level change (thermal expansion/contraction of seawater; deWolde et al., 1995; Schulz and Schäfer-Neth, 1998). Such low magnitudes are unreasonable given the >50 m estimates based on facies analysis, extent and depth of subaerial exposure features, and stratal geometries (e.g. Heckel, 1977; Rygel et al., 2008). Conversely, if we assume isotopic shifts were due only to ice-volume effects, the measured 0.5-0.9‰ changes in $\delta^{18}O$ during cycle development equate to ~45-80 m glacio-eustatic changes for the sampled cycles, assuming the relationship of 0.11‰ per 10 m sea-level change (Fairbanks and Matthews, 1978).

Using the Pleistocene as an analog, we assume a combination of ice-volume and SST effects controlled the measured isotopic variations, and assume SST and ice-volume effect contributions of ~30% and ~70%, respectively (Fairbanks and Matthews 1978; Fairbanks, 1989). Using this method, we estimate that the sampled Gray Mesa cycles were generated by >30-50 m glacio-eustatic changes accompanied by <1°C SST changes. However, Ca/Mg ratios and $\delta^{18}O$ data from planktonic foraminifera over the past 350 kyr suggest glacial-interglacial SST changes on the order of 3-5°C (Lea et al., 2000;2002). If we apply 3-5°C SST change as a minimum to sampled Pennsylvanian cycles, then the remaining isotopic shift equates to <25 m glacio-eustatic sea-level fluctuations, which would imply that SST change contributed ~70% of the total $\delta^{18}O$ value, double the

estimated contribution over the last few million years (Fairbanks and Matthews, 1978; Fairbanks, 1989).

The estimated >30-50 m magnitudes record minimum values and are less than those (~60-140 m) reported by Elrick and Scott (2010). The absence of lowstand and early transgressive deposits and variability in the extent of subaerial exposure and facies changes observed at Mesa Sarca indicate that this locality did not record the full extent of sea-level rise and fall and imply that the full magnitude of glacial-interglacial isotopic shift was even larger. Much like the Pleistocene, 10^5-10^6 yr fluctuations in the volume of glacial ice during the Pennsylvanian likely contributed to the variability of sea-level change between successive cycles (Rygel et al., 2008).

It is unclear why cycles 7 and 8 show initially increasing, then decreasing $\delta^{18}O$ values, with maximum values near mid cycle (Figure 5). Based on traditional facies analysis, which is used to interpret relative sea-level changes, these $\delta^{18}O$ versus facies relationships suggest that maximum glaciation occurred just above mid-cycle or below cycle tops, before deposition of the shallowest water facies at the cycle top. However, a more reasonable interpretation is that these cycles were generated in response to eustasy. We discuss $\delta^{18}O$ versus facies relationships using Figure 7, which outlines the differences between relative sea-level interpreted from facies analysis versus eustatic sea-level interpreted from a theoretical understanding of the combined effects of subsidence, sea-level change, and sedimentation (Jervey, 1988; Coe and Church, 2000). Shallowing-upward facies could be generated by sedimentation rates greater than eustatic sea-level rise rates. However, this hypothesis is unlikely because the tops of cycles 7 and 8 display evidence of prolonged subaerial exposure, including pedogenic calcretes and meteoric

$\delta^{13}C$ signatures, which can only form when absolute sea level falls and exposes the seafloor to meteoric waters and soil formation.

Increasing, then decreasing $\delta^{18}O$ in cycles 7 and 8 could also be generated by changes in evaporation rate and/or basin restriction, whereby increases in evaporation rate and/or basin restriction are recorded by greater $\delta^{18}O$ values. However, this hypothesis is unlikely because the greatest $\delta^{18}O$ values are recorded during the mid- to late regression when eustatic sea-level is high (Figure 7). If evaporation rates increased during this interval, exchange with the open ocean would have also increased due to sea-level rise, dampening the effect of evaporation rate on $\delta^{18}O$ values.

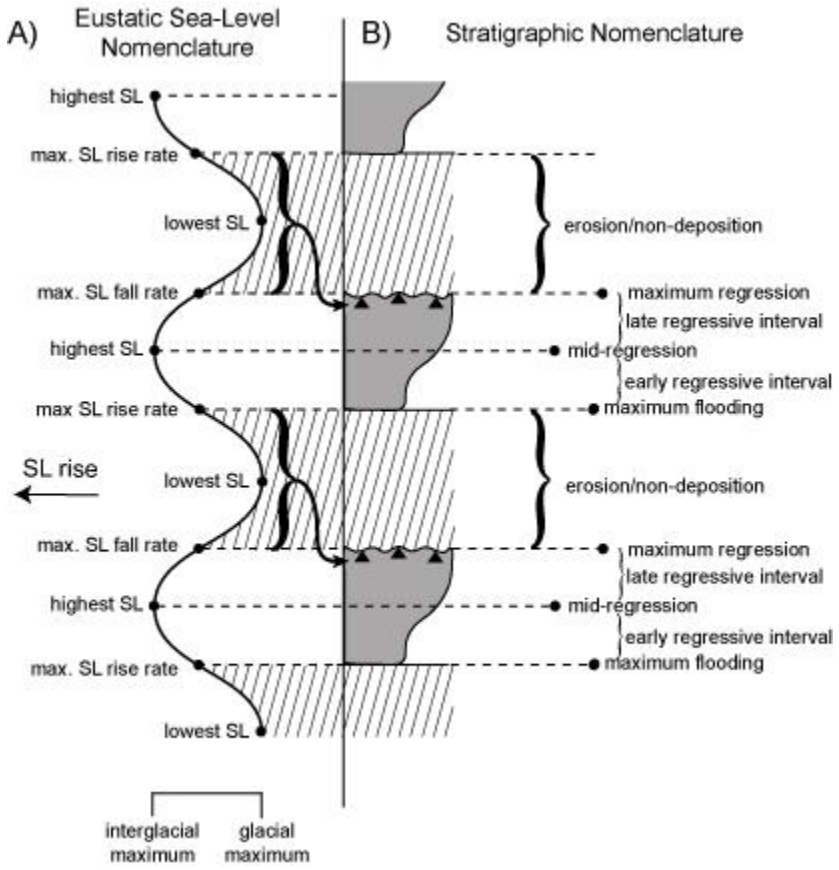

Figure 7. A) Simplified sinusoidal eustatic sea-level (SL) curve with labeled inflection points and maximum glacial-interglacial intervals. B) Stratigraphic nomenclature used in text with schematic asymmetric cycles similar to those observed in the Gray Mesa Formation with a narrower column representing deeper water facies and a wider column representing shallower water facies. Note that no deposition/erosion occurs during the late

eustatic fall, lowstand and early rise (diagonal lines) and a disconformity develops; subaerial exposure features develop at the cycle top during subaerial exposure (black triangles). During a single glacial-interglacial sea-level cycle, deposition during the initial transgression as the glaciers begin to melt is not recorded within the study area due to lack of accommodation space. Once accommodation space is created due to subsidence and rapid (maximum) SL rise rates, deposition occurs and is represented by deeper water deposits at the cycle base. SL continues to rise with additional glacial melting and reaches its highest position at the interglacial maximum (mid-regression). Because SL is rising at a slower rate after the maximum rate of SL rise inflection point (and assuming constant sedimentation rate), sediments above the maximum flooding zone reflect loss of accommodation space and is termed the early regressive interval. After the interglacial maximum, SL fall rates increase and is represented by the shallowest water deposits of the late regressive interval. The maximum regression is therefore defined in this study as the maximum regressive deposits recorded at the sampling locality.

Nd-isotope trends

Five of the eight sampled cycles are characterized by ε_{Nd} trends that are initially high at cycle base (maximum flooding), lowest near the mid-cycle (mid-regression), and return to high ε_{Nd} values at the cycle top (late regression; Figures 5 and 7). These trends suggest increasing continental weathering flux into the Lucero Basin during times of maximum flooding when sea-level was rising the fastest and until sea level reached its highest position at the interglacial maximum (mid-cycle). Subsequent increases in ε_{Nd} values suggest a reduction in continental weathering flux into the basin during initial sea-level fall. During sea-level lowstand, this inner shelf location was subaerially exposed (depositional hiatus) and no record of Nd-isotopes is available.

Four possible interpretations are explored to explain these dominant ε_{Nd} trends, each within the context of orbital-scale glacio-eustatic sea-level fluctuations. Fanton et al. (2002) interpret that ε_{Nd} increases and decreases recorded in Ordovician marine deposits represent influx from significantly different continental source areas during My-scale regression and transgression. In their scenario, the low-relief Precambrian shield (with low ε_{Nd}) was exposed during regression and submerged during transgression, which resulted in regressive marine deposits with low ε_{Nd} values and transgressive deposits with higher ε_{Nd} values. Applying this principle to the Lucero Basin, the observed ε_{Nd} trends could be produced if influx from older continental crust (with lower ε_{Nd} values) occurred

during high sea level (interglacial maximum), whereas influx from younger continental crust (with higher ε_{Nd} values) reached the basin during sea-level fall (glacier growth). This scenario is not reasonable for this study because the Lucero Basin was surrounded by Precambrian uplifts (Ancestral Rocky Mountains), all with similar ages of ~1.7 Ga whose ε_{Nd} at the time of deposition of Gray Mesa cycles is ~-30 to -25 calculated from measured $^{143}Nd/^{144}Nd$ and $^{147}Sm/^{144}Nd$ reported in Bennett and DePaolo (1987); see Table 1 for calculations. Maximum exposure of these Precambrian uplifts during falling and low sea levels (glacier growth and glacial maximum) would have generated ε_{Nd} trends opposite of those observed.

A second potential explanation for the observed ε_{Nd} trends would be changes in regional marine circulation patterns. The observed ε_{Nd} trends would result from regional marine currents transporting lower ε_{Nd} values from older continental source areas flowing into the Lucero Basin during rising and high sea level (interglacials), whereas marine currents transporting higher ε_{Nd} isotope values (sourced from younger continental crust or more open-ocean waters) would flow into the Lucero Basin during falling and low sea level (early, maximum, and late glacial intervals). Because Precambrian Ancestral Rocky Mountain uplifts throughout the U.S. Southwest have relatively uniform ε_{Nd} values (Bennett and DePaolo, 1987), it is unlikely that the Mesa Sarca ε_{Nd} trends record changes in influx from significantly different continental crust source areas and it is unlikely that the same marine circulation patterns would have occurred for six successive cycles formed during variable magnitude sea-level changes.

Instead, we explore two alternative mechanisms that can explain changes in continental weathering flux on orbital timescales. In a scenario in which eolian transport

dominated continental influx into the Lucero Basin, rising sea levels (early interglacials or cycle bases) are characterized by low eolian influx due to low wind intensities and/or greater humidity/wetter climate, and resultant high ε_{Nd} values. This would be followed by increasing eolian influx due to increasing winds/aridity during highest sea-levels (interglacial maximums or mid-cycles), resulting in low ε_{Nd} values. During subsequent sea-level fall (early glacial), eolian input would decline with decreasing wind intensity and/or aridity and a return to higher ε_{Nd} values. While a few studies from tropical and temperate Pacific Ocean cores report increased eolian input during Pleistocene or Holocene interglacial intervals (Rea et al., 1986; Hovan et al., 1991), the majority of findings from these studies suggest that glacial intervals are characterized by drier climates and greater wind intensities, whereas interglacial intervals have wetter climates and lower wind intensities globally (e.g. Zeist, 1967; Janecek and Rea, 1983; Wasson et al., 1984; Rea et al., 1991; Nanson et al., 1992; Wang, 1993; Rea, 1994; Rincón-Martinez et al., 2010). Without a process-oriented model explaining windier/more arid conditions during interglacial intervals, it is not reasonable to expect that wind behavior during glacial Pennsylvanian intervals opposed the dominant Pleistocene regime.

We suggest that the observed ε_{Nd} trends were likely controlled by orbitally-driven changes in continental weathering rates and/or fluvial sediment influx. Accordingly, the observed trends would develop if fluvial influx and/or chemical weathering rates were low (resulting in higher ε_{Nd} values), increasing during maximum sea-level rise rates (early interglacial), and were greatest, signaled by lower ε_{Nd} values, during sea-level highs (interglacial maxima); fluvial influx and/or weathering rates would then decrease (rising ε_{Nd} values) during the subsequent fall in sea level (early glacial) (Figure 7). We

suggest that the systematic changes in fluvial influx and/or chemical weathering rates were controlled by orbitally-forced changes in paleotropical precipitation and/or air temperature, in which increases in precipitation and/or air temperature resulted in increased fluvial influx and/or chemical weathering rates and decreases in precipitation and/or air temperature resulted in decreased fluvial influx and/or weathering rates.

Many modern watersheds are shown to be 'weathering limited', characterized by thinner soils with readily available unaltered minerals, such that weathering flux is limited by mineralogy (susceptibility to chemical weathering), precipitation, soil-water pH, and temperature (Stallard and Edmond, 1981; 1983; 1987; Kump et al., 2000). Global continental chemical weathering rates are shown to increase with rises in temperature and precipitation demonstrated by increases in fluvial discharge cation concentrations, Ca, Mg, K, HCO_3^-, and H_4SiO_4 (e.g., Bluth and Kump, 1994; White and Blum, 1995; Berner et al., 1998; Kump et al., 2000; Frank, 2002; West et al., 2005; Schmidt et al., 2006; Gislason et al., 2009; McKay et al., 2009; Kuwahara et al., 2010; Williams et al., 2010). Indeed, positive coupling of chemical weathering rates with precipitation and temperature is also demonstrated over orbitally-driven glacial-interglacial cycles (e.g. Burton and Vance, 2000; Piotrowski et al., 2005; Bokhorst et al., 2009; Kuwahara et al., 2010). Because air temperature often co-varies with precipitation, evaporation rates, and vegetation cover, it is difficult to separate the effects of temperature and precipitation on chemical weathering rates (Kump et al., 2000). To separate the effects of temperature and precipitation, White and Blum (1995) fit an Arrhenius-type equation to SiO_2 and Na fluxes. Although plots of weathering fluxes versus temperature correlate reasonably well, they significantly underestimate chemical

weathering rates, suggesting that precipitation dominates chemical weathering rates and that precipitation and temperature are positively coupled.

The relationship between drier glacials and wetter interglacials is consistent with results from paleoequatorial regions in the Late Pennsylvanian (Soreghan, 1994; Rankey et al., 1997) and Pleistocene-Holocene (e.g. Zeist, 1967; Janecek and Rea, 1983; Wasson et al., 1984; Rea et al., 1991; Nanson et al., 1992; Wang, 1993; Rea, 1994; Rincón-Martinez et al., 2010). In particular, planktonic foraminifera from the Bay of Bengal demonstrate cyclic variations in ε_{Nd} on glacial-interglacial timescales over the past 150 kyr due to variations in continental weathering flux (Burton and Vance, 2000). Each of these examples are characterized by cooler, drier climates during glacial maxima with a relatively low flux of fluvially-derived material (reflected by higher ε_{Nd}) and warmer, wetter interglacial intervals, in which flux of fluvially-derived material increases (reflected by lower ε_{Nd}) (Naimo et al., 2005; Kettner and Syvitski, 2009; Lewis et al., 2009, Burton and Vance, 2000).

Vance et al., (2009) suggest that the products of chemical weathering on glacial-interglacial timescales is moderated by post-glacial weathering pulses (fine-grained physical weathering products produced by subglacial grinding underneath continental glaciers; Bell and Laine, 1985; Anderson, 2007) released during glacial melting and retreat. Post-glacial weathering pulses are more likely to be observed in ferromanganese nodules in post-glacial lakes (Vance et al., 2009), deep-ocean ferromanganese crusts (Reynolds et al., 1999; Piotrowski et al., 2005), and marine sediments along high-latitude continental shelves (Scher et al., 2011). Low-latitude shelf localities are less likely to record post-glacial pulses because global transport of REEs such as Nd and Sm occur via

large-scale ocean circulation (i.e.-modern transport from the Labrador Surface Water current to the North Atlantic Deep Water current and then the Antarctic Bottom Water current; e.g., Burton et al., 1997; Piotrowski et al., 2005; Scher and Martin, 2006; Via and Thomas, 2006). Due to their low mobility, REEs will likely be scavenged by particulates before a high-latitude post-glacial weathering pulse can be recorded in marine sediments accumulating on a low-latitude shelf. In addition, the lack of co-variance between $\delta^{18}O$ and ε_{Nd} support the assumption that ε_{Nd} values are locally-derived (Figure 6).

One of the eight sampled cycles (cycle 6) records a progressive increase in ε_{Nd} values from cycle base to top and one cycle (cycle 8) shows an initial increase to peak ε_{Nd} values in the middle of the cycle followed by a decrease in values within the cycle cap (Figure 5). These variable trends may be due to fluctuations in sedimentation rate, thus recording an incomplete eustatic sea-level curve over cycle development (Figure 7). Long-term variations in the magnitude of Pliocene through Pleistocene orbital-scale climate forcing are a possible explanation for variations in continental weathering flux, if changes in the magnitude of climatic forcing control the proclivity of chemical versus mechanical weathering. Differences in ε_{Nd} between the acid soluble (AS) and acid insoluble (AIS) fraction of samples may elucidate whether ε_{Nd} values were incorporated into the crystal structure of carbonate minerals (suggesting chemical weathering dominated) or whether ε_{Nd} is a primary signature of the detrital component (suggesting mechanical weathering dominated). Such a test may also explain why sediments deposited during the interglacial maximum do not necessarily possess the greatest detrital (AIS) fraction.

It is important to note that if our hypothesis of increased continental weathering flux during sea-level highstands (interglacials) is due to increased precipitation (and as a

result, increased fluvial flux), then it opposes traditional sequence stratigraphic interpretations, where sea-level controls shoreline and fluvial base-level positions and by implication, the flux of continentally-derived sediment into the marine basin (e.g. Van Wagoner et al., 1988; Coe and Church, 2003). In the traditional sequence stratigraphic model, sea-level fall/lowstands are characterized by fluvial incision and increased fluvial transport to the marine basin, which would be recorded by an up-cycle increase in $\varepsilon_{Nd.}$ In contrast, our hypothesized model suggests that increased fluvial incision and/or transport of physical weathering products (solids) and dissolved chemical weathering products (dissolved load) (shown by decreased ε_{Nd}) coincide with intervals of sea-level rise and highstand (interglacial), followed by decreased fluvial incision and/or flux (shown by increasing ε_{Nd}) during sea-level fall/lowstand (glaciation) (Figure 7). Increased fluvial incision is indeed more likely to occur during maximum regression due to lowering of fluvial base level, however the type of weathering (physical versus chemical), the mechanism of transport (fluvial versus eolian) and weathering rates to generate transportable particles is dominated by local/regional, climatically controlled changes in precipitation and/or air temperature.

Results from this study highlight how orbital to suborbital variations in ε_{Nd} and $\delta^{18}O$ within marine strata can detect the response of continental weathering flux to orbitally-forced climate change and eliminates potential miscorrelations between geographically separated marine and coeval non-marine successions. These results demonstrate that Middle Pennsylvanian paleotropical continental weathering flux is generally in-phase with glacio-eustatic sea-level change and glacial growth/melting, and suggest that local/regional paleotropical continental weathering may be dependent upon climatically

controlled changes in fluvial flux due to fluctuations in precipitation and/or air temperature. These results highlight a promising new technique utilizing nearshore marine successions to evaluate regional continental weathering flux and climate change within the context of global sea-level and glacial-interglacial cycles.

Conclusions

1) $\delta^{18}O$ trends across targeted orbital-scale subtidal cycles support previous interpretations that these cycles formed in response to glacio-eustasy with magnitudes of between 30 and 50 m combined with ~1°C SST changes.

2) The majority of cycles sampled for ε_{Nd} analysis display trends indicating maximum continental weathering flux during interglacial maxima (sea-level highstands) when local paleotropical precipitation rates and/or paleotemperatures were the highest, facilitating maximum weathering rates and/or fluvial transport of weathered solutes to the study area. During lower sea-level stands (early and late glacial stages), continental weathering flux decreased, suggesting drier and/or cooler paleotropical climates. Because these cycles were deposited at an inner shelf location, no record is available for lowest sea-level positions (glacial maximum).

3) Our hypothesis of increased continental weathering influx during sea-level highstands (interglacials) is in contrast to traditional sequence stratigraphic interpretations and suggests that climatically controlled precipitation and/or air temperature fluctuations influenced continental weathering flux more than sea-level controlled shoreline/base line position in this paleotropical location.

CHAPTER 3

FLUCTUATIONS IN CONTINENTAL WEATHERING FLUX DURING TWO PALEOZOIC GREENHOUSE INTERVALS

Theiling, B.P., and Elrick, M.

Abstract

Previous utilization of Nd isotopes in marine successions as a proxy for evaluating regional-scale changes in continental weathering flux under icehouse global climate regimes typically describe a binary mixing model between relatively unradiogenic continental rocks and relatively radiogenic oceanic waters and demonstrate that increases in continental weathering flux occur during interglacial intervals as a result of increases in precipitation and/or air temperature. This study compares icehouse Nd isotope trends to those generated during two separate global greenhouse intervals of the Late Silurian and early Late Devonian. Upper Silurian ε_{Nd} ranges from -8.4 to -10.9 and show no consistent intra-cycle trend, due to averaging out of far-field source variations in continental weathering flux, relatively uniform Late Silurian sub-tropical climate, and/or subdued continental weathering and flux due to the absence of upland and inland vascular land plants. Upper Devonian ε_{Nd} ranges from -12.9 to -6.6, and demonstrate increased intra-cycle variation in ε_{Nd}, most likely due to enhanced chemical weathering due to widespread colonization of land plants with large root systems and an intensified hydrologic cycle due to evapotranspiration. The range in ε_{Nd} for Upper Silurian and Upper Devonian cycles support previous claims that the widespread transition from weathering of relatively unradiogenic Canadian Shield and Transcontinental Arch to the radiogenic Caledonian Mountain Belt had occurred by the Pridolian in mid-Laurentia and

the Frasnian in western Laurentia. Cycle-scale comparison of ε_{Nd} from sampled greenhouse cycles to an icehouse continental weathering-climate model suggests that only a portion of the complete transition from warmer and/or wetter climate to cooler and/or drier climate intervals may be recorded. Partial ε_{Nd} records observed in most Upper Devonian sampled cycles are likely produced as the result of the interplay between sedimentation rate, accommodation space, and eustasy.

Introduction

Recently, Nd isotopes have been used to detect significant orbital-scale or high-frequency (10^4-10^5 yr) changes in continental weathering flux during icehouse climates (Burton and Vance, 2000; Theiling et al., 2012)(Chapter 2), intervals characterized by large climate shifts and large changes in continental ice volumes. Observed continental weathering flux variations imply concurrent fluctuations in nutrient supply to oceans and pCO_2 uptake related to silicate weathering rate changes, both of which have important affects on the global carbon budget, climate, and marine biologic productivity.

As our global climate shifts to warmer, or greenhouse, modes, a question arises as to whether continental weathering flux changes occur on orbital-timescales during warmer climates and if so, are these flux changes enhanced by warmer temperatures and an intensified hydrologic cycle or damped by more stable/uniform climatic conditions? Furthermore, are fluctuations in continental weathering flux recorded in marine basins the result of local, regional, or far-field changes in weathering and erosion?

The objectives of this study are to 1) describe orbital-scale Nd isotope trends during two different cyclic greenhouse marine successions of Late Silurian and Late Devonian age, 2) compare these greenhouse Nd isotope trends to those recorded in Pleistocene and

Pennsylvanian icehouse orbital-scale cycles, and 3) evaluate continental weathering flux provenance using absolute Nd and Sm/Nd isotope ratios.

Climatic and Geologic Setting

Upper Silurian

Traditionally, the Late Silurian has been interpreted as a greenhouse interval based on high latitudinal reef (Copper 2002) and carbonate (Lubeseder 2008) distribution, a lack of glacial deposits (Lehnert et al. 2006), globally high sea levels (Copper 2002), and low $\delta^{18}O$ (Veizer et al. 1999). However, recent data from Upper Silurian marine deposits record a range of geochemical and stratigraphic fluctuations that indicate widespread and dynamic climatic conditions, including large positive $\delta^{13}C$ excursions (e.g. Joachimski et al., 2002; Munnecke et al. 2003; Saltzman, 2005), My-scale $\delta^{13}C$ and $\delta^{18}O$ fluctuations (Samtleben, 2000; Munnecke et al., 2003; Saltzman), and worldwide distribution of cyclic, orbital-scale upward-shallowing marine sedimentary cycles (parasequences) (Calder and Gibling, 1994; Brett et al., 1998; Cotter, 1998; Dorning and Harvey, 1999; Al-Shaieb et al., 2001; Bourque, 2001; Anderson and Goodwin, 2003; Skompski et al., 2008; Cramer, 2009).

During the Late Silurian, much of the Earth's continental mass was situated in the southern hemisphere, leaving the northern hemisphere largely covered by the Panthalassic Ocean. The Late Silurian saw the closure of the Iapetus Ocean, culminating in the collision of Laurentia with the newly-combined Baltica-Avalonia Terrane (Caledonide Orogengy: 425-420 Ma; Cocks and Torsvik, 2002). The resultant Laurussian continent was largely covered by an epeiric sea. Successive continental collisions from the Taconic (Late Ordovician), Caledonide (Late Silurian) and Acadian

(Late Silurian-Early Devonian) Orogenies generated ~2000 km of uplifted accreted terranes to the north and northeast portions of Laurentia. Although the timing of the Romanzof Orogeny is still debated to have begun in the Early-Middle Devonian (Embry, 1991; Trettin, 1991), the Romanzof and Klakas Orogenies may have generated uplifts along the northern edge of Laurentia as early as the Late Silurian (Bazard et al., 1995; Butler et al., 1997; Soja and Antoshkina, 1997; Soja et al., 2000; van Staal et al., 2009). Carlson (1999) suggests the relatively low relief Transcontinental Arch (extending from Minnesota to New Mexico) was exposed during the Late Silurian. The Southern Oklahoma Rift and Reelfoot Rift (Proterozoic) basins intersected the southern margin of Laurussia. (Cocks and Scotese, 1991; Golonka et al., 1994; Cocks and Torsvik, 2002). Carbonate ramps and platforms extended along this southern edge from present-day New Mexico to central Tennessee (Baarli et al., 2003).

Sampled Upper Silurian cycles (Pridolian-Ludlovian) of the Haragan-Henryhouse Formation were deposited in the Anadarko Basin of south-central Oklahoma on a tectonically quiescent, southeastward-dipping carbonate ramp, positioned ~20-30°S of the paleoequator (Figure 1) (Cocks and Scotese, 1991; Golonka et al., 1994; Cocks and Torsvik, 2002). The Haragan-Henryhouse Formation is unconformably underlain by the Clarita Formation (Wenlockian) and unconformably overlain by the Mississippian and Devonian Woodford Shale (Figure 1). Observed subtidal cycles are characterized by thinly bedded shale and nodular argillaceous skeletal mudstone/wackestone (substorm wave base) overlain by medium-bedded skeletal wackestone-packstone (near fairweather wave base) which show no evidence of subaerial exposure (Figure 8), though subaerial exposure features and karsting are observed in landward positions (Al-Shaieb et al.,

2001). Age control is based on conodont and graptolite biostratigraphy (Barrick et al., 1990). Those coeval Upper Silurian cycles with adequate biostratigraphic time control reveal cycle durations of between ~20-120 ky (Jeppsson, 1997; Crick et al., 2001; Cramer et al, 2009), suggesting orbital climate influences during this time.

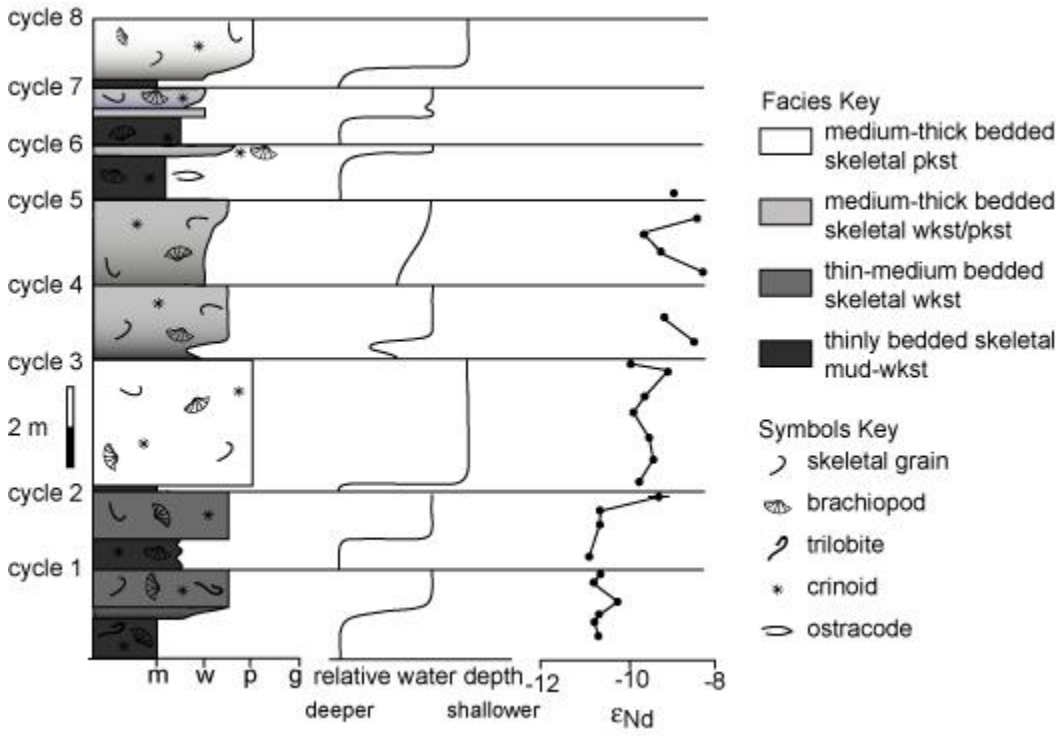

Figure 8. Upper Silurian (Pridolian-Ludlovian) cyclostratigraphy with interpreted changes in water depth based on facies changes and associated ε_{Nd} trends. Sampled section is within the *Oulodus elegans detorta* conodont Zone from the Haragan-Henryhouse Formation of central Oklahoma (~5 km south of Davis, Oklahoma). Long horizontal lines indicate cycle boundaries. m/s = lime-mudstone/shale, w (or wkst) = wackstone, p (or pkst) = packstone, g = grainstone.

Possible sources of continental weathering flux to the Anadarko Basin are the Transcontinental Arch to the north and northwest of the study locality and uplifts to the north and northeast due to the Caledonide Orogeny (Avalonia, Baltica, Meguma, Malverns, Cadomia, and Alexander Terranes) (Figure 1) (Nance and Murphy, 1996; Murphy, 2000; 2007; Baarli et al., 2003; Cocks and Torsvik 2011). Detrital zircons and Upper Silurian sedimentary rocks sourced from terranes accreted during the Caledonide

and Acadian Orogenies document variable Nd isotopic ratios (ε_{Nd}) and Nd model ages (τ_{DM}) (Figure 9; ε_{Nd} at t=410 Ma:~-12.0 to +7.0, τ_{DM}: ~0.9 to 2.0 Ga) (Clarke and Halliday, 1985; Gleason et al., 1985; Andre et al., 1986; Thorogood et al., 1990; Clarke et al., 1992; Pimental and Fuck, 1992; Nance and Murphy, 1996; Murphy et al., 1999; 2000; 2008; Murphy and Nance, 2002; Tull, 2002; Linnemann et al., 2012). ε_{Nd} (t=410 Ma) for the Canadian Shield and Transcontinental Arch ranges from -25 to -8 (Miller et al., 1986).

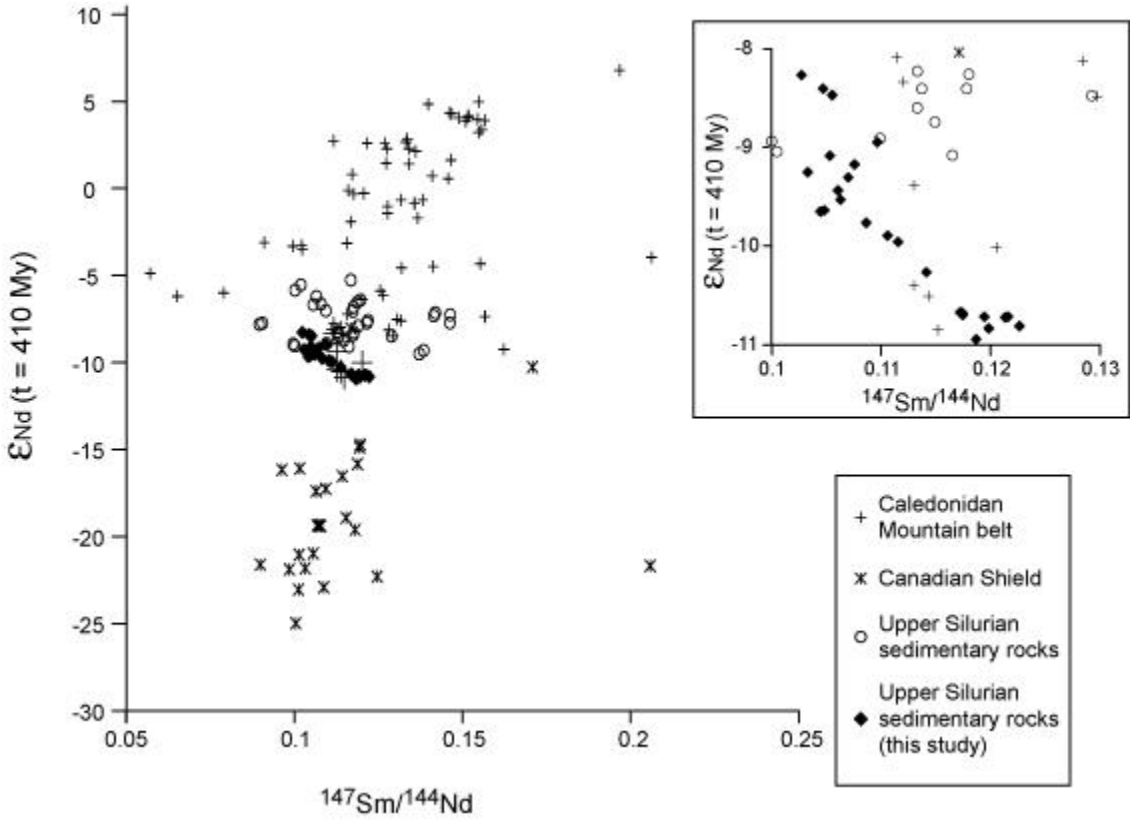

Figure 9. ε_{Nd} vs. $^{147}Sm/^{144}Nd$ of possible sources of continental weathering flux compared to other Upper Silurian sedimentary rocks and results from this study. Possible reservoirs and isotopic data include the Caledonian Mountain belt, which includes the Avalonian Terrane (Murphy and MacDonald, 1993; Murphy et al., 1996; 1999; 2000; 2008) and the Meguma Terrane (Clarke and Halliday, 1985; Clarke et al., 1993), the Canadian Shield and Transcontinental Arch (Canadian Shield: Miller et al., 1986). Upper Silurian sedimentary rocks shown for comparison from Thorogood (1990) and Gleason et al. (1995). Inset shows the same comparison, centered on the results from this study.

Upper Devonian

Evidence for Late Devonian greenhouse climates is based on comparable characteristics as that for the Late Silurian. Similar to Upper Silurian deposits, the Upper Devonian greenhouse interval records large, positive $\delta^{13}C$ excursions (e.g. Joachimski and Buggisch, 1993; Joachimski et al., 2002; Saltzman, 2005; van Geldern et al., 2006), My-scale $\delta^{18}O$ fluctuations (Joachmiski et al., 2009), and common orbital-scale upward-shallowing cycles (LaMaskin and Elrick, 1997; Gong et al., 2001; Yiming et al., 2001; Chen and Tucker, 2003; Ma et al., 2008; Zamanzadeh 2009; Whalen and Day, 2010).

The Late Devonian marks northward movement of Gondwana and initiation of Rheic ocean closure, ultimately ending in Pangean formation. Continuing continental collision from the Acadian Orogeny generated arc magmatism along the northeastern edge of Laurussia (Murphy et al., 1999). The Devonian also marks a shift from passive to active margin tectonics along the western edge of Laurussia, demonstrated by ophiolites, island arc rocks (Brouxel et al., 1987; Brouxel and LaPierre, 1988; Rouer et al., 1989; Dickinson, 2000; Nokleberg et al., 2000; Nelson and Colpron, 2007; Colpron and Nelson, 2009) and overthrust assemblages from the Romanzof (Late Silurian-Middle Devonian), and Antler and Ellesmerian (Late Devonian-Carboniferous) Orogenies (Embry, 1991; Trettin, 1991; Dickinson, 2000; Dickinson, 2009). Much of Laurussia's interior was covered by an epeiric sea after a major transgression in the Middle Devonian (Taghanic Onlap; Johnson, 1970), broken by small exposures of the Transcontinental Arch (Boucot et al., 2008).

Sampled Upper Devonian (late Givetian-Frasnian) cycles of the Guilmette and Devil's Gate Formation were deposited along a westward-deepening carbonate ramp which extended from Canada to Mexico. Central Nevada was positioned 10-20°S of the

paleo-equator during Late Devonian time (Torsvik and Cocks, 2004). The Devil's Gate Formation and coeval Guilmette Formation are underlain by the Bay State Dolomite (Givetian) and overlain by the Pilot Shale (Fammenian) (Figure 3). Of the many cycles observed at Devil's Gate and Gap Mountain, eight sampled subtidal cycles are characterized by thin, interbedded limestone and shale (rhythmites) or thin-bedded skeletal mudstone-wackestone (below storm wave base) overlain by medium- to thick-bedded skeletal mudstone-packstone, some of which contain in-growth-position Amphipora-type and/or lenticular stromatoporoids (near fair-weather wave base likely within photic zone). Half of the cycles record some initial deepening, followed by shallowing-upward facies trends (Figure 10).

Age control is based on conodont biostratigraphy, with samples coming from the *hassi* conodont Zone (e.g. Sandberg and Ziegler, 1996; Morrow and Sandberg, 2003). Coeval Upper Devonian cycles east of the study area record ~30-165 ky durations (LaMaskin and Elrick, 1997) and in other localities record ~20 ky durations (Chen and Tucker, 2003).

Possible sources of continental weathering flux (calculated at t=380 Ma) are immature ophiolites (ε_{Nd} = +3 to +8: Brouxel et al., 1987; Brouxel and LaPierre, 1988) and more mature arc volcanic (ε_{Nd} = -3 to -9: Rouer and LaPierre, 1989; Rouer et al., 1989) to the west, Grenville-aged crust from the Canadian Shield and Appalachian-Caledonian mobile belt to the north (ε_{Nd} = -27 to -8; Patchett et al., 1999; Dickinson, 2000), or the exotic Arctic Chukotka and Alexander terranes (ε_{Nd} = -8 to -0.5; Samson et al., 1989; Natal'in et al., 1999; Amato et al., 2009) to the northeast (Figure 11).

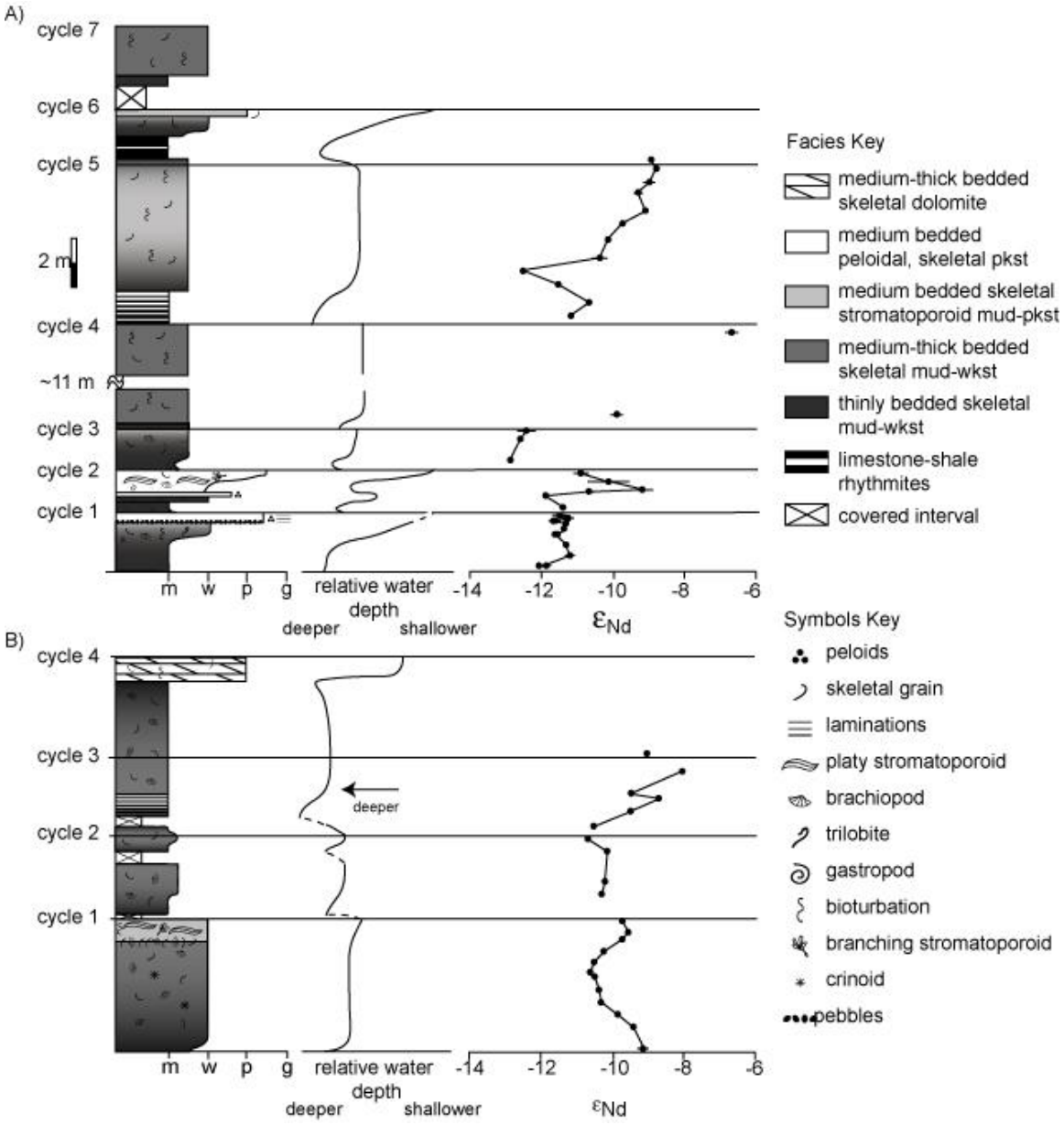

Figure 10. Cyclostratigraphy with interpreted changes in water depth based on facies changes and associated ε_{Nd} trends. A) Upper Devonian (Frasnian; hassi conodont Zone) cycles from the Devil's Gate Formation, central Nevada (Devil's Gate Pass, ~10 km northwest of Eureka, Nevada). B) Upper Devonian (Givetian-Frasnian; norrisi conodont Zone) cycles from the Guilmette Formation, southeastern Nevada (Gap Mountain, ~150 km southeast of Eureka, Nevada). Long horizontal lines indicate cycle boundaries. m/s = lime-mudstone/shale, w = wackstone, p = packstone, g = grainstone

Vascular land plant evolution

Fossil evidence of tetrads demonstrates that the emergence of primitive vascular land plants was established by the Middle Ordovician (Strother et al., 1996). The first

vascular plant, *Cooksonia*, appeared by the Middle Silurian, having a distinctive rigid body (due to development of lignin and cellulose), a vascular system (with vesicles and pathways for transporting water and nutrients through the body), and cellulose (used for preventing desiccation and blocking UV radiation) (Gerrieme et al., 2001). Yet, these early vascular land plants were rootless and spore-bearing, requiring water for reproduction. Between the Late Silurian and Late Devonian, land plants developed roots, leaves, secondary growths, and seeds (Sanderson et al., 2004). The production of seeds allowed plants to move inland and upland; invading land through streams, rivers, and lakes, then moist environments, and finally to hinterland and harsher regions (Yaalon, 1990; Park and Gierlowski-Kordesch, 2007).

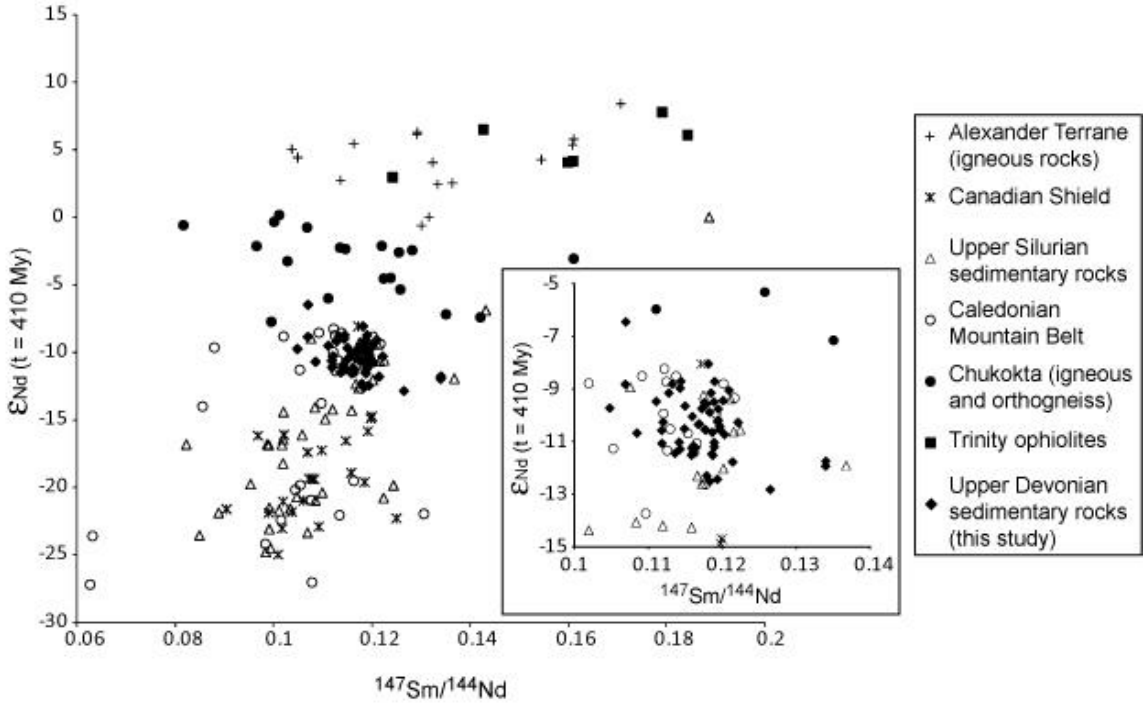

Figure 11. ε_{Nd} vs. $^{147}Sm/^{144}Nd$ of possible sources of continental weathering flux compared to other Upper Devonian sedimentary rocks from the Cordilleran miogeocline and results from this study. Possible reservoirs and isotopic data include the Caledonian Mountain Belt (Franklinian Mobile Belt; Patchett et al., 1999), the Canadian Shield (Miller et al., 1986), and western North American volcanics from the Trinity ophiolite (Brouxel et al., 1988; Brouxel and LaPierre, 1988), the Alexander Terrane (Samson et al., 1989), or the Arctic-Chukokta terrane (Natal'in et al., 1989; Amato et al., 2009). Data for the Cordilleran miogeocline from Boghossian et al.

(1996), Doughty and Chamberlain (1996), Garzione et al. (1997), and Patchett and Gehrels (1998). Inset shows the same comparison, centered on the results from this study.

Evolution and habitat diversification of vascular land plants had a profound effect on continental weathering. Chemical weathering by plants is due to four major processes: secretions of oxalic acid from roots, organic acids secreted by mycorrhyzal symbionts, bacterial decay of plant litter, and production of carbonic acid from the respiration of CO_2 by plant roots (Berner, 1992; Drever, 1994; Algeo et al., 1998). Berner (1992) suggests that the production of carbonic acid by root respiration is the most important in terms of continental weathering and the long-term carbon cycle. Therefore, the development of large root systems increased chemical weathering rates due to greater acid production from CO2-pumping into soils (Retallack, 1992) and a greater contact area of rootlets with soils (Fogel, 1985). The evolution of land plants resulted in rapid and dramatic drawdown of pCO_2 from the Silurian-Carboniferous, causing a decrease in average global temperature, increasing atmospheric O_2, and contributed to episodic anoxia in ocean bottom-waters (Berner, 1992; Cannfield, 1994; Algeo et al., 1995; 1998; Berner,1998; Edwards and Scott, 1998; Malkowski and Racki, 2009).

Previous Work

Marine apatite collected from cycles sampled in this study record two intra-cycle $\delta^{18}O$ trends (Theiling and Elrick, in prep., Chapter 1). The first trend illustrates a progressive increase in $\delta^{18}O$ coincident with facies-shallowing, similar in magnitude (1.3-3.1‰) to $\delta^{18}O$ trends observed in icehouse cycles generated by glacio-eustasy. Theiling and Elrick (in prep., Chapter 1) describe this result as an asymmetric $\delta^{18}O$ trend within an asymmetric cycle. The second trend observed illustrates initially decreasing, then increasing $\delta^{18}O$ values with <0.5 ‰ total magnitude of change, described as a

symmetric trend within an asymmetric cycle. They conclude that both isotopic trends support the hypothesis that these Late Silurian and Late Devonian greenhouse cycles developed in response to glacio-eustasy, but that recorded $\delta^{18}O$ are produced by the combination of changes in ice-volume, sea surface temperature, and changes in evaporation rate over orbital (glacial-interglacial) timescales.

Theiling and Elrick (in prep., Chapter 1) suggest that the interplay between sedimentation rate, subsidence and eustasy (Jervey, 1988) may cause only a portion of the total glacial to interglacial transition to be recorded. In typical, asymmetrical icehouse cycles with asymmetrical, increasing upward $\delta^{18}O$, sedimentation rate outpaces accommodation gains as a result of lowering sea-level from glacial growth. However, sedimentation rate that outpaces accommodation gains during peak interglacial conditions could generate low $\delta^{18}O$ in shallow-water facies (Figure 7; Jervey, 1988). Applying this model, Theiling and Elrick (in prep.) suggest that symmetric $\delta^{18}O$ trends within asymmetric cycles chronicle a more complete record of the glacial-interglacial climate transition, where decreasing and low $\delta^{18}O$ values represent the transition into maximum interglacial intervals and $\delta^{18}O$ increases record the transition into full glacial intervals (Figures 2, 5, and 7). In contrast, asymmetric cycles with asymmetric (increasing upward) $\delta^{18}O$ trends record only the interglacial to glacial portion of the climatic transition.

Methodology

REE systems such as Sm-Nd are ideal for studies of continental weathering flux in marine successions because the seawater REE budget is dominated by continental input (Goldstein and Jacobsen, 1988). Due to the short oceanic residence time of Nd ($<10^2$ yr),

Nd-isotopic ratios will be incorporated into marine sedimentary deposits before homogenization by oceanic mixing (oceanic mixing time ~10^3 yrs). In addition, REE are immobile (insoluble) and therefore, relatively unsusceptible to diagenesis (McLennan, 1989; Banner, 2004). The slightly larger ionic radius of Nd over Sm (lanthanide contraction) makes Nd 'more incompatible,' resulting in preferential partitioning of Nd into the crust during mantle melting and differentiation. As a result, Sm/Nd for the continental crust is ~40% lower than the depleted mantle and imparts significantly different isotopic ratios for each reservoir.

The decay of ^{147}Sm to ^{143}Nd results in emission of an alpha particle ($t_{1/2}$ = 106 Ga). Measurements of $^{143}Nd/^{144}Nd$ are typically expressed in comparison to the bulk earth $^{143}Nd/^{144}Nd$ (chondritic undifferentiated reservoir (CHUR)) as ε_{Nd}, where ε_{Nd} = $(^{143}Nd/^{144}Nd_{sample}/^{143}Nd/^{144}Nd_{CHUR}$ -1)*10,000. Due to preferential partitioning of Nd versus Sm in the continental crust, continental crust is typified by more unradiogenic ε_{Nd} (-20 for crust with a mean τ_{DM} of 2 Ga; Goldstein and Jacobsen, 1987) compared to more radiogenic mid-ocean ridge basalts (MORB) (> +8; Shirey, 1991). τ_{DM} represents the weighted average of the sample's crustal residence time, which can include many compositional and aged sources. Therefore, Nd isotopes can be utilized for regional-scale continental weathering flux studies to evaluate orbital- and suborbital-scale climate changes across varying climate zones/belts. ε_{Nd} in marine deposits can serve as a proxy for changes in the regional continental weathering flux, and can be used to track paleo-ocean circulation (e.g. Martin and Macdougall, 1995; Reynolds et al., 1999; Thomas, 2004; Piotrowski et al., 2005; Puceat et al., 2005; Scher and Martin, 2006; Via and

Thomas, 2006; MacLeod et al., 2008) and emergence/flooding of continental landmass (Fanton et al., 2002; Theiling et al., 2012).

These previous utilizations of Nd isotopes make several important assumptions: 1) rare earth elements (REE) such as Sm and Nd are immediately scavenged by particulates; the Sm/Nd ratio was recorded during or very soon after sedimentary deposition, 2) isotopic evolution of Sm and Nd is linear, 3) no isotopic exchange occurred after deposition, 4) Sm/Nd record the weighted average of all sources of REE (Thorogood, 1990), and most importantly, 5) fluctuations in Nd isotopic ratios are the result of a simple binary mixing line between a source of continental weathering flux (low Sm/Nd) and a relatively homogenous (higher Sm/Nd) local ocean/epeiric sea value. As a result, increases in continental weathering flux or changes in weathering source generate changes in Sm/Nd. Therefore, the Sm-Nd system is best utilized on sea floor ferromanganese crusts and/or nodules (Piotrowski et al., 2004; 2005) or on passive margin platform marine deposits because these environments are distant enough from singular sources of weathering material that the recorded marine Sm and Nd isotopic ratios will reflect a weighted average of binary mixing.

Neodymium isotopic analyses were performed on whole rock, collected at 0.1-1 m increments using a modified method of Theiling et al. (2012) (Chapter 2). Determination of $^{147}Sm/^{144}Nd$ was accomplished using a spike of known $^{147}Sm/^{150}Nd$. $^{147}Sm/^{144}Nd$ was calculated from measurements of $^{147}Sm/^{152}Nd$. Initial $^{143}Nd/^{144}Nd$ values were calculated using approximated ages of deposition of 410 Ma (Henryhouse-Haragan Formation), 385 Ma (Guilmette Formation), and 380 Ma (Devil's Gate Formation). All analyses were performed on a Thermo Neptune multi-collector inductively coupled plasma mass

spectrometer (MC-ICPMS) at the University of New Mexico Radiogenic Isotope Laboratory. The La Jolla Nd isotopic standard was run with each batch, obtaining a mean $^{143}Nd/^{144}Nd$ of 0.511825 ± 4e-5 (2σ), which is within the accepted range of values for the standard (Pier et al., 1989). An internal REE standard spiked with $^{147}Sm/^{150}Nd$ was run with each batch to check Sm isotope measurement accuracy, obtaining a mean value of 0.575496 ± 9e-5 (2σ), which is within the accepted range of values for this standard. Error is reported on initial ε_{Nd} (t = estimated age of deposition) for each sample, calculated by combining the error on replicate analyses of $^{143}Nd/^{144}Nd$ and $^{147}Sm/^{152}Nd$. ε_{Nd} error ranges between 0.04 and 0.49 ε-units and averages 0.10 ε-units (2σ) (Table 3, Figure 8, 10). Error bars of less than 0.30 ε-units are smaller than data points and are therefore not shown in Figures 8 and 10.

Results

Upper Silurian

Arbuckle Mountains

Sm and Nd isotopic results for Upper Silurian cycles are presented in Table 3 and Figure 8. ε_{Nd} (t=410 My) over the entire sampled ARB section range from -8.4 to -10.9. Trends and offsets of ε_{Nd} within each sampled cycle vary. ε_{Nd} trends of cycle 1 show a slight shift to higher values in the middle of the cycle.. Nd values in cycle 2 are initially low, then increase into the cycle cap. ε_{Nd} from cycle 3 shows slight increases and decreases with a shift to lower values at the cycle cap. Cycle 4 has limited samples but shows a shift to lower values into the mid cycle. is initially high and decreases by 0.7 ε-units. Cycle 5 records a symmetric shift from high to low then back to high values in the cycle cap.

distance above stratigraphic base (m)	$^{143}Nd/^{144}Nd$	apparent ε_{Nd}	$^{147}Sm/^{144}Nd$	$^{143}Nd/^{144}Nd$ initial	ε_{Nd} (t)	$f_{Sm/Nd}$
Upper Silurian (t = 410 My)						
Arbuckle Mountains						
0.6	0.511887	-14.7	0.1213095	0.5115610	-10.7	-0.383
0.6 (2)	0.511888	-14.6	0.1215794	0.5115615	-10.7	-0.382
0.9	0.511886	-14.7	0.1226119	0.5115566	-10.8	-0.377
1.1	0.511882	-14.7	0.1194111	0.5115615	-10.7	-0.393
1.4	0.511891	-14.6	0.1141252	0.5115845	-10.3	-0.420
1.9	0.511877	-14.8	0.1198189	0.5115555	-10.8	-0.391
2.1	0.511878	-14.8	0.1171955	0.5115638	-10.7	-0.404
2.5	0.511868	-15.0	0.1186684	0.5115498	-10.9	-0.397
3.3	0.511878	-14.8	0.1174402	0.5115625	-10.7	-0.403
3.6	0.511879	-14.8	0.1174020	0.5115636	-10.7	-0.403
4.0	0.511921	-14.0	0.1069953	0.5116337	-9.3	-0.456
4.3	0.511902	-14.4	0.1086354	0.5116102	-9.8	-0.448
4.9	0.511912	-14.2	0.1060618	0.5116270	-9.4	-0.461
5.4	0.511908	-14.2	0.1062867	0.5116222	-9.5	-0.460
6.0	0.511900	-14.4	0.1105870	0.5116035	-9.9	-0.438
6.4	0.511898	-14.4	0.1048205	0.5116166	-9.6	-0.467
7.0	0.511928	-13.9	0.1053173	0.5116450	-9.1	-0.465
7.2	0.511900	-14.4	0.1115466	0.5116003	-10.0	-0.433
7.7	0.511960	-13.2	0.1055301	0.5116764	-8.5	-0.463
8.3	0.511929	-13.8	0.1075625	0.5116404	-9.2	-0.453
9.4	0.511963	-13.2	0.1027315	0.5116868	-8.3	-0.478
9.9	0.511914	-14.1	0.1033040	0.5116365	-9.2	-0.475
10.3	0.511897	-14.5	0.1044664	0.5116160	-9.6	-0.469
10.7	0.511961	-13.2	0.1047075	0.5116797	-8.4	-0.468
11.3	0.511946	-13.5	0.1096511	0.5116520	-8.9	-0.443
Upper Devonian (t = 385 My)						
Gap Mountain						
0.0	0.511972	-13.0	0.1184101	0.5116738	-9.1	-0.398
1.0	0.511962	-13.2	0.1200381	0.5116591	-9.4	-0.390
1.5	0.511934	-13.7	0.1182175	0.5116364	-9.9	-0.399
2.0	0.511907	-14.3	0.1167249	0.5116128	-10.3	-0.407
2.5	0.511911	-14.2	0.1196080	0.5116091	-10.4	-0.392
3.0	0.511905	-14.3	0.1196111	0.5116033	-10.5	-0.392
3.2	0.511896	-14.5	0.1186014	0.5115967	-10.7	-0.397
3.6	0.511899	-14.4	0.1176392	0.5116024	-10.5	-0.402
4.0	0.511924	-13.9	0.1220882	0.5116164	-10.3	-0.379
4.5	0.511944	-13.5	0.1194033	0.5116427	-9.8	-0.393
4.8	0.511949	-13.4	0.1177662	0.5116522	-9.6	-0.401
5.3	0.511939	-13.6	0.1171866	0.5116432	-9.7	-0.404
6.3	0.511908	-14.2	0.1168518	0.5116137	-10.3	-0.406
6.8	0.511919	-14.0	0.1193175	0.5116181	-10.2	-0.393
8.0	0.511922	-14.0	0.1194069	0.5116213	-10.2	-0.393
8.5	0.511896	-14.5	0.1202465	0.5115929	-10.7	-0.389
9.0	0.511899	-14.4	0.1176980	0.5116019	-10.6	-0.402
9.6	0.511952	-13.4	0.1175606	0.5116552	-9.5	-0.402
10.1	0.511996	-12.5	0.1189012	0.5116962	-8.7	-0.396
10.3	0.511956	-13.3	0.1188297	0.5116567	-9.5	-0.396
11.2	0.512028	-11.9	0.1180707	0.5117308	-8.0	-0.400
11.9	0.511983	-12.8	0.1208766	0.5116787	-9.1	-0.385

Devil's Gate						
0.2	0.511869	-15.0	0.1339258	0.5115315	-11.9	-0.319
0.2 (2)	0.511879	-14.8	0.1339559	0.5115410	-11.7	-0.319
0.6	0.511877	-14.8	0.1188483	0.5115772	-11.0	-0.396
1.0	0.511868	-15.0	0.1188752	0.5115687	-11.2	-0.396
1.4	0.511849	-15.4	0.1159820	0.5115567	-11.4	-0.410
1.4 (2)	0.511844	-15.5	0.1157904	0.5115524	-11.5	-0.411
1.6	0.511858	-15.2	0.1158460	0.5115661	-11.3	-0.411
1.8	0.511863	-15.1	0.1160228	0.5115705	-11.2	-0.410
1.9	0.511851	-15.3	0.1186661	0.5115522	-11.5	-0.397
1.9	0.511854	-15.3	0.1185275	0.5115550	-11.5	-0.397
2.0	0.511865	-15.1	0.1141222	0.5115777	-11.0	-0.420
2.2	0.511852	-15.3	0.1142415	0.5115645	-11.3	-0.419
2.4	0.511860	-15.2	0.1163434	0.5115669	-11.2	-0.409
2.85	0.511846	-15.5	0.1213554	0.5115396	-11.8	-0.383
3.0	0.511894	-14.5	0.1148268	0.5116040	-10.5	-0.416
3.4	0.511937	-13.7	0.1110190	0.5116573	-9.5	-0.436
3.8	0.511869	-15.0	0.1084295	0.5115956	-10.7	-0.449
4.2	0.511804	-16.3	0.1264433	0.5114854	-12.8	-0.357
5.0	0.511800	-16.4	0.1182576	0.5115014	-12.5	-0.399
5.5	0.511810	-16.2	0.1178462	0.5115126	-12.3	-0.401
5.9	0.511909	-14.2	0.1047253	0.5116446	-9.7	-0.468
20.7	0.512082	-10.8	0.1068851	0.5118126	-6.4	-0.457
21.3	0.511857	-15.2	0.1117903	0.5115754	-11.1	-0.432
21.8	0.511882	-14.7	0.1117629	0.5116007	-10.6	-0.432
22.5	0.511843	-15.5	0.1135589	0.5115564	-11.4	-0.423
23.0	0.511807	-16.2	0.1192906	0.5115058	-12.4	-0.394
23.5	0.511900	-14.4	0.1119519	0.5116173	-10.3	-0.431
24.2	0.511920	-14.0	0.1158886	0.5116280	-10.0	-0.411
24.8	0.511938	-13.6	0.1149264	0.5116487	-9.6	-0.416
25.3	0.511971	-13.0	0.1142433	0.5116834	-9.0	-0.419
26.0	0.511958	-13.3	0.1127109	0.5116737	-9.2	-0.427
26.4	0.511977	-12.9	0.1131970	0.5116914	-8.8	-0.425
26.9	0.511985	-12.7	0.1143370	0.5116967	-8.7	-0.419
27.2	0.511960	-13.2	0.1068472	0.5116906	-8.8	-0.457

Table 3. Measured $^{143}Nd/^{144}Nd$, apparent ε_{Nd} (value at present), measured $^{147}Sm/^{144}Nd$, and $^{143}Nd/^{144}Nd$, ε_{Nd} (t), and $f_{Sm/Nd}$ where t = estimated time of deposition.

In total, the Upper Silurian samples exhibit an up-section increase in ε_{Nd} of 2.7 ε-units and an up-section decrease in $^{147}Sm/^{144}Nd$. $^{147}Sm/^{144}Nd$ versus ε_{Nd} (t = 410 My) are shown in Figure 8 and are compared to terranes and crustal material accreted to Laurentia during the Caledonide and Acadian Orogenies. Calculated τ_{DM} for Upper Silurian samples is 1.6-2.1 Ga.

Upper Devonian

Gap Mountain

Neodymium isotopic results for Upper Devonian cycles at Gap Mountain (GM) are presented in Table 3 and Figure 10. ε_{Nd} (t=385 My) over the entire sampled GM section ranges from -10.7 to -8.0. Trends and offsets of ε_{Nd} within each sampled cycle vary. ε_{Nd} of cycle 1 records a symmetric trend of initially high, then decreasing values toward mid-cycle, then increases progressively into the cycle cap. Cycle 2 demonstrates essentially stable values with a small shift to lower values in the cycle cap. Cycle 3 shows a large up-cycle increase in ε_{Nd} values.

Devil's Gate

Neodymium isotopic results for Upper Devonian cycles from Devil's Gate (DG) are presented in Table 3 and Figure 10. ε_{Nd} (t=380 My) over the entire sampled DG section ranges from -12.9 to -6.6 and decreases by ~3.2 e-units from the base to the top of the sampled section. Trends and offsets of ε_{Nd} within each sampled cycle vary. Cycle 1 records an initial increase in ε_{Nd} values followed by relatively stable values to the cycle cap. ε_{Nd} from cycle 2 demonstrates an abrupt increase, then decrease in values into the cycle cap. Cycle 3 shows an abrupt decrease to lower values, then a steady increase up-cycle. Although incompletely sampled, cycle 4 cap records an anomalously high ε_{Nd} value of -6.6. Cycle 5 records a relatively symmetric trend of decreasing values followed by increasing and high values in the cycle cap.

Discussion

Provenance

Middle Silurian-Upper Devonian sedimentary rocks from across the United States and Canada record a transition from unradiogenic source rocks (ε_{Nd} = -27 to -15) to a more radiogenic source (ε_{Nd} = -10 to -5) (Figure 12). This transition is observed in the Canadian Cordilleran miogeocline and mid-continental United States during the Silurian (Gleason et al., 1994; 1995; Patchett et al., 1999) and in the western United States Cordilleran miogeocline during the Middle and Upper Devonian (Boghossian et al., 1996; Garzione et al., 1997; Patchett and Gehrels, 1997). ε_{Nd} from all three sampled successions from this study lie between -12 and -8, with the exception of one sample from the Devil's Gate Formation (-6.4; Figure 10), supporting the claim that this source change had occurred by the at least the Pridolian (Oklahoma study area) and Frasnian (Nevada study area) (Figure 12).

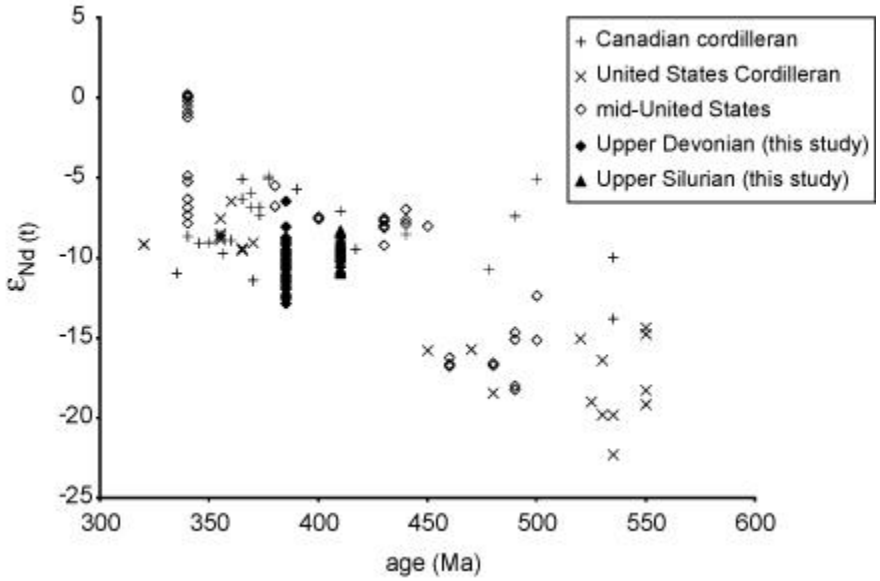

Figure 12. ε_{Nd} vs. age (Ma) for sampled Upper Silurian and Upper Devonian cycles compared to other sedimentary rocks, indicating that the shift from relatively unradiogenic to radiogenic ε_{Nd} had occurred in each of the sampled marine basins by the time of deposition. ε_{Nd} data from the Canadian Cordilleran (Garzione et al.,1997; Patchett and Gehrels,1998), United States Cordilleran (Boghossian et al.,1996), and mid-United States (Gleason et al., 1995).

Accretion, uplift, and weathering of relatively radiogenic crustal material from the Caledonide Orogeny (Figure 9) during the Late Silurian-Late Devonian are the most likely sources of continental weathering flux that generated the observed range in ε_{Nd} (Figures 9 and 11). Two processes may have generated this range: mixing of a radiogenic and unradiogenic source, or introduction of a source with similar isotopic ratios to those observed. The most probable sources of large-scale binary mixing are the strongly unradiogenic Canadian Shield and Transcontinental Arch (ε_{Nd} = -25 to -15; Miller et al., 1986) and strongly radiogenic terranes of the Caledonian-Appalachian mobile belt (ε_{Nd} = -5 to +7; Murphy et al., 1996; 1999; 2000; 2008) (Figure 9). To estimate the contributions of these end-members to sampled Upper Silurian limestones, we utilize the mixing model equations of Langmuir et al. (1978), assuming an average $^{143}Nd/^{144}Nd$ value for radiogenic Caledonide terranes (Murphy et al., 1996; 1999; 2000; 2008) and Archean-aged Canadian Shield and Transcontinental Arch rocks (Miller et al., 1999). Binary mixing between these sources suggests that approximately 45% of all Nd was sourced from strongly radiogenic Caledonide terranes (i.e. Avalonia terrane) and 55% was sourced from the Canadian Shield and/or Transcontinental Arch. Due to the inner-shelf position of the sampled successions, deposition is biased toward highstand through lowstand deposition. As a result, the Transcontinental Arch was likely submerged during much of the recorded intervals, implying that enormous quantities of unradiogenic material would have been sourced from intermittent exposures of the Transcontinental Arch or Canadian Shield. The greater weathering ability of exposed terranes and overlap in Nd values with samples from a mixture of strongly radiogenic and more unradiogenic terranes within the Caledonide mobile belt (Figures 9 and 11)

suggests introduction of continental weathering flux from these far-field accreted and uplifted terranes (e.g. Stallard and Edmond, 1983; Raymo et al., 1988; Berner, 1994).

Eolian and fluvial processes demonstrate transport over remarkable continental distances. Prevailing southwestwardly winds for southern hemisphere subtropical latitudes suggest eolian-derived detritus is a possible component to mid-southern Laurentia during the Late Silurian. However, Late Devonian northwestward prevailing winds for western Laurentia render wind-blown material an unlikely source of Nd for the studied Upper Devonian successions.

Basins ranging from Ordovician-Carboniferous age across Laurentia contain detrital zircons (Dickinson and Gehrels, 2003), sedimentary ε_{Nd}, and paleocurrents (Gleason et al., 1994; 1995; Patchett et al., 1999; Boghossian et al., 1996; Garzione et al., 1997; Patchett and Gehrels, 1997) traceable to the Caledonian-Appalachian orogenic belt, invoking large fluvial systems that traversed the width of Laurentia. The modern Amazon River basin encompasses a similarly large continental area (~2.5-3x10^6 km^2: Revenga et al., 1998), traveling ~3000 km from the Andes Mountains to the Atlantic Ocean. Immature Amazonian Quarternary-aged quartz sands demonstrate transport of continental weathering flux over ~3000 km in a single phase (Johnsson et al., 1988; Potter, 1978), implying single-phase transport for trans-continental paleo-rivers.

Boghossian et al. (1996) and Patchett et al. (1999) suggest a multi-phase transport of Caledonian-Appalachian detrital material across Laurentia, whereby extensive weathering of the Caledonian-Appalachian orogenic belt, beginning in the Ordovician, deposited material in an extensive foreland basin that was later uplifted, eroded, transported further and re-incorporated into younger deposits. Indeed, crystallization

ages, paleocurrent directions, and comparision of observed ε_{Nd} to Caledonian basement ε_{Nd} demonstrate that Siluro-Devonian sedimentary rocks from the Canadian miogeocline were sourced from the Caledonian orogeny via the Franklinian mobile belt of northern Canada, suggesting multi-phase transport of Caledonian weathered material (Patchett et al., 1999). Similarly, Grenville-aged detrital zircons suggest that trans-Laurentian river systems were established by at least the Neoproterozoic and demonstrate a multi-phase process of weathering, deposition, lithification and reworking of detrital material (Ross and Parrish, 1991; Rainbird et al 1992; 1997; Stewart et al., 2001).

Intracycle-scale Nd-isotope trends

Source area changes

If our far-field Caledonian source area interpretations are correct, then this implies that any potential variations in the source material(s) would have been averaged out by the time continental weathering flux reached the studied marine basins, whether transport and deposition was single or multi-phase. Therefore, it is not unreasonable to assume binary mixing would occur between an average Caledonian source and ocean waters and/or the Canadian Shield/Transcontinental Arch over orbital timescales.

Cyclic ε_{Nd} trends due to changes in source material are demonstrated in an Upper Ordovician mixed carbonate-siliciclastic succession (Fanton et al., 2002). In their study, platform emergence due to My-scale sea-level fall exposed low ε_{Nd} Precambrian basement rocks from the Canadian Shield and Transcontinental Arch, generating lower marine ε_{Nd} values in the sampled marine succession. Platform flooding due to My-scale sea-level rise submerged low ε_{Nd} rocks, increasing ε_{Nd} values in the sampled marine succession. This scenario is unlikely in either Upper Silurian or Upper Devonian

sampled successions because observed ε_{Nd} are not low enough to suggest periodic sourcing from the adjacent unradiogenic Transcontinental Arch or Canadian Shield. Likewise, the similar range in ε_{Nd} of our samples with Caledonian source rocks, suggests that observed cycle-scale variation in ε_{Nd} trends are not a result of source area changes, but rather are generated by binary mixing with ocean waters.

Orbital-scale climate changes

If our binary mixing interpretation is correct then we can compare observed Upper Silurian and Upper Devonian greenhouse ε_{Nd} trends to those observed in icehouse cycles of Burton and Vance (2000), Piotrowski et al. (2005), and Theiling et al. (2012). ε_{Nd} trends from previously studied icehouse cycles demonstrate decreasing ε_{Nd} into interglacial intervals and increasing ε_{Nd} into glacial intervals due to increases and decreases, respectively, in continental weathering and/or transport. Theiling et al. (2012) proposed a climate-weathering model for platform marine sedimentary systems in which decreases in ε_{Nd} into mid-cycle deposits (sea-level highstand or interglacials) are generated by increases in continental weathering flux that result from increases in precipitation and/or air temperature. Increases in ε_{Nd} into cycle caps are generated by decreases in continental weathering flux from decreases in precipitation and/or air temperature. Hypothesized fluctuations in precipitation and/or air temperature may manifest as climatically-driven fluctuations in fluvial and/or eolian input to a marine basin. The Theiling et al. (2012) climate-weathering model is shown in comparison to the stratigraphic-eustatic model of Jervey (1988) in Figure 13, which illustrates schematic intra-cycle ε_{Nd} trends produced during wet/warm (interglacial) and dry/cool (glacial) intervals.

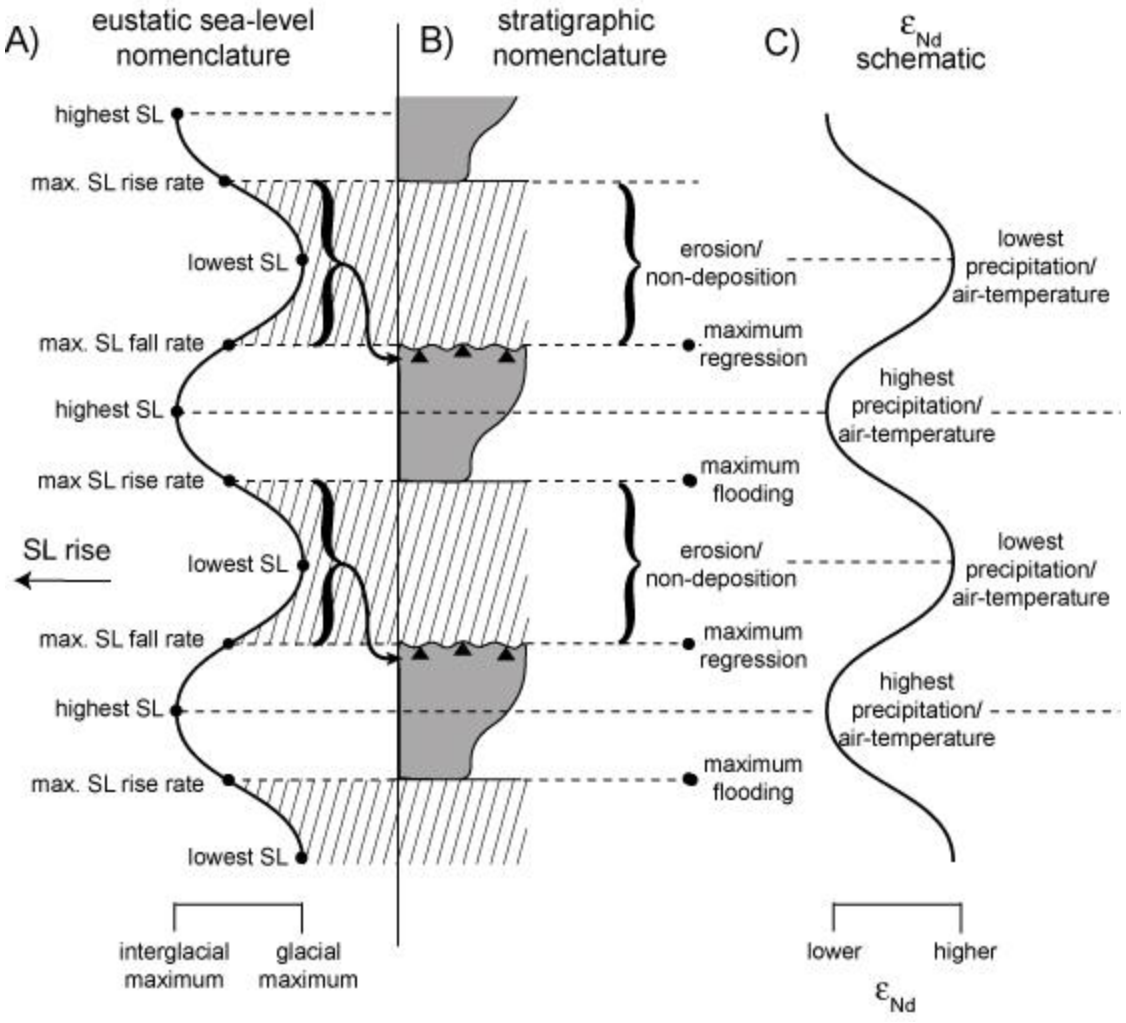

Figure 13. A) Simplified sinusoidal eustatic sea-level (SL) curve with labeled inflection points and maximum glacial-interglacial intervals. B) Stratigraphic nomenclature with schematic asymmetric cycles similar to those observed in sampled Upper Silurian and Upper Devonian cycles with a narrower column representing deeper water facies and a wider column representing shallower water facies. Note that no deposition/erosion occurs during the late eustatic fall, lowstand and early rise (diagonal lines) and a disconformity develops; subaerial exposure features develop at the cycle top during subaerial exposure (black triangles). During a single glacial-interglacial sea-level cycle, deposition during the initial transgression as the glaciers begin to melt is not recorded within the study area due to lack of accommodation space. Once accommodation space is created due to subsidence and rapid (maximum) SL rise rates, deposition occurs and is represented by deeper water deposits at the cycle base. SL continues to rise with additional glacial melting and reaches its highest position at the interglacial maximum (mid-regression). Because SL is rising at a slower rate after the maximum rate of SL rise inflection point (and assuming constant sedimentation rate), sediments above the maximum flooding zone reflect loss of accommodation space. After the interglacial maximum, SL fall rates increase and is represented by the shallowest water deposits. C) Schematic of d18O trend due to changes in ice-volume and sea surface temperatures (SST) over successive glacial-interglacial intervals. D) Schematic of eNd due to changes in precipitation and/or air temperature as a direct result of glacial-interglacial cycles. Modified from Theiling et al. (2012).

Most sampled Upper Silurian cycles demonstrate relatively steady intra-cycle ε_{Nd}, with the exception of cycles 2 and 5 (Figure 8), as opposed to larger variations in ε_{Nd}

observed in sampled Upper Devonian cycles (Figure 10). Such small cycle-scale ε_{Nd} variations in this succession suggest orbital-scale changes in continental weathering flux were not as profound during the Late Silurian in relation to the Late Devonian. Smaller Upper Silurian intra-cycle variations may be generated by a lag between the time of climate fluctuation and subsequent continental weathering, and the time required to transport continental weathering flux from a far-field Caledonide source, which could average out any initial variations in continental weathering flux.

This scenario is in opposition to continental weathering sources of Fanton et al. (2002) and Theiling et al. (2012). In these studies, changes in climate and continental weathering flux were readily apparent because flux was sourced from uplifts <100 km away from sampled marine basins. Furthermore, these sampled successions were sometimes subaerially exposed, suggesting these localities were sometimes directly fed by local fluvial waters from nearby uplifts. While the proposed lag time between weathering and deposition is likely for such far-field transport to the sampled Upper Silurian basin, larger intra-cycle variations observed in similarly-sourced Upper Devonian cycles suggest that averaging out of far-field flux did not generate small Upper Silurian variation.

A relatively uniform ε_{Nd} trend may also be generated by a relatively constant warm and/or wet Late Silurian subtropical climate. Modeling of, and proxy data from greenhouse intervals suggest that increased greenhouse temperatures intensify the hydrologic cycle (Pagani et al., 2006; Clementz and Sewall, 2011; Berra, 2012), leading to overall increased rainfall patterns. An intensified greenhouse hydrologic cycle implies more intense and relatively constant continental weathering and flux. However, this

scenario is inadequate because Upper Devonian ε_{Nd} shows greater intra-cycle variation, implying that fluctuations in continental weathering flux may occur during greenhouse intervals.

Perhaps the most likely scenario is that the lack of inland and upland vascular land plants during the Late Silurian contributed to relatively uniform weathering. Vascular plants prior to the Middle Devonian were rootless, contributing to chemical breakdown of rock/proto-soil due to production of oxalic, humic, and carbonic acids, but providing little stabilization of the land-surface (Algeo et al., 1998). Therefore, before upland and inland land plant colonization, continental weathering was primarily a product of erosion and mass-wasting. As plants developed large root systems, chemical weathering increased due to both greater acid production from pumping of CO_2 into soil (Retallack, 1992) and a greater contact area of rootlets with soils (Fogel, 1985).

In the modern record, we observe that fluctuations in climate have a profound effect on plants. During wetter and/or warmer intervals, roots penetrate deeper and generate increased chemical weathering, while plant roots are smaller during drier and/or cooler intervals, generating decreased weathering. As a result, changes in continental weathering rates as a result of fluctuations in climate may not have been as pronounced before the evolution of land plants with large root systems and colonization of upland and inland land areas (Middle-Late Devonian). Instead, erosion due to tectonic uplift (Stallard and Edmond, 1983) may have dominated continental weathering flux before the Middle-Late Devonian.

It is also possible that minimal plant colonization of land during the Late Silurian contributed to a relatively suppressed greenhouse hydrologic cycle. Increased

atmospheric instability typical of warmer climates is enhanced by evapotranspiration, whereby water is transferred directly from a plant to the atmosphere. Therefore, the effect of plants on the hydrologic cycle is to promote recirculation of water in the atmosphere, increasing cloud-cover and precipitation (Algeo et al., 1998; Shuckle and Mintz, 1982). Without widespread distribution of land plants, the Late Silurian hydrologic cycle may have been less intense than the Late Devonian.

In opposition to the relatively steady record of continental weathering flux observed in these Upper Silurian cycles, sampled upper Devonian cycles record greater variability in ε_{Nd}. 5 of 7 cycles record high ε_{Nd} values (low continental weathering flux) during falling/lowstand sea-level and low ε_{Nd} values (high continental weathering flux) during sea-level highstands. 2 of 7 cycles show symmetric ε_{Nd} trends within asymmetric cycles, one of which demonstrates an in-phase symmetric $\delta^{18}O$ trend (Theiling and Elrick, in prep., Chapter 1). Similar to symmetric $\delta^{18}O$ intra-cycle trends, these symmetric ε_{Nd} trends argue that these particular cycles preserve a more complete transition from glacial-interglacial-glacial stages (Figure 13). Both trends and these magnitudes are similar to Pennsylvanian and Pleistocene studies, suggesting that increases in precipitation and/or air temperature generate increases in continental weathering flux and decreases in precipitation and/or air temperature generate decreases in continental weathering flux.

We suggest that these two trends are generated as a result of the interplay between sedimentation rate, subsidence and eustasy, illustrated by combining the sedimentation-eustasy model of Jervey (1988) and the ε_{Nd}-weathering-climate model of Theiling et al. (2012). Symmetric ε_{Nd} trends will be recorded in asymmetric cycles under the following conditions: if sedimentation rate outpaces accommodation gains during peak cool and/or

dry conditions, lowest ε_{Nd} will be recorded when sea-level is highest, between maximum flooding and mid-regression and high ε_{Nd} will be recorded in shallow-water facies during maximum sea-level fall (Figure 13). However, an asymmetric ε_{Nd} trend may be recorded in an asymmetric cycle if accommodation gains outpaced sedimentation rate during the transition from peak glacial to peak interglacial (highest sea-level position). After the maximum interglacial (highest sea-level), sedimentation rate begins to outpace accommodation gains, recording only the top half of the idealized ε_{Nd} trend (Figure 13).

Increased variation in continental weathering flux during the Late Devonian is likely due to the more widespread distribution and diversification of land plants, increasing chemical weathering rates (Knoll and James, 1987; Johnson, 1993; Drever, 1994) and precipitation from evapotranspiration, leading to dramatic drawdown in pCO_2 and cooling global climate (Shukla and Mintz, 1982; Berner, 1992; 1998; Edwards and Scott, 1998; Algeo et al., 1998; Malkowski and Racki, 2009). Indeed, Algeo et al. (1995) describe a critical shift in continental weathering flux and oceanic nutrient influx occurring in the Devonian as a result of inland and upland habitation of vascular land plants and increased root penetration. Late Devonian climate changes are expected given the appearance of well-documented ice sheets in South America within a few million years (e.g., Veevers and Powell, 1987; Frakes and Francis, 1988; Frakes et al., 1992; Ziegler et al., 1997; Hyde et al., 1999; Isbell et al., 2003; Blakey, 2008; Fielding et al., 2008; Buggisch et al., 2011; Isbell et al., 2012).

Conclusions

1) ε_{Nd} and $^{147}Sm/^{144}Nd$ values for both Silurian and Devonian successions suggest far-field Caledonide source area, which implies trans-Laurentian fluvial systems transported weathered material.

2) Silurian intra-cycle ε_{Nd} trends are relatively steady across individual orbital-scale cycles, implying relatively constant continental weathering flux. Constant flux may be related to a) a lag between the time of weathering and the time of deposition, effectively averaging out initial variations, b) relatively constant continental weathering flux due to warm and/or wet sub-tropical climate, or c) lower chemical weathering rates and precipitation due to the absence of widespread upland and inland vascular land plants.

3) Devonian record increased intra-cycle ε_{Nd} variability similar in appearance and magnitude to icehouse ε_{Nd} trends, with higher continental weathering flux (lower ε_{Nd} values) during sea-level highstand (warmer/wetter stages) and lower continental weathering flux (higher ε_{Nd} values) during falling sea-levels (cooler/drier stages). Increased ε_{Nd} variability may have resulted from evolution and inland and upland colonization of land plants, increasing chemical weathering rates due to evolution of large root systems and increasing precipitation as a result of evapotranspiration.

SUPPLEMENTAL A

OXYGEN ISOTOPE DATA AND INTERPRETATIONS FROM UPPER SILURIAN APATITIC BRACHIOPODS AND CONODONT PEARLS COLLECTED FROM THE ARBUCKLE MOUNTAINS, OKLAHOMA

Introduction

Oxygen isotopic data from Theiling and Elrick (in prep., Chapter 1) suggests that sea-level fluctuations observed from facies changes of Upper Silurian and Upper Devonian marine greenhouse successions were glacially-driven, implying that greenhouse intervals can support both very warm sea surface temperatures (SST) and polar glacial ice. Due to the difficulty in recovering sufficient coniform conodonts at each Upper Silurian sampling interval (typically ~100-300 elements), apatitic inarticulate brachiopod fragments and conodont pearls were collected in addition to conodont elements whenever possible. The stronger PO_4 bond in apatite as opposed to the weaker CO_3 bond found in most calcitic and aragonitic brachiopod or whole-rock samples suggests that biogenic apatites are less susceptible to diagenetic recrystallization (Longinelli and Nuti, 1973; Kolodny et al., 1983; Luz et al., 1984; Lécuyer et al., 1996) and that biogenic apatite is precipitated in equilibrium with ambient seawater (Longinelli and Nuti, 1973; Kolodny et al., 1983; Lécuyer et al., 1996). Although some studies have demonstrated offsets in apatitic inarticulate brachiopod versus conodont (Luz et al. 1984; Kastner et al., 1990; Kolodny and Luz, 1991; Wenzel et al., 2000) and fish tooth apatite (Zigate et al., 2010) $\delta^{18}O$ due to partial recrystallization, the similarity of brachiopod to conodont and fish $\delta^{18}O$ imply that apatitic brachiopods may be used to evaluate relative changes in $\delta^{18}O$.

The purpose of this study is to compare $\delta^{18}O$ data from coniform conodont elements of *Belodella* condonts collected from the Upper Silurian (Haragan-Henryhouse Formation) in the Arbuckle Mountains of central Oklahoma (Theiling and Elrick, in prep.; Chapter 1) with coeval conodont pearls and apatitic inarticulate brachiopods to assess whether these brachiopods and pearls generate similar $\delta^{18}O$ trends to coniform conodont elements. The geologic setting, sampling intervals and analytical techniques are described in Theiling and Elrick (in prep.; Chapter 1).

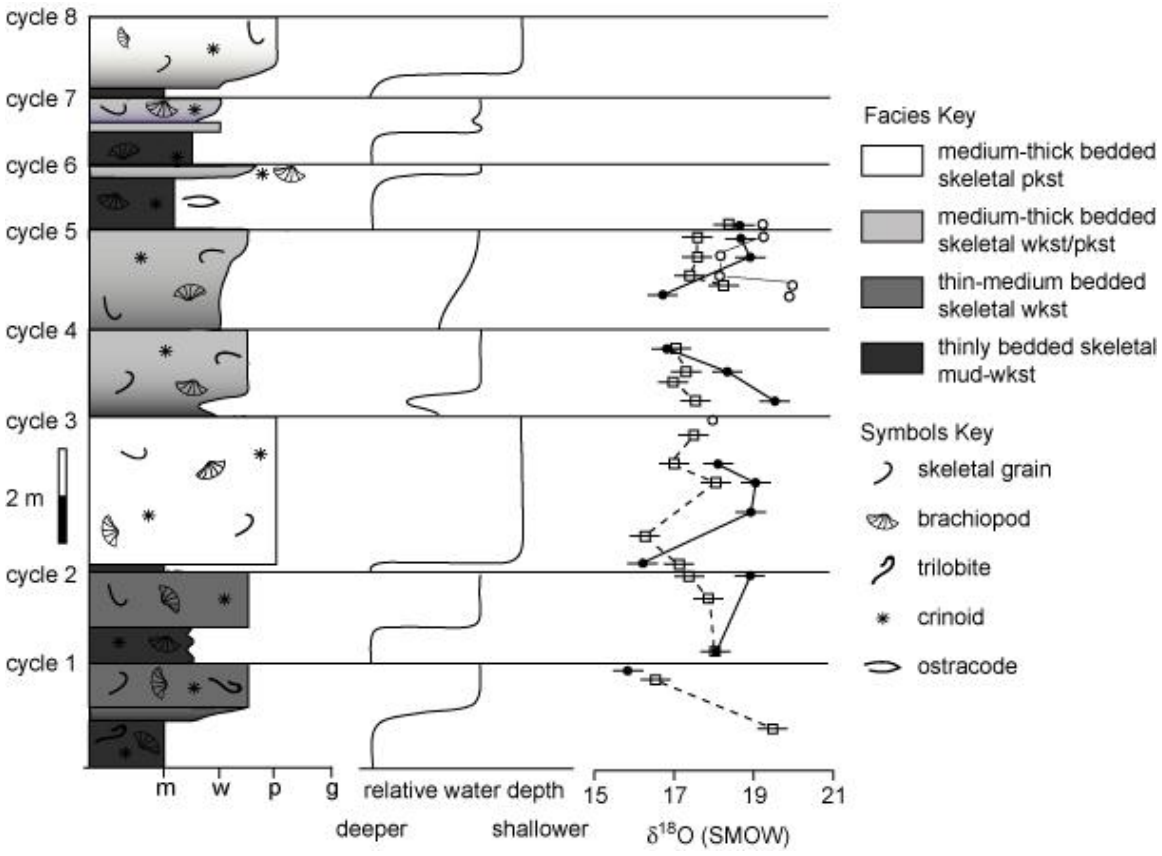

Figure 14. Upper Silurian (Pridolian-Ludlovian) cyclostratigraphy with interpreted changes in water depth based on facies changes and associated $\delta^{18}O$ trends. Sampled section is within the *Oulodus elegans detorta* conodont Zone from the Haragan-Henryhouse Formation of central Oklahoma (~5 km south of Davis, Oklahoma). All $\delta^{18}O$ data points are single analyses and/or averaged from replicate analyses. Coniform conodont $\delta^{18}O$ data (filled circles) from Theiling and Elrick (in prep). $\delta^{18}O$ data symbols: open squares = phosphatic brachiopods, open circles = conodont pearls. Long horizontal lines indicate cycle boundaries. m/s = lime-mudstone/shale, w (or wkst) = wackstone, p (or pkst) = packstone, g = grainstone.

Results

Conodont Pearls

Oxygen isotopic results from conodont pearls are presented in Table 4 and Figure 14. $\delta^{18}O$ over the entire sampled section ranges from 18.1‰ to 20.0‰. Only cycle 5 contained sufficient conodont pearls throughout the cycle to generate a trend; decreasing $\delta^{18}O$ toward mid-cycle, followed by increasing $\delta^{18}O$ into the cycle cap. The total intra-cycle change in $\delta^{18}O$ over this cycle is 1.9‰.

distance from stratigraphic base (m) Conodont pearls	$\delta^{18}O$ (‰) SMOW
7.4	18.4
9.9	19.9
10.1	19.6
10.1	20.4
10.3	17.6
10.3	18.1
10.3	18.3
10.3	18.5
10.7	18.5
10.7	17.7
11.1	18.7
11.1	19.7
11.3	19.4
11.3	18.9
11.3	19.2
11.3	19.3

Table 4. $\delta^{18}O$ from sampled apatitic inarticulate brachiopods and conodont pearls with stratigraphic depth.

Apatitic inarticulate brachiopods	
0.9	19.3
0.9	20.0
0.9	19.1
1.9	16.7
1.9	16.3
2.5	17.5
2.5	16.5
2.5	19.7
2.5	18.5
3.6	17.9
3.6	17.9
4.1	17.3
4.1	17.3
4.1	17.5
4.3	17.2
4.3	17.1
4.3	16.7
4.3	17.6
4.9	17.7
4.9	14.8
6.0	18.8
6.0	17.8
6.0	17.9
6.0	18.3
6.0	17.6
6.4	19.8
6.4	16.8
6.4	17.2
6.4	16.5
6.4	16.8
6.4	18.0
6.4	17.1
6.4	16.5
7.0	16.7
7.0	17.5
7.0	18.3
7.7	17.2
7.7	18.0
7.7	17.4
8.1	17.0
8.3	17.3
8.8	17.0
10.1	18.7
10.1	17.7
10.1	18.4
10.3	17.4
10.7	17.6
10.7	17.6
11.1	17.5
11.1	17.4
11.1	17.8
11.3	18.4

Phosphatic brachiopods

Oxygen isotopic results from phosphatic brachiopods are presented in Table 4 and Figure 14. $\delta^{18}O$ from brachiopods over the entire sampled section ranges from 16.3‰ to 19.5‰. Only two samples contained sufficient brachiopods from cycle 1 to measure $\delta^{18}O$, suggesting decreasing $\delta^{18}O$ up-cycle of 3.0‰. Cycle 2 demonstrates decreasing $\delta^{18}O$ upward with a total intra-cycle change of 0.7‰. Cycle 3 demonstrates a zig-zag pattern; initially decreasing $\delta^{18}O$, followed by an increase toward mid-cycle deposits, then a decrease in $\delta^{18}O$ into cycle cap deposits. The total intra-cycle change for cycle 3 is 1.8‰. Cycle 4 demonstrates a decrease upward with a total intra-cycle change of 0.5‰. Cycle 5 exhibits initially decreasing, then increasing $\delta^{18}O$ with a total intra-cycle change of 0.9‰.

Discussion

Conodont pearls

Only one of the five sampled cycles (cycle 5) contained sufficient conodont pearls to generate an intra-cycle trend, which is similar to brachiopod data but opposes platform conodont data (Figure 14). A trend of decreasing, then increasing $\delta^{18}O$ for analyzed pearls and brachiopods suggests increasing SST and/or decreasing ice-volume into mid-cycle deposits, followed by decreasing SST and/or increasing ice-volume. If the hypothesis proposed by Theiling and Elrick (in prep., Chapter 1) and Chapter 3 is correct, whereby decreasing, then increasing $\delta^{18}O$ is indicative of a more complete record of the transition from glacial-interglacial-glacial, then these brachiopod and pearl data demonstrate a more complete climatic record than coniform conodont data (Figure 7). However, because this result was produced in only one sampled cycle, it is equally or

more plausible that conodont pearl and brachiopod trends from cycle 5 were generated as a result of diagenetic recrystallization.

Apatitic inarticulate brachiopods

Two comparative trends between coniform conodont and apatitic brachiopods emerge from these analyses: in-phase or opposing $\delta^{18}O$. Conodont and brachiopod $\delta^{18}O$ trends are similar and in-phase in cycles 3 and 4, with conodont $\delta^{18}O$ enriched by -0.8‰ to +2.5‰ (+1.4‰ average). This offset is also observed between conodont pearl and brachiopod samples in cycle 5 (although the trends oppose platform conodont $\delta^{18}O$), where pearls are enriched by +0.5‰ to +1.7‰. Similar enrichment of conodont $\delta^{18}O$ versus brachiopod $\delta^{18}O$ is widely observed (Luz et al. 1984; Kastner et al., 1990; Kolodny and Luz, 1991; Lecuyer et al., 1996; Wenzel and Joachimski, 1996; Wenzel et al., 2000; Elrick et al., 2011). Lower $\delta^{18}O$ of coeval apatitic brachiopods may be the result of post-mortem phosphate addition (Lecuyer et al., 1998) from the degradation of chitinous organic layers that alternate with fibrous carbonate-fluorapatite (francolite) (Iijima and Moriwaki, 1990; Williams et al., 1992; Cusack et al., 1997).

Partial recrystallization of apatitic brachiopods is also suggested by higher SST estimated from brachiopods; brachiopod samples estimate SST of 30-38°C (34°C average) whereas coeval conodonts estimate 21-37°C SST (27°C average) (ocean $\delta^{18}O$ assumed at -1‰; Kolodny et al., 1983). Estimations of SST using the equation of Puceat et al. (2011) produce unreasonably high SSTs ~8°C higher than estimations using the equation of Kolodny et al. (1983). However, these SST estimations support the hypothesis that brachiopod trends may be used to assess relative changes in $\delta^{18}O$, supporting the claim that these Upper Silurian cycles were generated by glacio-eustasy.

Opposing $\delta^{18}O$ trends between conodont pearl and brachiopod versus coniform conodonts observed in cycles 1 and 5 may be described by vital effects, diagenetic recrystallization, differing water temperature due to deep or shallow-water habitats, or out-of-phase climate transitions recorded by conodonts versus apatitic brachiopods. Due to the lack of data documenting similar isotopic inconsistencies between pearls and elements of conodonts, we cannot further comment on whether conodont pearls are subject to vital effects or recrystallization. To avoid possible interspecies differences in $\delta^{18}O$ (Bassett et al., 2005), all conodont samples were composed of coniform elements of *Belodella*. However, due to the fragmentary preservation of apatitic brachiopod samples recovered, we were unable to separate brachiopods by species. As a result, brachiopod $\delta^{18}O$ may include a component of interspecies biologic fractionation of $\delta^{18}O$.

The benthic nature of brachiopods versus nektonic conodonts may suggest differences in $\delta^{18}O$ result from water temperatures at the sea-floor as opposed to surface waters (Picard et al., 1998). However, the shallow water depths estimated for this platform are < 100 m (Theiling and Elrick, in prep., Chapter 1), implying any differences in water temperature between brachiopod and conodont habitats are insignificant (Adlis et al., 1988; Levitus and Boyer, 1994).

If opposing brachiopod and conodont $\delta^{18}O$ trends indeed record a climatic transition, cycle 2 implies that warmest SST and smallest glacial ice-volumes occurred when the sea-level fall rate was near or at a maximum and that coolest SST and largest glacial ice-volumes occurred when sea-level rise rate was near or at a maximum (Figure 7). Similarly, brachiopod $\delta^{18}O$ from cycle 5 may demonstrate an as a more complete record of the glacial-interglacial climate transition that is out-of-phase with conodont $\delta^{18}O$.

Conclusions

$\delta^{18}O$ data from the sampled Upper Silurian greenhouse section demonstrate that apatitic brachiopods and conodont pearls generate both similar and opposing trends to coniform conodont $\delta^{18}O$. Because apatitic brachiopods recovered from these deposits were too fragmentary to allow for species separation, variable $\delta^{18}O$ trends may be due to vital effects or partial recrystallization. If analyzed brachiopod and conodont pearl samples were not subject to vital effects or recrystallization, these samples suggest that brachiopod and conodont pearl samples sometimes record $\delta^{18}O$ out-of-phase with coniform conodont element $\delta^{18}O$.

SUPPLEMENTAL B

RARE EARTH ELEMENT AND SM-ND CATION EXTRACTION COLUMN EXPERIMENT

Introduction

Separation of Sm and Nd from carbonates in the studies presented in previous chapters were accomplished through ion exchange chromatography. Ion exchange chromatography methods for rare earth elements (REE) are typically generated for use with silicate materials, which require strong acids (e.g. HF) to dissolve sample powders and rocks. Carbonate rocks sampled for these studies however, may be dissolved using weak acids (e.g. HCl). Carbonate samples collected for the preceding studies are typified by very low concentrations of REE relative to silicate rocks. Due to the low REE concentrations expected for these samples, it was necessary to determine a more precisely the amount of eluent required to elute REE in the first phase of extraction and Sm and Nd in the second phase of extraction using the ion exchange columns and resins available in the clean lab at the Radiogenic Isotope Laboratory at the University of Mexico. Here I present the results of two ion extraction experiments and a revised methodology for extraction of REE and Sm and Nd at the Radiogenic Isotope Laboratory at the University of New Mexico.

Methodology

Ion Exchange chromatography

In liquid ion exchange chromatography, a sample dissolved in a weak acid (mobile phase) is introduced (loaded) onto an ion exchange resin (stationary phase), typically composed of a sulfonic or carboxylonic acid. TRU Resin is used for REE extractions

(Horwitz et al., 1993). Sequential addition of eluent induces downward movement of the mobile phase while increasing the partitioning between ions in the solution based on ion charge, size, and K_D (distribution coefficient). Small, lesser charged ions with low K_D will elute first. In the first stage of extraction, REE are separated from $^{+2}$Ca, $^{+2}$Mg, and $^{+2}$Sr ions that dominate carbonate samples. Sm and Nd are separated and collected in a second stage extraction utilizing long TRU Resin filled columns, which allows REE to partition from small additions of 0.18 N HCl eluent.

Traditional Sm and Nd extraction method

Each whole-rock sample was prepared using the method described in Theiling et al. (2012). REE were extracted using a method modified from Asmerom et al. (1999). The soluble fraction of powdered whole-rock samples were dissolved in 4mL 1N HNO_3, centrifuged, and the supernate was loaded onto 250 μL cation exchange columns filled with TRU-SP resin, cleaned and conditioned with 1N HNO_3. Each addition of eluent was allowed to drip completely through the columns to ensure reproducibility of the methodology and precision of separations. After sample loading, 2mL 1N HNO_3 was added to columns to partition REE from ions that dominate carbonate samples (primarily $^{+2}$Ca, $^{+2}$Mg, and $^{+2}$Sr). REE were then collected during addition of 2mL 0.1% HNO_3.

Longer exchange columns were used for partitioning REE using a method modified from Asmerom et al. (1999). Columns were cleaned by allowing 10 mL 6N HCl to drip through; a strong acid ensures effective removal of any ions from previous separations. This cleaning procedure was also performed at the end of each sample separation. 0.18N HCl were added to REE columns in two separate increments, such that the mobile and stationary phases have the same pH when the sample is introduced, termed conditioning.

The sample was loaded onto the columns in a 0.2mL solution of 0.18N HCl. Each addition of eluent was allowed to drip through the column completely to ensure precision and reproducibility of REE partitioning. To partition REE, two increments of 0.2mL 0.18N HCl were added to columns, followed by 0.5mL 0.18N HCl, 1mL HCl, and 16mL 0.18N HCl. Nd was then collected by adding 8mL 0.18N HCl. 2 mL 0.5N HCl were then added to move Sm ions downward in the resin. Sm was collected by adding 4mL 0.5N HCl to columns.

REE extraction phase				
traditional method	eluent added	sample	^{146}Nd (cps)	^{147}Sm (cps)
2mL 0.1% HNO3	1mL 0.1% HN_3O	1	1400	540
	1mL 0.1% HN_3O	2	500	1550
clean columns/	1mL 0.1% HN_3O	3	15000000	17500000
discard waste	1mL 0.1% HN_3O	4	1800000	1900000
	1mL 0.1% HN_3O	5	100000	100000
Sm-Nd extraction phase				
16mL 0.18N HCl	12mL 0.18N HCl			
	4 mL 0.18N HCl	1	90000	500
8mL 0.18N HCl	2 mL 0.18N HCl	2	90000	180
	2 mL 0.18N HCl	3	90000	100
	2 mL 0.18N HCl	4	90000	100
	2 mL 0.18N HCl	5	600000	100
2 mL 0.18N HCl	2 mL 0.18N HCl	6	450000	100
4 mL 0.18N HCl	2 mL 0.5N HCl	7	70000	8000
	2 mL 0.5N HCl	8	35000	200000
clean columns/	2 mL 0.5N HCl	9	5000	90000
discard waste	2 mL 0.5N HCl	10	1600	450000

Table 5. Counts per second (cps) of ^{146}Nd and ^{147}Sm for each aliquot collected during both REE and Sm and Nd extraction phases of experiment #1. Aliquots collected are compared to traditional method eluent addition. Traditional collection intervals are indicated by gray shaded areas.

Sm and Nd extraction experiment #1

Efficiency of REE extraction was tested using a REE standard of known concentration. 1mL increments of 0.1% HNO_3 eluent were added to columns during the collection step to determine which increment contained the highest concentrations of Sm and Nd. Each 1mL aliquot was collected and analyzed separately on a Thermo Finnigan

X-Series II ICPQ-MS at the University of New Mexico Radiogenic Isotope Laboratory. Amounts of Sm and Nd collected are expressed in counts per second (cps) of ^{146}Nd and ^{147}Sm because these isotopes are not subject to isobaric interferences. The results of this experiment are detailed in Figure 15 and Table 5. The 3rd and 4th aliquots of eluent produced maximum cps, suggesting the traditional method will not sufficiently collect REE in carbonate samples. As a result, we altered the method to add two aliquots of 2mL 0.1% HNO_3. REE are now collected during the second addition of 0.1% HNO_3.

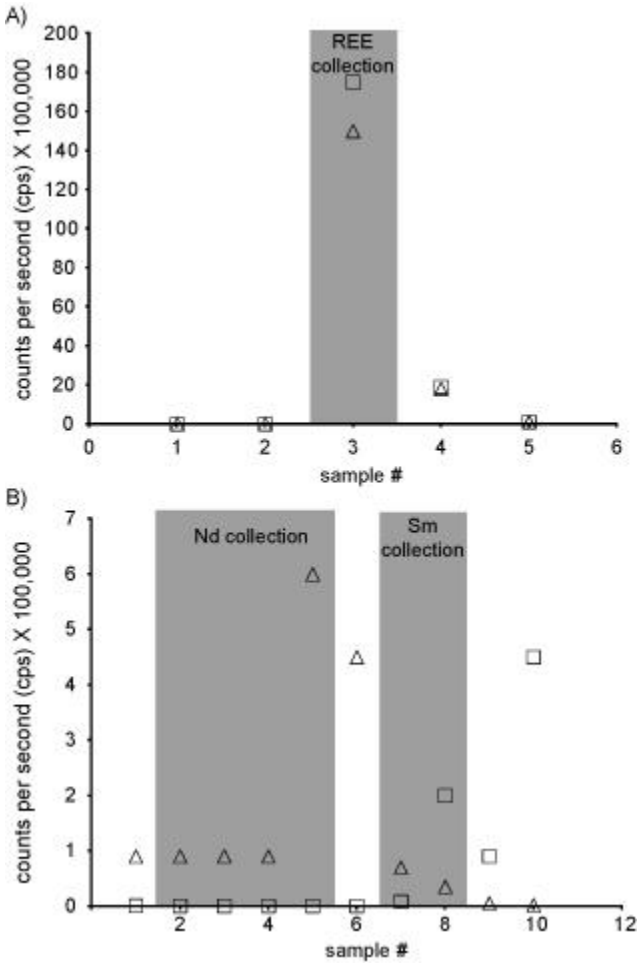

Figure 15. Histogram of counts per second (cps) for each sample collection aliquot taken during extraction experiment #1. Nd = open triangles, Sm = open squares. Traditional collection intervals are indicated by shaded rectangles. Eluent amounts for each sample are given in Table 1. a) REE extraction experiment. b) Sm and Nd extraction experiment.

Determination of the separation and collection efficiency of Sm and Nd during the second phase of extraction was performed similarly to the REE extraction experiment. In the traditional method, Nd is collected during addition of 8mL 0.18N. We separated this collection phase into four increments of 2mL 0.18N HCl. Likewise, Sm is traditionally collected in a later phase using 4mL 0.5N HCl, but was similarly separated into 2mL increments for this experiment. The results of this experiment are shown in Figure 15 and Table 5 and indicate that Nd collection may be sufficient, but that Sm collection needs modification.

Sm-Nd extraction phase				
traditional method load sample	eluent added load sample	sample	^{146}Nd (cps)	^{147}Sm (cps)
0.2 mL 0.18N HCl	0.2 mL 0.18N HCl			
0.2 mL 0.18N HCl	0.2 mL 0.18N HCl			
0.5 mL 0.18N HCl	0.5 mL 0.18N HCl			
1 mL 0.18N HCl	1 mL 0.18N HCl			
16 mL 0.18N HCl	8 mL 0.18N HCl			
	4 mL 0.18N HCl	1	300000	200
	4 mL 0.18N HCl	2	1200000	150
8 mL 0.18N HCl	1 mL 0.18N HCl	3	1600000	150
	1 mL 0.18N HCl	4	1800000	200
	1 mL 0.18N HCl	5	2000000	300
	1 mL 0.18N HCl	6	2200000	300
	1 mL 0.18N HCl	7	2200000	300
	1 mL 0.18N HCl	8	2100000	200
	1 mL 0.18N HCl	9	2000000	250
	1 mL 0.18N HCl	10	2000000	250
2 mL 0.5N HCl	1 mL 0.5N HCl	11	1800000	250
	1 mL 0.5N HCl	12	200000	10000
4 mL 0.5N HCl	1 mL 0.5N HCl	13	170000	1200000
	1 mL 0.5N HCl	14	38000	5000000
	1 mL 0.5N HCl	15	18000	5000000
	1 mL 0.5N HCl	16	9500	5000000
clean columns/ discard waste	1 mL 0.5N HCl	17	5000	2200000
	1 mL 0.5N HCl	18	3800	390000
	1 mL 0.5N HCl	19	2000	50000
	1 mL 0.5N HCl	20	1500	13000

Table 6. Counts per second (cps) of ^{146}Nd and ^{147}Sm for each aliquot collected during only the Sm and Nd extraction phase of experiment #2. Aliquots collected are compared to traditional method eluent addition. Traditional collection intervals are indicated by gray shaded areas.

Sm and Nd extraction experiment # 2

Results from the REE extraction efficiency in the first experiment promoted alteration of the REE extraction methodology whereby REE are collected during a second aliquot addition of 2mL 0.1% HNO3. We used this altered extraction during the first phase of REE collection for the second experiment. In this experiment, traditional collection intervals of Nd and Sm (second extraction phase) were further subdivided to determine the most accurate collection phase for each cation (Table 6). The 16mL 0.18N HCl eluent addition was subdivided into 8mL, 4mL and 4mL additions. The 8mL 0.18N HCl Nd collection phase, 2mL 0.5N HCl intermediary phase, and 4mL 0.5N HCl Sm collection phase were each subdivided into 1mL increments. Each aliquot was analyzed for cps ^{146}Nd and ^{147}Sm similar to the first experiment. The results of this experiment are shown in Figure 16 and Table 6. This experiment demonstrates that Nd is eluted from the column earlier than predicted using the modified REE extraction method and that Sm

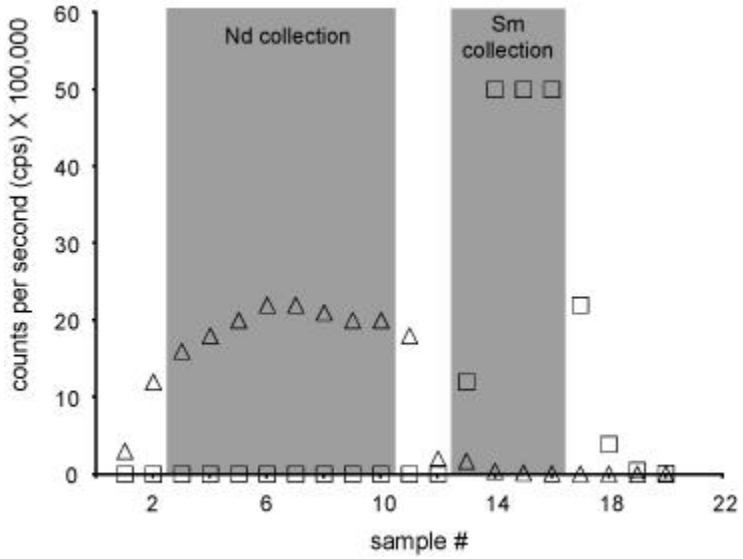

Figure 16. Histogram of counts per second (cps) for ^{146}Nd and ^{147}Sm of each sample collection aliquot taken during Sm and Nd extraction experiment #2. Nd = open triangles, Sm = open squares. Traditional collection intervals are indicated by shaded rectangles. Eluent amounts for each sample are given in Table 2.

continues eluting after collection ends using the traditional method. As a result of these observations, 15.5 mL 0.18N HCl is now added to the column before Nd collection. Nd is collected using 8.5 mL 0.18N HCl. Likewise, Sm is now collected with 5 mL 0.5N HCl instead of the traditional 4mL.

Revised Sm and Nd extraction methodology

Carbonate sample preparation for REE extraction

1) Drill ~250 mg of powder from clean whole rock samples, taking care to avoid stylolites, intraclasts, large skeletal grains, veins and heavily weathered surfaces with a diamond Dremel© drill bit. Clean drill bit with 5-10% HCl, dionized water, then ethanol between samples to avoid contamination.

2) Take powder vials into clean lab contained inside a Ziploc© bag to minimize dust contamination in the lab.

3) Label a clean 15mL Teflon© collection beaker and obtain mass (g).

   a) After placing beaker inside scale, use static gun 2-3 times.

   b) Close doors to scale before obtaining mass measurement.

4) Tare scale with collection beaker on scale, then remove collection beaker from scale.

5) Carefully tap sample powder into collection beaker.

6) Use static gun on sample powder in beaker before closing collection beaker with lid.

7) Place closed collection beaker + sample onto the scale, use static gun, close doors, and obtain mass.

8) Clean up any sample powder that may have fallen onto table with a clean Kimwipe© and ethanol.

9) Place sample under fume hood onto the glass plates on the left side of the fume hood.

10) Add 6N HCl dropwise to each sample until dissolved. Begin by adding ~10 drops, allowing the reaction to begin violently. Then, add drops until the reaction has completed.

11) Transfer acid soluble (AS) and acid insoluble (AIS) fractions to a labeled 15 mL centrifuge tube, using 6N HCl in squeeze bottle to remove AIS fractions if necessary. Cover centrifuge tube with small squares of Parafilm©.

12) Place tubes into centrifuge containers. Make sure that centrifuge containers are within ~0.025 g of each other so that the centrifuge is well-balanced. Use the large scale in the cabinet underneath the table scale for this measurement. If extra mass is needed, use scraps of weigh paper (often found near the centrifuge from previous users).

13) Turn on centrifuge. This will take ~4 min.

14) During this time, clean collection beakers using the following method:

a) Turn on tap water. Use 18MΩ water to rinse beakers. Use a clean Kimwipe© to wipe out any excess sample material.

b) Rinse with 18MΩ 3 times.

c) Pour a small amount (2-3 mL) of 6N HCl from the bottle labeled: "For cleaning purposes only"

d) Screw cap back on tightly, place on hotplate on setting 2 for 5-10 min. Do not increase temperature on hotplate above setting 3 because it will melt Teflon beakers.

e) Place beakers on glass plate under hood until cool enough to handle.

f) Turn back on tap water, shake beaker, remove cap, and pour liquid down drain. Rinse beaker 3 times with 18MΩ water.

g) Fill ~halfway with 18MΩ, screw cap tightly, and place beaker back on hotplate for 5-10 min.

h) Take off hotplate as before, pour liquid down drain, and rinse 3 times with 18MΩ water.

i) Fill again halfway with 18MΩ, screw cap tightly, and place beaker back on hotplate for 5-10 min.

j) Take off hotplate as before, pour liquid down drain, and rinse 3 times with 18MΩ water.

k) Your collection beaker is now clean only for future use with its labeled sample.

15) Remove centrifuge tube containers from centrifuge. Carefully peel back Parafilm©, taking care not to disturb the AIS fraction at the bottom.

16) Very carefully pour the AS (liquid) sample into your newly cleaned labeled collection beaker.

17) Place the Parafilm© cover back on the centrifuge tube in the event that you want to analyze AIS fractions later.

18) Take collection beaker + AS fraction to hotplate. Remove lid. Let sample dry down on hotplate setting 3 (2+ hours).

19) Once dry, remove from hotplate onto glass plate, and dissolve sample dropwise in 7N HNO_3. (~10-15 drops or until reaction is complete).

20) Place back on hotplate until dry.

21) Once dry, remove from hotplate onto glass plate, and dissolve sample dropwise in 15N HNO_3. (~10 drops or until reaction is complete). This phase often does not completely dissolve until placed back on the hotplate.

22) Place back on hotplate until dry.

23) Once dry, remove from hotplate onto glass plate and dissolve in 2mL 1N HNO_3

24) Bring sample (in 2mL 1N HNO_3) into weigh room. Obtain mass of each sample using procedure outlined above in steps #3-4 as a guideline.

25) Weigh Sm-Nd spike before and after use on large scale in lower cabinet and record masses in Spikes and Standards Book.

26) Add 2 drops of Sm-Nd spike to sample and obtain spike mass (g) for each sample.

27) Screw lid on tightly and allow sample to flux on hotplate for a few minutes (lower heat setting ~1-2).

28) Carefully pour spiked sample into clean 20mL centrifuge tube, cover with parafilm, and centrifuge, using procedure outlined in step #12-13 above.

29) Carefully remove centrifuge tube from container and pipette $^2/_3$ to ¾ of the AS liquid from the tube and load into cleaned and conditioned REE columns.

REE extraction

1) Add TRU-SPS resin powder to a 15mL Teflon collection beaker.

2) Add 18MΩ water to resin powder in beaker and stir.

3) Obtain 250μL columns at equilibrium with 2N HCl acid. Rinse with 18MΩ water:

a) Turn tap water on.

b) Turn 18MΩ water on and rinse column, first shaking column to remove 2N HCl, then rinsing with 18MΩ water and shaking out water 3 times.

c) Fill entire column with 18MΩ water. Using thumb and forefinger, pinch top of column closed and flick column to ensure that no air bubbles are present in narrow part of column.

d) Bring column (still filled with 18MΩ) to lab station and place in column holder, with a small glass waste beaker underneath each column.

4) Mix resin powder and water by gently swirling a clean pipette tip in mixture. Then, pipette resin/water mixture in 0.5-1 mL increments into clean 250mL columns. This entire process should be done before the 18MΩ water already in the columns drips through, which may take several seconds.

5) After the first pipette increment of resin/water, wait for resin to settle into column to determine whether additional resin/water is needed. Only the stem of the column should be filled with resin. The amount of acid used in future steps is calibrated for having to travel through the amount of resin contained in only the stem of the column. If too much resin is added to column, use pipette to remove excess resin and discard in waste beaker underneath column. To avoid possible contamination of resin, do not put excess resin back into Teflon beaker with clean resin/water mixture.

6) Add additional resin/water as needed until only narrow column is filled with resin. Allow 18MΩ water to drip through into waste beaker.

7) Add 3mL 0.1% HNO_3 to columns to clean resin. Allow to drip through completely.

8) Add 1mL 1N HNO_3 to condition columns. Allow to drip through completely.

9) Add the top $^2/_3$ to ¾ of the supernate from centrifuged sample (see step #28-29 from "Sample prep for REE columns") to your cleaned and conditioned REE columns. This will be approximately 1.5mL. Allow to drip through completely.

10) Add 2mL 1N HNO_3. Allow to drip through completely.

11) Replace waste beaker underneath column with cleaned and labeled collection beaker.

12) Add 2mL 0.1% HNO_3. Allow to drip through completely.

13) Add 2mL 0.1% HNO3 and COLLECT REE's in collection beaker.

14) Dry down collected sample on the hotplate or by leaving uncovered under the fume hood overnight.

15) Clean waste beakers:

a) Turn on tap water.

b) Pour acid mixture down drain, using tap water to dilute.

c) Rinse beakers 3 times in 18MΩ water.

d) Place upside down on towel next to sink.

16) Clean columns:

a) Turn on tap water.

b) Using 18MΩ water, fill and rinse columns until all resin is gone from column.

c) Place column back into bottle with other 250µL columns. Add more 2N HCl if necessary. Replace cap tightly. Shake bottle so that 2N HCl may fill columns inside bottle.

17) Clean lab station with ethanol.

Sm and Nd extractions

1) Remove columns from containers filled with 6N HCl. Place beakers (acid waste beaker) under each column and secure column through upper and lower holes in rack. Wash column and resin by adding 10mL 6N HCl.

2) While columns are being washed, add 0.2mL 0.18N HCl to dried REE separate sample in collection beaker. Screw cap on tightly and flux on hotplate setting ~1 for ~10min. Take off hotplate and set onto glass to continue dissolution until columns are ready.

3) Add 3mL 0.18N HCl to columns to condition.

4) Add 2 mL of 0.18N HCl to columns to condition.

4) Bring sample (in 0.2mL 0.18N HCl) to workstation. Using a clean pipette for every sample, load sample onto column.

5) Add 0.2 mL of 0.18N HCl to column.

6) Add 0.2 mL of 0.18N HCl to column.

7) Add 0.5 mL of 0.18N HCl to column.

8) Add 1 mL of 0.18N HCl to column.

9) Add 15.5 mL of 0.18N HCl.

10) Clean collection beakers using the method described in "Sample prep for REE columns".

11) Replace waste acid beaker with clean, labeled collection beaker (Adding to your original label: "Nd").

12) Add 8.5 mL of 0.18N HCl and COLLECT Nd in clean collection beaker.

13) Remove collection beaker with Nd separate and place on hotplate (setting 3) to dry.

14) Place waste acid beaker underneath column, and add 2 mL of 0.5N HCl.

15) Label a new 15mL collection beaker with sample designation + "Sm". Replace waste acid beaker with "Sm" collection beaker, add 5 mL of 0.5N HCl and COLLECT Sm in clean collection beaker.

16) Remove collection beaker with Sm separate and place on hotplate to dry.

17) Add 10mL 6N HCl to clean columns. After adding 10mL, use the squirt bottle for 6N HCl to squirt around inside of column to remove any possible contaminants.

18) Rinse acid waste beakers 3 times with 18MΩ water. Place Sm-Nd columns back into containers filled with 6N HCl, nested inside cleaned acid waste beakers. Clean lab station if necessary.

18) When Nd and Sm separates are dry (usually next day or another day), add 1 mL of 3% $HN0_3$ to each. Cover tightly and flux (hotplate setting 1-2) for ~10min. Remove and place on glass plate. Allow to sit for a few hours, if possible, to maximize voltage signal on Neptune.

19) Carefully pour into labeled sample vials and cap tightly. Bring to lab with Neptune for analysis.

REFERENCES

Adlis, D.S., Grossman, E.L., Yancey, T.E., & McLerran, D.R. (1988). Isotope stratigraphy and paleodepth changes of Pennsylvanian cyclical sedimentary deposits. Palaios, 3, 487-506.

Ahrens, C.D. (1991). Essentials of Meteorology: An Invitation to the Atmosphere, 3rd edition. Brooks/Cole Thomson Learning, Pacific Grove, CA, 464p.

Algeo, T., Wilson, J.L., & Lohmann, K.C. (1991). Eustatic and tectonic controls on cyclic sediment accumulation patterns in Lower-Middle Pennsylvanian strata of the Orogrande Basin, New Mexico. NMGS Guidebook 42, 203-212.

Algeo, T.J., Berner, R.A., Maynard, J.B., & Scheckler, S.E. (1995). Late Devonian oceanic anoxic events and biotic crises: 'rooted' in the evolution of vascular land plants? GSA Today, 5, 64-66.

Algeo, T.J., Scheckler, S.E., & Scott, A.C. (1998). Terrestrial-marine teleconnections in the Devonian: Links between the evolution of land plants, weathering processes, and marine anoxic events [and discussion]. Philosphical Transactions of the Royal Society of London: Biological Sciences, 353, 113-130.

Al-Shaieb, Z., Puckette, J., & Blubaugh, P. (2001). The Hunton Group: Sequence stratigraphy, facies, dolomitization, and karstification. Oklahoma Geological Survey Circular, 105, 17-29.

Amato, J.M., Toro, J., Miller, E.L., Gehrels, G.E., Farmer, G.L., Gotllieb, E.S., & Till, A.B. (2009). Late Proterozoic-Paleozoic evolution of the Arctic Alaska-Chukotka terrane based on U-Pb igneous and detrital zircon ages: Implications for Neoproterozoic paleogeographic reconstructions. Geological Society of America Bulletin, 121, 1219-1235.

Amzy, K., Veizer, J., Bassett, M.G., & Copper, P. (1998). Oxygen and carbon isotopic composition of Silurian brachiopods: Implications for coeval seawater and glaciations: GSA Bulletin, 110, 1499-1512.

Anderson, R.Y. (1982). A long geoclimatic record from the Permian. Journal of Geophysical Research, 87, 7285-7294.

Anderson, E.J., & Goodwin, P.W. (2003). Facies and paleoenvironments of the Keyser formation in the context of its cyclic structure *In* Way, J.H. & others, (eds.) Geology on the Edge: Selected Geology of Bedford, Blair, Cambria, and Somerset Counties, Guidebook, 68th Annual Field Conference of Pennsylvania Geologists, 1-18.

André, L., Hertogen, J., & Deutsch, S. (1986). Ordovician–Silurian magmatic provinces in Belgium and the Caledonian orogeny in the middle Europe. Geology, 14, 879–882.

Asmerom, Y. (1999). Th-U fractionation and mantle structure. Earth and Planetary Science Letters, 166, 163-175.

Arens, N.C., & Jahren, A.H. (2000). Carbon isotope excursion in atmospheric CO_2 at the Cretaceous-Tertiary boundary: Evidence from terrestrial sediments. Palaios, 15, 314-322.

Arthur, M.A., Bottjer, D.J., Dean, W.E., Fischer, A.G., Hattin, D.E., Kauffman, E.G., Pratt, L.M., & Scholle, P.A. (1986). Rhythmic bedding in Upper Cretaceous pelagic carbonate sequences; varying sedimentary response to climatic forcing. Geology, 14, 153-156.

Baarli, G.B., Johnson, M.E., & Antoshkina, A.I. (2003). Silurian stratigraphy and paleogeography of Baltica. New York State Museum Bulletin, 493, 3-34.

Banner, J.L. (2004). Radiogenic Isotopes: Systematics and applications to earth surface processes and chemical stratigraphy. Earth-Science Reviews 65, 141-194.

Barrick, J.E. (1975). Silurian conodonts of the Clarita Formation, Arbuckle Mountains, Oklahoma. [M.S. Thesis] University of Iowa, Iowa City, 207pp.

Barrick, J.E., Klapper, G., & Thomas, A. (1990). Late Ordovician-Early Devonian conodont succession in the Hunton Group, Arbuckle Mountains and Anadarko Basin, Oklahoma. Oklahoma Geological Survey Guidebook, 55-62.

Barrick, J.E., & Klapper, G. (1992). Late Silurian-Early Devonian conodonts from the Hunton Group (upper Henryhouse, Haragan, and Bois d'Arc formations), south-central Oklahoma. Oklahoma Geological Survey Bulletin, 145, 19-65.

Bassett, D.J., MacLeod, K.G., & Ethington, R.L. (2005). Differences in the oxygen isotopic composition of Upper Ordovician conodont species. GSA Abstracts with Programs 37, 457.

Bassett, D., MacLeod, K.G., Miller, J.F., & Ethington, R.L. (2007). Oxygen isotopic composition of biogenic phosphate and the temperature of Early Ordovician seawater. Palaios 22, 98-103.

Bazard, D.R., Butler, R.F., Gehrels, G., & Soja, C.M. (1995). Early Devonian paleomagnetic data from the Lower Devonian Karheen Formation suggest Laurentia-Baltica connection for the Alexander terrane. Geology, 23, 707–710.

Bennett, V.C., & DePaolo, D.J. (1987). Proterozoic crustal history of the Western United States as determined by neodymium isotopic mapping. Geological Society of America Bulletin 99, 674-685.

Berner, R.A. (1992). Weathering, plants and the long-term carbon cycle. Geochimica et Cosmochimica Acta, 56, 3225-3231.

Berner, R.A. (1994). 3 GEOCARB II: A revised model of atmospheric CO_2 over Phanerozoic time. American Journal of Science, 294, 56-91.

Berner, R.A., Lenton, M.T., & Beerling, D.J. (1998). The carbon cycle and CO_2 over Phanerozoic time: The role of land plants [and discussion]. Philosophical Transactions of the Royal Society of London, Biological Sciences, 353, 75-82.

Berner, R.A. (2001). Modeling atmospheric oxygen over Phanerozoic times. Geochimica et Cosmochimica Acta, 65, 685–694.

Berra, F. (2012). Sea-level fall, carbonate production, rainy days: How do they relate? Insight from Triassic carbonate platforms (Western Tethys, Southern Alps, Italy). Geology, 40, 271-274.

Bice, K.L., Huber, B.T., & Norris, R.D. (2003). Extreme polar warmth during the Cretaceous greenhouse? Paradox of the late Turonian delta (super 18) O record at Deep Sea Drilling Project Site 511. Paleoceanography, 18, 11.

Blakey, R.C. (2008). Gondwana paleogeography from assembly to breakup—a 500 m.y. odyssey *In* Fielding, C.R., Frank, T.D., Isbell, J.L., (eds.) Resolving the Late Paleozoic Ice Age in Time and Space: Geological Society of America Special Paper, 441, 1-28.

Bluth, G.J.S., & Kump, L.R. (1994). Lithologic and climatologic controls of river chemistry. Geochimica et Cosmochimica Acta, 58, 2341-2359.

Boghossian, N.D., Patchett, P.J., Ross, G.M., & Gehrels, G.E. (1996). Nd isotopes and the source of sediments in the miogeocline of the Canadian Cordillera. The Journal of Geology, 104, 259-277.

Bokhorst, M.P., Beets, C.J., Markovic, S.B., Gerasimenko, N.P., Matviishina, Z.N., & Frechen, M. (2009). Pedo-chemical climate proxies in late Pleistocene Serbian-Ukrainian loess sequences. Quaternary International 198, 113-123.

Bornemann, A., Norris, R.D., Friedrich, O., Beckmann, B., Schouten, S., Damaste, J.S., Vogel, J., Hoffman, P., & Wagner, T. (2008). Isotopic evidence for glaciation during the Cretaceous supergreenhouse. Science, 319, 189-192.

Boucot, A.J., Poole, F.G., Amaya-Martínez, R., Harris, A.G., Sandberg, C.A., & Page, W.R. (2008). Devonian brachiopods of southwesternmost Laurentia: biogeographic affinities and
tectonic significance. Geological Society of America Special Paper, 442, 77–97.

Bourque, P. (2001). Sea level, synsedimentary tectonics, and reefs: implications for hydrocarbon exploration in the Silurian-lowermost Devonian Gaspé Belt, Québec Appalachians. Bulletin of Canadian Petroleum Geology, 49, 217-237.

Brett, C.E., Goodman, W.M., Loduca, S.T., Pratt, B., & Tetreault, D. (1998). Silurian-Early Devonian sequence stratigraphy, cycles, and paleoenvironments of the Niagara Peninsula area of Ontario, Canada. Geological Society of America, Annual Meeting Field Trip Guidebook, 16.

Brouxel, M., LaPierre, H., Michard, A., & Albarede, F. (1987). The deep layers of a Paleozoic arc: Geochemistry of the Copley-Balaklala volcanics (California). Earth and Planetary Science Letters, 85, 386-400.

Brouxel, M., & LaPierre, H. (1988). Geochemical study of an early Paleozoic island-arc-backarc basin system. Part 1: The Trinity Ophiolite (northern California). Geological Society of America Bulletin, 100, 1111-1119.

Bryant, J.D., Koch, P.L., Froelich, P.N., Showers, W.J., & Genna, B.J. (1996). Oxygen isotope partitioning between phosphate and carbonate in mammalian apatite. Geochimica et Cosmochimica Acta 60, 5145-5148.

Buggisch, W., Wang, X., Alekseev, A.S., and Joachimski, M.M. (2011). Carboniferous-Permian carbon isotope stratigraphy of successions from China (Yangtze platform), USA (Kansas) and Russia (Moscow Basin and Urals). Palaeogeography, Palaeoclimatology, Palaeoecology, 301, 18-38.

Burton, K.W., Ling, H.F., & O'Nions, R.K. (1997). Closure of the central American Isthmus and its effect on deep water formation in the North Atlantic. Nature, 386, 382-385.

Burton, K.W., & Vance, D. (2000). Glacial-interglacial variations in the neodymium isotope composition of seawater in the Bay of Bengal recorded by planktonic Foraminifera. Earth and Planetary Science Letters, 176, 425-441.

Butler, R.F., Gehrels, G.E., & Bazard, D.R. (1997). Paleomagnetism of Paleozoic strata of the Alexander terrane, southeastern Alaska. Geological Society of America Bulletin, 109, 1372–1388.

Calder, J.H., & Gibling, M.R. (1994). The Euramerican Coal Province: controls on Late Paleozoic peat accumulation. Palaeogeography, Palaeoclimatology, Palaeoecology, 106, 1-21.

Cannfield, D.E. (1994). Factors influencing organic carbon preservation in marine sediments. Chemical Geology, 114, 315-329.

Caputo, M.V., & Crowell, J.C. (1985). Migration of glacial centers across Gondwana during the Paleozoic era. Geological Society of America Bulletin, 96, 1020–1036.

Carlson, M.P. (1999). Transcontinental Arch; a pattern formed by rejuvenation of local features across central North America. Tectonophysics, 305, 225-233.

Chen, D., & Tucker, M.E. (2003). The Frasnian-Famennian mass extinction: insights from high-resolution sequence stratigraphy and cyclostratigraphy in South China. Palaeogeography, Palaeoclimatology, Palaeoecology, 193, 87-111.

Cisne, J.L. (1986). Earthquakes recorded stratigraphically on carbonate platforms. Nature, 323, 320-322.

Clarke, D.B., & Halliday, A.N. (1985). Sm/Nd isotopic investigation of the age and origin of the Meguma Zone metasedimentary rocks. Canadian Journal of Earth Sciences, 22, 102-107.

Clarke, D.B., Chatterjee, A.K., & Giles, P.S. (1992). Petrochemistry, tectonic history, and Sr-Nd systematic of the Liscomb Complex, Megume Lithotectonic Zone, Nova Scotia. Canadian Journal of Earth Sciences, 30, 449-464.

Clementz, M.T., & Sewall, J.O. (2011). Latitudinal gradients in greenhouse seawater delta (super 18) O; evidence from Eocene Sirenian tooth enamel. Science, 332, 455-458.

Cocks, L.R.M., & Scotese, C.R. (1991). The global biogeography of the Silurian Period. Special Papers in Palaeontology, 44, 109-122.

Cocks, L.R.M., & Torsvik, T.H. (2002). Earth geography from 500 to 400 million years ago: a faunal and palaeomagnetic review. Journal of the Geological Society of London, 159, 631–644.

Cocks, L.R.M., & Torsvik, T.H. (2011). The Paleozoic geography of Laurentia and western Laurussia: A stable craton with mobile margins. Earth-Science Reviews, 106, 1-51.

Coe, A.L., Church, K.D. (2003). The Sedimentary Record of Sea-Level Change, Angela L. Coe (ed.) Cambridge University Press, 57-98.

Colpron, M., & Nelson, J.L. (2009). A Palaeozoic Northwest Passage: incursion of
Caledonian, Baltican and Siberian terranes into eastern Panthalassa, and the early evolution of the North American Cordillera. Geological Society of London. Special Publication, 318, 273–307.

Copper, P. (2000). Megareefs in a super greenhouse; the 80 million year long mid-Paleozoic, Siluro-Devonian interval. Geological Society of America Abstracts with Programs, 32, 313.

Copper, P., & Scotese, C.R. (2003). Megareefs in Middle Devonian supergreenhouse climates. Geological Society of America Special Paper, 370, 209-230.

Cotter, E. (1998). Silurian coastal sedimentation and meter-scale rhythms in the Appalachian foreland basin of Pennsylvania. Bulletin-New York State Museum (1976), 491, 229-237.

Cramer, B.D. (2009). Chapter 2: Extending astrochronology into the lower Paleozoic, *in* Application of Integrated High-Resolution Biochemostratigraphy to Paleozoic Chronostratigraphic Correlation: Recalibrating the Silurian System [Ph.D. thesis]: Columbus, The Ohio State University, 37–46.

Crick, R.E., Ellwood, B.B., Hladil, J., El Hassani, A., Hrouda, F., & Chlupác, I. (2001). Magnetostratigraphy susceptibility of the Přídolian-Lochkovian (Silurian-Devonian) GSSP (Klonk, Czech Republic) and a coeval sequence in Anti-Atlas Morocco. Palaeogeography, Palaeoclimatology, Palaeoecology, 167, 73-100.

Crowell, J.C. (1999). Pre-Mesozoic ice ages: Their bearing on understanding the climate system. Geological Society of America Memoir, 192, 1–106.

Culver, S.J., Farrell, K.M., Mallinson, D.J., Willard, D.A., Horton, B.P., Riggs, S.R., Theiler, E.R., Wehmiller, J.F., Parham, P., Snyder, S.W., & Hillier, C. (2011). Micropaleontologic record of Quaternary paleoenvironments in the central Albemarle Embayment, North Carolina, U.S.A. Palaeogeography, Palaeoclimatology, Palaeoecology, 305, 227-249.

Cusack, M., Williams, A., & Buckman, J.O. (1997). Shell biochemistry *In* Kaesler, R.L. (ed.) Treatise on Invertebrate Paleontology, Part H. Brachiopods, Revised 1, Geological Society of America and University of Kansas, 243-266.

Dickinson, W.R. (2000). Geodynamic interpretation of Paleozoic tectonic trends oriented
oblique to the Mesozoic Klamath–Sierran continental margin in California. Geological Society of America Special Paper, 347, 200–245.

Dickinson, W.R., & Lawton, T.F. (2003). Sequential intercontinental suturing as the ultimate control for Pennsylvanian Ancestral Rocky Mountains deformation. Geology, 31, 609-612.

Dickinson, W.R. (2009). Anatomy and global context of the North American Cordillera.
Geological Society of America Memoir, 204, 1–29

Dorning, K.J., & Harvey, C. (1999). Wenlock cyclicity, palynology, and stratigraphy in the Buildwas, Coalbrookdale, and Much Wenlock Limestone Formations, Shropshire, England. Bollettino della Societa Paleontologica Italiana, 38, 155-166.

Drever, J.I. (1994). The effect of land plants on weathering rates of silicate minerals. Geochimica et Cosmochimica Acta, 58, 3209-3216.

Edwards, D., & Scott, A.C. (1998). Climate signals in Paleozoic land plants [and discussion]. Philosophical Transactions of the Royal Society of London, Biological Sciences, 353, 141-157.

Elrick, M., Berkyova, S., Klapper, G., Sharp, Z., Joachimski, M., & Fryda, J. (2009). Stratigraphic and oxygen isotope evidence for My-scale glaciations driving eustasy in the Early-Middle Devonian greenhouse world. Palaeogeography, Palaeoclimatology, Palaeoecology, 276, 170-181.

Elrick, M., & Scott, L.A. (2010). Carbon and oxygen isotope evidence for high-frequency (104-105 yr) and My-scale glacioeustasy in Middle Pennsylvanian cyclic carbonates (Gray Mesa Formation), central New Mexico. Palaeogeography, Palaeoclimatology, Palaeoecology, 285, 307-320.

Elrick, M., Rieboldt, S., Saltzman, M., & McKay, R.M. (2011). Oxygen-isotope trends and seawater temperature changes across the Late Cambrian Steptoean positive carbon-isotope excursion (SPICE event). Geology, 39, 987-990.

Embry, A.F. (1991). Middle-Upper Devonian clastic wedge of the Arctic Islands *In* Trettin, H.P. (ed.) Geology of the Innutian orogen and Arctic platform of Canada and Greenland Geological Survey of Canada, Geology of Canada No 3, 263-279.

Emiliani, C. (1955). Pleistocene temperatures. Journal of Geology, 63, 538-578.

Emiliani, C. (1966). Isotopic paleotemperatures. Science, 154, 851-857.

Epstein, S., Buschbaum, R., Lowenstam, H.A, & Urey, H.C. (1953). Revised carbonate-water isotopic temperature scale. Geological Society of America Bulletin, 64, 1315-1326.

Fairbanks, F.G., & Matthews, R.K. (1978). The marine oxygen isotope record in Pleistocene coral, Barbados, West Indies. Quaternary Research, 10, 181-196.

Fanton, K., Holmden, C., Nowlan, G., & Haidl, F. (2002). $^{143}Nd/^{144}Nd$ and Sm/Nd stratigraphy of Upper Ordovician epeiric sea carbonates. Geochimica et Cosmochimica Acta, 66, 241-255.

Fairbanks, F.G. (1989). A 17,000-year glacio-eustatic sea level record; influence of glacial melting rates on the Younger Drays event and deep-ocean circulation. Nature, 342, 637-642.

Fairbanks, F.G., & Matthews, R.K. (1978). The marine oxygen isotope record in Pleistocene coral, Barbados, West Indies. Quaternary Research, 10, 181-196.

Faure, H., Walter, R.C., & Grant, D.R. (2002). The coastal oasis: ice age springs on emerged continental shelves. Global and Planetary Change, 33, 47-56.

Fielding, C.R., Frank, T.D., Birgenheier, L.P., Rygel, M.C., Jones, A.T., & Roberts, J. (2008). Stratigraphic imprint of the Late Palaeozoic Ice Age in eastern

Australia: A record of alternating glacial and-non-glacial climate regime. Geological Society of London Journal, 165, 129-140.

Fogel, R. (1985). Roots as primary producers in below-ground ecosystems *In* Fitter, A.H., Atkinson, D., Read, D.J., Usher, M.B., (eds). Ecological Interactions in soil: plants, microbes, and animals. Blackwell, Oxford, 23-46.

Forster, A., Schouter, S., Baas, M., & Sinninghe Damste, J. (2007). Mid-Cretaceous (Albian-Santonian) sea surface temperature record of the tropical Atlantic Ocean. Geology, 35, 919-922.

Frakes, L.A., & Francis, J.E. (1988). A guide to Phanerozoic cold polar climates from high-latitude ice-rafting in the Cretaceous. Nature, 333, 547-549.

Frakes, L.A., Francis, J.E., & Syktus, J.I. (1992). Climate Modes of the Phanerozoic. Cambridge University Press, Cambridge. 274p.

Frank, M. (2002). Radiogenic isotopes: tracers of past ocean circulation and erosional input. Reviews of Geophysics, 40, 1-38.

Gale, A.S., Hardenbol, J., & Hathaway, B. (2002). Global correlation of the Cenomanian (Upper Cretaceous) sequences: evidence for Milankovitch control on sea level. Geology, 30, 291-294.

Garzione, C.N., Patchett, P.J., Ross, G.M., & Nelson, J. (1997). Provenance of Paleozoic sedimentary rocks in the Canadian Cordilleran miogeocline: a Nd isotopic study. Canadian Journal of Earth Science, 34, 1603-1618.

van Geldern, R., Joachimski, M.M., Day, J., Jansen, U., Alvarez, F., Yolkin, E.A., & Ma, X.-P. (2006). Carbon, oxygen and strontium isotope records of Devonian brachiopod shell calcite. Palaeogeography, Palaeoclimatology, Palaeoecology, 240, 47-67.

Gerriene, P., Bergamashi, S., Pereira, E., Rodrigues, M.A.C., Steemans, P. (1991). An Early Devonian flora, including *Cooksonia*, from the Paraná Basin (Brazil). Revelations in Palaeobotanical Palynology, 116, 19-38.

Gleason, J.D., Patchett, P.J., Dickinson, W.R., & Ruiz, J.R. (1994). Nd isotopes link Ouachita turbidites to Appalachian sources. Geology, 22, 347-350.

Gleason, J.D., Patchett, P.J., Dickinson, W.R., & Ruiz, J. (1995). Nd isotopic constraints on sediment sources of the Ouachita-Marathon fold belt. Geological Society of America Bulletin, 107, 1192-1210.

Gislason, S.R., Oelkers, E.H., Eiriksdottir, J., Torsannder, P., & Oskarsson, N. (2009). Direct evidence of the feedback between climate and weathering. Earth and Planetary Science Letters, 277, 213-222.

Goldhammer, R. K., & Elmore, R. D. (1984). Paleosols capping regressive carbonate cycles in the Pennsylvanian Black Prince Limestone, Arizona. Journal of Sedimentary Petrology, 54, 1124–1137

Goldstein, S.J., & Jacobsen, S.B. (1987). The Nd and Sr isotopic systematic of river-water dissolved material; implications for the sources of Nd and Sr in seawater. Chemical Geology, 66, 245-272.

Goldstein, S.J., & Jacobsen, S.B. (1988). Nd and Sr isotopic systematics of river water suspended material: implications for crustal evolution. Earth and Planetary Science Letters, 87, 249-265.

Goldhammer, R.K. (1987). Platform carbonate cycles, Middle Triassic of northern Italy; the interplay of local tectonics and global eustasy (Dissertation). Johns Hopkins University, Baltimore, Maryland, 548 pp.

Golonka, J., Ross, M.I., & Scotese, C.R. (1994). Phanerozoic paleogeographic and paleoclimatic modeling maps. Memoir-Canadian Society of Petroleum Geologists, 17, 1-47.

Gong, Y.M., Li, B.H., Wany, C.Y., & Wu, Y. (2001). Orbital cyclostratigraphy of the Devonian Frasnian-Famennian transition in South China. Palaeogeography, Palaeoclimatology, Palaeoecology, 168, 237-248.

Hay, W.W., & Leslie, M.A. (1990). Could possible changes in global groundwater reservoir cause eustatic sea-level fluctuations? *In* R. Revelle, (Panel Chairman), Sea- Level Change: National Academy Press, Washington D.C, 161-170.

Heckel, P.H. (1977). Origin of phosphatic black shale facies in Pennsylvanian cyclothems of mid-continent North America. American Association of Petroleum Geologists Bulletin, 61, 1045-1068.

Heckel, P.H. (1994). Evaluation of evidence for glacio-eustatic control over marine
Pennsylvanian cyclothems in North America and consideration of possible tectonic effects, *In* Dennison, J.M., and Ettensohn, F.R., eds., Tectonic and eustatic controls on sedimentary cycles. SEPM (Society for Sedimentary Geology) Concepts in Sedimentology and Paleontology 4, 65–87.

Herman, A.B., & Spicer, R.A. (1996). Palaeobotanical evidence for a warm Cretaceous Arctic Ocean. Nature, 380, 330-333.

Horwitz, E.P., Chiarizia, R., Dietz, M.L., Diamond, H., & Nelson, D. (1993). Separation and preconcentration of actinides from acidic media by extraction chromatography. Analytica Chimica Acta, 281, 361-372.

Hovan, S.A., Rea, D.K., & Pisias, N.G. (1991). Late Pleistocene continental climate and oceanic variability recorded in Northwest Pacific sediments. Paleoceanography, 6, 349-370.

Hyde, W.T., Crowley, T.J., Tarasov, L., & Paltier, W.R. (1999). The Pangean ice age: studies with a coupled climate-ice sheet model. Climate Dynamics, 15, 619-629.

Iacumin, P., Bocherens, H., Mariotti, A., & Longinelli, A. (1996). Oxygen isotope analysis of co-existing carbonate and phosphate in biogenic apatite: a way to monitor diagenetic alteration of bone phosphate? Earth and Planetary Science Letters, 142, 1-6.

Iijima, M., & Moriwaki, Y. (1990). Orientation of apatite and organic matrix in *Lingula unguis* shell. Calcified Tissue International, 47, 237-242.

Immenhauser, A., & Scott, R.W. (2002). An estimate of Albian sea-level amplitudes and its implications for the duration of stratigraphic hiatuses. Sedimentary Geology, 152, 19-28.

Immenhauser, A. (2009). Estimating palaeo-water depth from the physical rock record. Earth Science Reviews, 96, 107-139.

Isbell, J.L.,Miller,M.F.,Wolfe, K.L., & Lenaker, P.A. (2003). Timing of the late Paleozoic glaciations in Gondwana: Was glaciation responsible for the development of Northern Hemisphere cyclothems? *in* Chan, M.A., Archer, A.W. (Eds.), Extreme Depositional Environments: Mega End-members in Geologic Time. Geological Society of America Special Paper, 370, 5–24.

Isbell, J.L., Miller, M.F., Wolfe, K.L., & Lenaker, P.A. (2003). Timing of late Paleozoic glaciations in Gondwana: was glaciations responsible for the development of northern hemisphere cyclothems? *In* Chan, M.A., Archer, A.W., (eds.) Extreme depositional environments: mega end members in geologic time: Geological Society of America Special Paper, 370, 5-24.

Isbell, J.L., Henry, L.C., Gulbranson, E.L., Limarino, C.O., Frasier, M.L., Koch, Z.J., Ciccioli, P.L., & Dineen, A.A. (2012). Glacial paradoxes during the late Paleozoic ice age: Evaluating the equilibrium line altitude as a control on glaciations. Gondwana Research, 22, 1-19.

Jahren, A.H., Amundson, R., Kendall, C., & Wigand, P. (2001). Paleoclimatic reconstruction using the correlation in delta (super 18) O of hackberry carbonate and environmental water, North America. Quaternary Research, 56, 252-263.

Janecek, T.R., & Rea, D.K. (1983). Eolian deposition in the Northeast Pacific Ocean; Cenozoic history of atmospheric circulation. Geological Society of America Bulletin, 94, 730-738.

Jeppsson, L. (1997). The anatomy of the Mid-Early Silurian Ireviken Event and a scenario for P-S events *In* Brett, C.E., Baird, G.C., (eds.) Paleontological events; stratigraphic, ecological, and evolutionary implications. Columbia University Press, New York, NY.

Jervey, M.T. (1988). Quantitative geological modeling of siliciclastic rock sequences and their seismic expressions, *In* Wilgus, C.K., Hastings, B.S., Kendall, C.G.St.C., Posamentier, H.W., Ross, C.A., and Van Wagoner, J.C., (eds.) Sea-Level Changes; An Integrated Approach.
Society of Economic Paleontologists and Mineralogists, Special Publication, 42, 47–69.

Joachimski, M.M., & Buggisch, W. (1993). Anoxic events in the late Frasnian-Causes of the Frasnian-Famennian faunal crisis? Geology, 21, 675-678.

Joachimski, M.M., Pancost, R.D., Freeman, K.H., Ostertag-Henningh, C., & Buggisch, W. (2002). Carbon isotope geochemistry of the Frasnian-Famennian transition. Palaeogeography, Palaeoclimatology, Palaeoecology, 181, 91-109.

Joachimski, M.M., Geldern, R., Breisig, S., Bruggisch, W., & Day, J. (2004). Oxygen isotope evolution of biogenic calcite and apatite during the Middle and Late Devonian. International Journal Earth Science, 93, 542–553.

Joachimski, M.M., von Bitter, P.H., & Buggisch, W. (2006). Constraints on Pennsylvanian glacioeustatic sea-level changes using oxygen isotopes on conodont apatite. Geology, 34, 277–280.

Joachimski, M.M., Breisig, S., Buggisch, W., Talent, J.A., Mawson, R., Gereke, M., Morrow, J.R., Day, J., & Weddige, K. (2009). Devonian climate and reef evolution: Insights from oxygen isotopes in apatite. Earth and Planetary Science Letters, 284, 599-609.

Johnson, J.G. (1970). Taghanic Onlap and the end of North American Devonian provinciality. Geological Society of America Bulletin, 81, 2077–2106.

Johnsson, M.J. (1993). The system controlling the composition of clastic sediments. *In* Johnson, M.J., Basu, A. (eds.) Processes controlling the composition of clastic sediments. Geological Society of America Special Paper no 284, 1-19.

Johnsson, M.J., Stallard, R.F., & Meade, R.H. (1988). First-cycle quartz arenites in the Orinoco river basin, Venezuela and Colombia. Journal of Geology, 96, 263-277.

Karlstrom, K.E., Amato, J.M., Williams, M.L., Heizler, M., & Shaw, C.A. (20040. Proterozoic tectonic evolution of the New Mexico region; a synthesis. Special Publication New Mexico Geological Society, 11, 1-34.

Kastner, M., Garrison, R.E., Kolodny, Y., Reimers, C.E., & Shemesh, A. (1990). Coupled changes of oxygen isotopes in PO_4^{3-} and CO_3^{2-} in apatite, with emphasis on the Monterey Formation, California *In* Burnett, W.C. and Riggs, S.R., (eds.) Phosphate deposits of the world, vol. 3. Neogene to modern Phosphorites, Cambridge University Press, Cambridge, 312-324.

Kelly, V.C., & Wood, G.H. (1946). Lucero uplift, Valencia, Socorro, and Bernalillo counties, New Mexico. U.S.G.S. Oil and Gas Inventory Preliminary Map 47.

Kettner , A.J., & Syvitski, J.P.M. (2009). Fluvial responses to environmental perturbations in the Northern Mediterranean since the Last Glacial Maximum. Quaternary Science Reviews, 28, 2386-2397.

Kidder, D.L., & Worsley, T.R. (2010). Phanerozoic Large Igneous Provinces (LIPs), HEATT (Haline Euxinic Acidic Thermal Transgression) episodes, and mass extinctions. Palaeogeography, Palaeoclimatology, Palaeoecology, 295,162-191.

Kluth, C.F., & Coney, P.J. (1981). Plate tectonics of the Ancestral Rocky Mountains. Geology, 9,10–15.

Kolodny, Y., Luz, B., & Navon, O. (1983). Oxygen isotope variations in phosphate of biogenic apatites; I Fish bone apatite; rechecking the rules of the game. Earth and Planetary Science Letters, 64, 398-404.

Kolodny, Y., & Luz, B. (1991). Oxygen isotopes in phosphate of fossil fish—Devonian to recent *In* Taylor, H.T.J. (ed.) Stable isotope geochemistry: A tribue to Samuel Epstein, 65-76.

Knoll, M.A., & James, W.C. (1987). Effect of the advent and diversification of vascular land plants on mineral weathering through geologic time. Geology, 15, 1099-1102.

Kues, B.S., & Giles, K.A. (2004). The Late Paleozoic Rocky Mountains system in New Mexico. Special Publication-New Mexico Geological Society, 11, 95-136.

Kump, L.R., Brantley, S.L., & Arthur, M.A. (2000). Chemical weathering, atmospheric CO2, and climate. Annual Reviews in Earth and Planetary Science, 28, 611-667.

Kuwahara, Y., Masudome, Y., Paudel, M.R., Fujii, R., Hayashi, T., Mampuku, M., & Sakai, H. (2010). Controlling weathering and erosion intensity on the southern slope of the central Himalaya by the Indian summer monsoon during the last glacial. Global and Planetary Change, 71, 73-84.

LaMaskin, T.A., & Elrick, M. (1997). Sequence stratigraphy of the Middle to Upper Devonian Guilmette Formation, southern Egan and Schell Creek ranges, Nevada *In* Klapper, G., Murphy, M.A., and Talent, J.A., (eds.) Paleozoic sequence stratigraphy, biostratigraphy, and biogeography: Geological Society of America Special Publication, 321, 89-112.

Langmuir, C.H., Vocke, R.D., & Hanson, G.N. (1978). A general mixing equation with applications to Icelandic basalts. Earth and Planetary Science Letters, 37, 380-392.

Laurin, J., Meyers, S.R., Sageman, B.B., & Waltham, D. (2005). Phase-lagged amplitude modulation of hemipelagic cycles: A potential tool for recognition and analysis of sea-level change. Geology, 33, 569-572.

Lea, D.W., Pak, D.K., & Spero, H.J. (2000). Climate impact of Late Quaternary equatorial Pacific sea surface temperature variations. Science, 289, 1719-1724.

Lea, D.W., Martin, P.A., Pak, D.K., & Spero, H.J. (2002). Reconstructing a 350 ky history of sea level using planktonic Mg/Ca and oxygen isotope records from a Cocos Ridge core. Quaternary Science Reviews, 21, 283-293.

Lécuyer, C., Grandjean, P., & Emig, C.C. (1996). Determination of oxygen isotope fractionation between water and phosphate from living lingulides: Potential application to palaeoenvironmental studies. Palaeogeography, Palaeoclimatology, Palaeoecology, 126, 101-108.

Lecuyer, C., Grandjean, P., Barrat, J.-A., Nolvak, J., Emig, C., Paris, F., & Robardet, M. (1998). D18O and REE contects of phosphatic brachiopods: A comparison between modern and lower Paleozoic populations. Geochimica et Cosmochimica Acta, 62, 2429-2436.

Lehnert, O., Joachimski, M.M., Rfyda, J., Buggisch, W., Calner, M., Jeppsson, L., & Eriksson, M.E. (2006). The Ludlow Lau event; another glaciation in the Silurian greenhouse? Geological Society of America Abstracts with Programs, 38, 183.

Levitus, S., & Boyer, T. (1994). World Ocean Atlas 1994, Volume 4, Temperature. NOAA Atlas NESDIS 4, U.S. Department of Commerce, Washinton, D.C.

Lewis, C.J., McDonald, E.V., Sancho, C., Pena, J.L., & Rhodes, E.J. (2009). Climatic implications of correlated upper Pleistocene glacial and fluvial deposits of the Cinca and Gallego Rivers (NE Spain) based on OSL dating and soil stratigraphy. Global and Planetary Change, 67, 141-152.

Linnemann, U., Herbosch, A., Liegeois, J.-P., Pin, Christian, Gartner, A., & Hofmann, M. (2012). The Cambrian to Devonian odyssey of the Brabant Massif within Avalonia: A review with new zircon ages, geochemistry, Sm-Nd isotopes, stratigraphy, and palaeogeography. Earth-Science Reviews, 112, 126-154.

Lisiecki, L.E., & Raymo, M.E. (2005). A Pliocene-Pleistocene stack of 57 globally distributed benthic $\delta^{18}O$ records. Paleoceanography, 20, 1003.

Longinelli, A., & Nuti, S. (1973). Revised phosphate-water isotopic temperature scale. Earth and Planetary Science Letters, 19, 373-376.

Lozovsky, V.R., & Yarshenko, O.P. (1994). The Permian/Triassic boundary in the continental series of the Moscow syneclise: recent achievements. Permophiles, 24, 54-59.

Lubeseder, S. (2008). Palaeozoic low-oxygen, high-latitude carbonates; Silurian and Lower Devonian nautiloid and scyphocrinoid limestones of the Anti-Atlas (Morocco): Palaeogeography, Palaeoclimatology, Palaeoecology, 264, 195-209.

Luz, B., Kolodny, Y., & Kovach, J. (1984). Oxygen isotope variations in phosphate of biogenic apatites, III. Conodonts. Earth and Planetary Science Letters, 69, 255-262.

Ma, X.P., Wang, C.Y., Racki, G., & Racka, M. (2008). Facies and geochemistry across the Early-Middle Frasnian transition (Late Devonian) on South Chine carbonate shelf: Comparison with the Polish reference succession. Palaeogeography, Palaeoclimatology, Palaeoecology, 269, 130-151.

MacLeod, K.G., Martin, E.E., & Blair, S.W. (2008). Nd isotopic excursion across Cretaceous ocean anoxic event 2 (Cenomanian-Turonian) in the tropical North Atlantic. Geology, 36, 811-814.

Marcantino, F., Thomas, D.J., Woodard, S., McGee, S., McGee, D., & Winckler, G. (2009). Extraterrestrial ^{3}He in Paleocene sediments from Shatsky Rise: Constraints on sedimentation rate variability. Earth and Planetary Science Letters, 287, 24-30.

Malkowski, K., & Racki, G. (2009). A global biogeochemical perturbation across the Silurian-Devonian boundary: ocean-continent-biosphere feedbacks. Palaeogeography, Palaeoclimatology, Palaeoecology, 276, 244-254.

Martin, J.L. (1971). Stratigraphic analysis of Pennsylvanian strat in the Lucero region of west-central New Mexico [Ph.D. dissertation], University of New Mexico, 196 pp.

Martin, E.E., & Macdougall, J.D. (1995). Sr and Nd isotopes at the Permain/Triassic boundary: A record of climate change. Chemical Geology, 125, 73-99.

Massari, F., Capraro, L., & Rio, D. (2007). Climatic modulation of timing of systems-tract development with respect to sea-level changes (Middle Pleistocene of Crotone, Calabria, southern Italy). Journal of Sedimentary Research, 77, 461-468.

McLennan, S.M. (1989). Rare earth elements in sedimentary rocks: Influence of provenance and sedimentary processes *In* Lipin , B.R., McKay, G.A., (eds.) Geochemistry and Mineralogy of Rare Earth Elements. Reviews in Mineralogy, 21, 169-200.

McKay, C.P., Molaro, J.L., & Marinova, M.M. (2009). High frequency rock temperature data from hyper-arid desert environments in the Atacama and the Antarctic dry valleys and implications for rock weathering. Geomorphology, 110, 182-187.

Miller, R.G., O'Nions, R.K., Hamilton, P.J., & Welin, E. (1986). Crustal residence ages of clastic sediments, orogeny and continental evolution. Chemical Geology, 57, 87-99.

Miller, K.B., McCahon, T.J., & West, R.R. (1996). Lower Permian (Wolfcampian) paleosol bearing cycles of the U.S. Midcontinent: evidence of climatic cyclicity. Journal of Sedimentary Research, 66, 71–84.

Miller, K.G., Barrera, E., Olsson, R.K., Sugarman, P.J., & Savin, S.M. (1999). Does ice drive early Maastrichtian eustasy? Geology, 27, 783-786.

Morrow, J.R., & Sandberg, C.A. (2003). Late Devonian sequence and event stratigraphy across the Frasnian-Famennian (F-F) boundary, Utah and Nevada *In* Harries, P.J. (ed.) High resolution approaches in stratigraphic paleontology. Kluwer Academic Publishers, London, 351-419.

Mundil, R., Zuehlke, R., Bechstaedt, T., Peterhaensel, A., & Egenhoff, S.O. (2003). Cyclicities in Triassic platform carbonates: synchronizing radio-isotopic and orbital clocks. Terra Nova, 15, 81-87.

Munnecke, A., Samtleben, C., & Bickert, T. (2003). The Ireviken Event in the lower Silurian of Gotland, Sweden-relation to similar Palaeozoic and Proterozoic events. Palaeogeography, Palaeoclimatology, Palaeoecology, 195, 99-124.

Murphy, A.E., Sageman, B.B., & Hollander, D.J. (2000). Eutrophication by decoupling of the marine biogeochemical cycles of C, N, and P: a mechanism for the Late Devonian mass extinction. Geology, 28, 427-430.

Murphy, J.B., van Staal, C.R., & Keppie, J.D. (1999). Middle to late Paleozoic Acadian orogeny in the northern Appalachians: a Laramide-style plume-modified orogeny? Geology, 27, 653–656.

Murphy, J.B., Strachan, R.A., Nance, R.D., Parker, K.D., & Fowler, M.B. (2000). Proto-Avalonia: 1.2-1.0 Ga tectonothermal event and constraints for the evolution of Rodinia. Geology, 28, 1071-1074.

Murphy, J.B., Dostal, J., & Keppie, J.D. (2008). Neoproterozoic-Early Devonian magmatism in the Antigonish Highlands, Avalon terrane, Nova Scotia: Tracking the evolution of the mantle and crustal sources during the evolution of the Rheic Ocean. Tectonophysics, 461, 181-201.

Murphy, J.B. (2007). Geological evolution of middle to late Paleozoic rocks in the Avalon terrane of northern mainland Nova Scotia, Canadian Appalachians: a record of tectonothermal activity along the northern margin of the Rheic Ocean in the Appalachian–Caledonide orogen. Geological Society of America Special Paper, 423, 413–435.

Murphy, B.J., & Nance, R.D. (2002). Sm-Nd isotopic systematic as tectonic tracers: an example from West Avalonia in the Canadian Appalachians. Earth-Science Reviews, 59, 77-100.

Naimo, D., Adamo, P., Imperato, M., & Stanzione, D. (2005). Mineralogy and geochemistry of a marine sequence, Gulf of Salerno, Italy. Quaternary International, 140-141, 53-63.

Nance, R.D., & Murphy, J.B. (1996). Basement isotopic signatures and Neoproterozoic paleogeography of Avalonian-Cadomian and related terranes in the circum North Atlantic *In* Nance, R.D., Thompson, M.D., (eds.) Avalonian and related Peri-Gondwanan Terranes of the Circum North Atlantic. Geological Society of America Special Paper, 304, 333-346.

Nanson, G.C., Price, D.M., & Short, S.A. (1992). Wetting and drying of Australia over the past 300 ka. Geology, 20, 791-794.

Natalin, B.A., Amato, J.M., Toro, J., & Wright, J.E. (1999). Palaeozoic rocks of northern
Chukotka Peninsular, Russian Far East: implications for the tectonics of the Arctic region. Tectonics, 18, 977–1003.

Nelson, J., & Colpron, M. (2007). Tectonics and metallogeny of the British Columbia, Yukon and Alaskan Cordillera, 1.8 Ga to the present. Geological Association of Canada, Mineral Deposits Division, Special Publication, 5, 755–791.

Nokleberg, W.J., Parfenov, L.M., Monger, J.W.H., Norton, I.O., Khanchuk, A.I., Stone, D.B., Scotese, C.R., Scholl, D.W., & Fujita, K. (2000). Phanerozoic tectonic evolution of the Circum-North Pacific. United States Geological Survey, Professional Paper, 1626, 1–122.

Olson, P. E., & Kent, D. V. (1999). Long-period Milankovitch cycles from the Late Triassic and Early Jurassic of eastern North America and their implications for the calibration of the Early Mesozoic time-scale and the long-term behavior of the planets. Philosophical Transactions of the Royal Society of London, 357, 1761-1786.

O'Neil, J.R., Roe, L.J., Reinhard, E., & Blacke, R.E. (1994). A rapid and precise method of oxygen isotope analysis of biogenic phosphate. Israel Journal of Earth Science, 43, 203-212.

Osleger, D.A. (1991). Subtidal carbonate cycles: Implications for allocyclic versus autocyclic controls. Geology, 19, 917-920.

Pagani, M., Pedentchouk, N., Huber, M., Sluijs, A., & Schouten, S. (2006). Arctic hydrology during global warming at the Palaeocene/Eocene Thermal Maximum. Nature, 442, 671-675.

Park, L.E., & Gierlowski-Kordesch, E.H. (2007). Paleozoic lake faunas: Establishing aquatic life on land. Palaeogeography, Palaeoclimatology, Palaeoecology, 249, 160-170.

Patchett, P.J., & Gehrels, G.E. (1998). Continental influence on Canadian Cordilleran terranes from Nd isotopic study, and significance for crustal growth processes. The Journal of Geology, 106, 269-280.

Patchett, P.J., Roth, M.A., Canale, B.S., de Freitas, T.A., Harrison, J.C., Embry, A.F., & Ross, G.M. (1999). Nd isotopes, geochemistry, and constraints on sources of sediments in the Franklinian mobile belt, Arctic Canada. Geological Society of America Bulletin, 111, 578-589.

Pekar, S., Hucks, A., Fuller, M., & Li, S. (2005). Glacioeustatic changes in the early and middle Eocene (51-42 Ma): shallow-water stratigraphy from ODP Leg 189 Site 1171 (South Tasman Rise) and deep-sea delta O-18 records. Geological Society of America Bulletin, 117, 1081-1093.

Picard, S., Garcia, J.-P., Lecuyer, C., Sheppard, S.M.F., Cappetta, H., & Emig, C.C. (1998). D18O values of coexisting brachiopods and fish: Temperature differences and estimates of paleo-water depths. Geology, 26, 975-978.

Pier, J.G., Podosek, F.A, Luhr, J.A., Brannon, J.C., & Ara-Gomez, J.J. (1989). Spinel-Iherzolite-bearing Quaternary volcanic centers in San Luis Potosi, Mexico, 2. Sr and Nd isotope systematics. Journal of Geophysical Research, 94, 7941-7951.

Pimentel, M.M., & Fuck, R.A. (1992). Neoproterozoic crustal accretion in central Brazil. Geology, 20, 375-379.

Piotrowski, A.M., Goldstein, S.L., Hemming, S.R., & Fairbanks, R.G. (2004). Earth and Planetary Science Letters, 225, 205-220.

Piotrowski, A.M., Goldstein, S.L., Hemming, S.R., & Fairbanks, R.G. (2005). Temporal relationships of carbon cycling and ocean circulation at glacial boundaries. Science, 307, 1933-1938.

Potter, P.E. (1978). Petrology and chemistry of modern big river sands. Journal of Geology, 86, 423-449.

Pucéat, E., Lécuyer, C., & Reisberg, L. (2005). Neodymium isotope evolution of NW Tethyan upper ocean waters throughout the Cretaceous. Earth and Planetary Science Letters, 236, 706-720.

Pucéat, E., Joachimski, M.M., Bouilloux, A., Monna, F., Bonin, A., Motreuil, S., Moriniere, P., Henard, S., Mourin, J., Dera, G., & Quesne, D. (2010). Revised phosphate-water fractionation equation reassessing paleotemperatures derived from biogenic apatite. Earth and Planetary Science Letters, 298, 135-142.

Rankey, E.C. (1997). Relations between relative changes in sea level and climate shifts:
Pennsylvanian–Permian mixed carbonate–siliciclastic strata, western United States. Geological Society of America Bulletin, 109, 1089–1100.

Rainbird, R.H., Heaman, L.M., & Young, G. (1992). Sampling Laurentia: Detrital zircon geochronology offers evidence for an extensive Neoproterozoic river system originating from the Grenville orogen. Geology, 20, 351-354.

Rainbird, R.H., McNicoll, V.J., Theriault, R.J., Heaman, L.M., & Abbott, J.G. (1997). Pan-continental river system draining Grenville Orogen recorded by U-Pb and Sm-Nd geochronology of Neoproterozoic quartzarenites and mudrocks, northwestern Canada. Journal of Geology, 105, 1-17.

Raymo, M.E., Ruddiman, W.F., & Froelich, P.N. (1988). Influence of late Cenozoic mountain building on ocean geochemical cycles. Geology, 16, 649-653.

Raymo, M.E., & Ruddiman, W.F. (1992). Tectonic forcing of late Cenozoic climate. Nature, 359, 117-122.

Raymo, M. E. Lisiecki, L. E., & Nisancioglu, K. H. (2006). Plio-Pleistocene ice volume, Antarctic climate, and the global $\delta^{18}O$ record. Science, 313, 492-495.

Rea, D.K., Chambers, L.W., Chuey, J.M., Janecek, T.R., Leinen, M., & Pisias, N.G. (1986). A 420,000-year record of cyclicity in oceanic and atmospheric processes from the eastern Equatorial Pacific. Paleoceanography, 1, 577-586.

Rea, D.K., Pisias, N.G., & Newberry, T. (1991). Late Pleistocene paleoclimatology of the central Equatorial Pacific; flux patterns of biogenic sediments. Paleoceanography, 6, 227-244.

Rea, D.K. (1994). The paleoclimatic record provided by eolian deposition in the deep sea; the geologic history of wind. Reviews of Geophysics, 32, 159-195.

Retallack, G.J. (1985). Fossil soils as grounds for interpreting the advent of large plants and animals on land. Philosophical Transactions of the Royal Society of London Biological Sciences, 309, 105-142.

Retallack, G.J. (1992). Paleozoic paleosols *In* Martini, I.P., Chesworth, W., (eds.) Weathering and Paleosols. Elsevier, Amsterdam, 543-564.

Revenga, C., Murray, S., Abramovitz, J., & Hammond, A. (1998). Watersheds of the world-Ecological value and vulnerability. World Resources Institude and World Watch Institute.

Reynolds, B.C., Frank, M., & O'Nions, R.K. (1999). Nd- and Pb-isotope time series from Atlantic ferromanganese crusts: Implications for changes in provenance and paleocirculation over the last 8 Myr. Earth and Planetary Science Letters, 173, 381-396.

Rincón-Martínez D., Lamy F., Contreras S., Leduc G., Bard E., Saukel C., Blanz T., Mackensen A., & Tiedemann R. (2010). More humid interglacials in Ecuador during the past 500 kyr linked to latitudinal shifts of the equatorial front and the Intertropical Convergence Zone in the eastern tropical Pacific. Paleoceanography, 25, 2210.

Ross, G.M., & Parrish, R.R. (1991). Detrital zircon geochronology of metasedimentary rocks in the southern Omineca Belt, Canadian Cordillera. Canadian Journal of Earth Sciences, 28, 1254-1270.

Rouer, O., Lapierre, H., Mascle, G., Coulon, C., & Albers, J. (1989). Geodynamic implications of Devonian silicic arc magmatism in the Sierra Nevada and Klamath Mountains, California. Geology, 17, 177-180.

Rouer, O., & Lapierre, H. (1989). Comparison between two Palaeozoic island-arc terranes in northern California (eastern Klamath and northern Sierra Nevada): geodynamic constraints. Tectonophysics, 169, 341-349.

Rygel, M.C., Fielding, C.R., Frank, T.D., & Birgenheier, L.P. (2008). The magnitude of Late Paleozoic glacioeustatic fluctuations: a synthesis. Journal of Sedimentary Research, 78, 500-511.

Saltzman, M. (2005). Phosphorus, nitrogen, and the redox evolution of the Paleozoic oceans. Geology, 33, 573-576.

Samson, S.D., McClelland, W.C., Patchett, P.J., Gehrels, & Anderson, R.G. (1989). Evidence from neodymium isotopes for mantle contributions to Phanerozoic crustal genesis in the Canadian Cordillera. Nature, 337, 705-709.

Samtleben, C., Munnecke, A., & Bickert, T. (2000). Development of facies and C/O-isotopes in transects through the Ludlow of Gotland: Evidence for global and local influences on a shallow-marine environment. Facies, 43,1-38.

Sandberg, C.A., & Ziegler, W. (1996). Devonian conodont biochronology in geologic time calibration. Senckenbergiana Lethaea, 76, 259-265.

Sanderson, M.J., Thorne, J.L., Wilkstrom, N., & Bremer, K. (2004). Molecular evidence on plant divergence times. American Journal of Botany, 91, 1656-1665.

Scher, H.D., & Martin, E.E. (2006). Timing and climatic consequences of the opening of Drake Passage. Science, 312, 428-430.

Scher, H.D., Bohaty, S.M., Zachos, J.C., & Delaney, M.L. (2011). Two-stepping into the icehouse; east Antarctic weathering during progressive ice-sheet expansion at the Eocene-Oligocene transition. Geology, 39, 383-386.

Schmidt, R., Kamenik, C., Tessadri, R., & Koining, K.A. (2006). Climatic changes from 12,000 to 4,000 years ago in the Austrian central Alps tracked by

sedimentological and biological proxies of a lake sediment core. Journal of Paleolimnology, 35, 491-505.

Schulz, M., & Schäfer-Neth, C. (1997). Translating Milankovitch climate forcing into eustatic fluctuations via thermal deep water expansion; a conceptual link. Terra Nova, 9, 228-231.

Scotese, C.R. (2001). Quicktime Computer Animations, PALEOMAP Project Department of Geology, University of Texas at Arlington, Arlington, Texas.

Scotese, C. R., & Galonka, J. (1992). PALEOMAP Paleogeographic Atlas, PALEOMAP Progress Report No. 20, Department of Geology, University of Texas at Arlington, Arlington, Texas, 34 pp.

Scott, L.A. & Elrick, M. (2004). Cycle and sequence stratigraphy of Middle Pennsylvanian (Desmoinsian) strata of the Lucero Basin, central New Mexico *In* Lucas, S.G. and Zeigler, K.E, (eds.), Carboniferous-Permian transition, New Mexico Museum of Natural History and Science Bulletin, 31-41.

Sellwood, B.W., & Valdes, P.J. (2006). Mesozoic climates: General circulation models and the rock record. Sedimentary Geology, 190, 269-287.

Shackleton, N.J., & Opdyke, N.D. (1973). Oxygen isotope and palaeomagnetic stratigraphy of Equatorial Pacific Core V28-238: Oxygen isotope temperatures and ice volumes on a 105 and 106 year scale. Quaternary Research, 3, 39-55.

Shackleton, , N.J., Imbrie, J., & Pisias, N.G. (1988). The evolution of oceanic oxygen-isotope variability in North Atlantic over the past three million years. Philosphical Transactions of the Royal Society of London, Biological Sciences, 318, 1191.

Shirey, S.B. (1991). The Rb-Sr, Sm-Nd and Re-Os isotopic systems; a summary and comparison of their applications to the cosmochronology and geochronology of igneous rocks. Applications of radiogenic isotope systems to problems in geology, Short course handbook, 19, 103-166.

Shishkin, M.A., & Ochev, V.G. (1993). The Permo-Triassic transition and the Early Triassic history of the Euramerican tetrapod fauna. Bulletin-New Mexico Museum of Natural History and Science.

Shukla, J., & Mintz, Y. (1982). Influence of land-surface evapotranspiration on the Earth's climate. Science, 215, 1498-1500.

Skompski, S., Luczynski, P., Drygant, D., Kozlowski, W., 2008. High-energy sedimentary events in lagoonal successions of the Upper Silurian of Podolia, Ukraine. Facies 54, 277-296.

Soja, C.M., & Antoshkina, A.I. (1997). Coeval development of Silurian stromatolite reefs in Alaska and the Ural Mountains: Implications for paleogeography of the Alexander terrane. Geology, 25, 539-542.

Soja, C.M., White, B., Antoshkina, A., Joyce, S., Mayhew, L., Flynn, B., & Gleason, A. (2000). Devolopment and decline of a Silurian stromatolite reef complex, Glacier Bay National Park, Alaska. Palaois, 18, 225-235.

Soreghan, G.S. (1994). Stratigraphic responses to geologic processes: Late Pennsylvanian eustasy and tectonics in the Pedrogosa and Orogrande basins, Ancestral Rocky Mountains: Geological Society of America Bulletin, 106, 1195-1211.

Soreghan, G.S., & Giles, K.A. (1999). Amplitudes of Late Pennsylvanian glacioeustasy.
Geology, 27, 255–258.

van Staal, C.R., Whalen, J.B., Valverde-Vaquero, P., Zagorevski, A., & Rogers, N. (2009). Pre-Carboniferous, episodic accretion-related, orogenesis along the Laurentian margin of the northern Appalachians. Geological Society, London, Special Publications, 327, 271-316.

Stallard, RF, & Edmond, J.M. (1981). Geochemistry of the Amazon 1. Precipitation chemistry and the marine contribution to the dissolved load at the time of peak discharge. Journal of Geophysical Research, 86, 9844–9854.

Stallard, RF, & Edmond, J.M. (1983). Geochemistry of the Amazon 2. The influence of geology and weathering environment on the dissolved load. Journal of Geophysical Research, 88, 9671–9688.

Stallard, R.F., & Edmond, J.M. (1987). Geochemistry of the Amazon 3.Weathering chemistry and limits to dissolved inputs. Journal of Geophysical Research,92, 8293–8302.

Sweet, A.G., & Harris, W.C. (1988). Mechanical and chemical techniques for separating microfossils from rock, sediment, and residue matrix. Special Publication, Paleontological Society, 4, 70-86.

Stampfli, G.M., & Borel, G.D. (2002). A plate tectonic model for the Paleozoic and Mesozoic constrained by dynamic plate boundaries and restored synthetic isochrones. Earth and Planetary Science Letters, 196, 17-33.

Stewart, J.H., Gehrels, G.E., Barth, A.P., Link, P.K., Christie-Blick, N., & Wrucke, C.T. (2001). Detrital zircon provenance of Mesoproterozoic to Cambrian arenites in the western United States and northwestern Mexico. Geological Society of America Bulletin, 113, 1343-1356.

Stoll, H.M., & Schrag, D.P. (2000). High-resolution stable isotope records from the Upper Cretaceous rocks of Italy and Spain: Glacial episodes in a greenhouse planet? Geological Society of America Bulletin, 112, 308-319.

Strother, P.K., Al-Hajni, S., & Traverse, A. (1996). New evidence for land plants from the lower Middle Ordovician of Saudi Arabia. Geology, 24, 55-58.

Theiling, B.P., Elrick, M., & Asmerom, Y. (2012). Increased continental weathering flux during orbital-scale sea-level highstands: Evidence from Nd and O isotope trends in Middle Pennsylvanian cyclic carbonates. Palaeogeography, Palaeoclimatology, Palaeoecology, 342-343, 17-26.

Theiling, B.P., & Elrick, M. Oxygen isotopic evidence for orbital-scale glacial ice-volume changes during middle Paleozoic (Silurian and Devonian) greenhouse time intervals. (In preparation).

Thomas, D.J. (2004). Evidence for deep-water production in the North Pacific Ocean during the early Cenozoic warm interval. Nature, 430, 65-68.

Thorogood, E.J. (1990). Provenance of the pre-Devonian sediments of England and Wales: Sm-Nd isotopic evidence. Journal of the Geological Society, London, 147, 591-594.

Torsvik, T.H., Smethurst, M.A., Meert, J.G., Van der Voo, R., McKerrow,W.S., Brasier, M.D., Sturt, B.A., & Walderhaug, H.J. (1996). Continental break-up and collision in the Neoproterozoic: a tale of Baltica and Laurentia. Earth Science Reviews, 40, 229–258.

Torsvik, T.H., & Cocks, L.R.M. (2004). Earth geography from 400 to 250 Ma: a palaeomagnetic, faunal and facies review. Journal of the Geological Society of London, Biological Sciences, 161, 555–572.

Trettin,H.P. (Ed.), (1991). Geology of the Innuitian Orogen and Arctic Platform of Canada and Greenland. Geological Survey of Canada: Geology of Canada, 3, 1–569.

Tull, J.F. (2002). Southeastern margin of the middle Paleozoic shelf, southwesternmost Appalachians: Regional stability bracketed by Acadian and Alleghanian tectonism. Geological Society of America Bulletin, 114, 643-655.

Van der Voo, R. (1994). True polar wander during the middle Palaeozoic. Earth and
Planetary Science Letters, 122, 239–243.

Vance, D., Teagle, D.A.H., & Foster, G.L. (2009). Variable Quaternary chemical weathering fluxes and imbalances in marine geochemical budgets. Nature, 458, 493-496.

Van Wagoner, J.C., Posamentier, H.W., Mitchum, R.M., Vail, P.R., Sarg, J.F., Loutit, T.S., & Hardenbol, J. (1988). An overview of the fundamentals of sequence stratigraphy and key definitions, *In* Wilgus, C.K., Hastings, B.S., Kendall, C.G.St.C., Posamentier, H.W., Ross, C.A., and Van Wagoner, J.C. (eds.), Sea Level Changes: An Integrated Approach. SEPM, Special Publication, 42, 39–45.

Veevers, J.M., & Powell, C.McA. (1987). Late Paleozoic glacial episodes in Gondwanaland reflected in transgressive-regressive depositional sequences in Euramerica. Geological Society of America Bulletin, 98, 475-487.

Veizer, J., Ala, D., Amzy, K., Bruckschen, P., Buhl, D., Bruhn, F., Carden, G.A.F., Diener, A., Ebneth, S., Godderis, Y., Jasper, T., Korte, C., Pawellek, F., Podlaha,O.G., & Strauss, H. (1999). $^{87}Sr/^{86}Sr$, $\delta^{13}C$, and $\delta^{18}O$ evolution of Phanerozoic seawater. Chemical Geology, 161, 59-88.

Via, R.K., & Thomas, D.J. (2006). Evolution of Atlantic thermohaline circulation: Early Oligocene onset of deep-water production in the North Atlantic. Geology, 34, 441-444.

Wang,Y. (1993). Lacustrine carbonate chemical sedimentation and climatic-environmental evolution--a case study of Qinghai lake and Daihai lake, China. Oceanologia et Limnologia Sinica, 24, 31-36.

Wasson, R. J., Smith, G. I., & Agrawal, D.P. (1984). Late Quaternary sediments, minerals, and inferred geochemical history of Didwana Lake, Thar Desert, India. Palaeogeography, Palaeoclimatology, Palaeoecology, 46, 345-372.

Wengerd, S.A. (1959). Regional geology as related to the petroleum potential of the Lucero region, west-central New Mexico. New Mexico Geological Society Guidebook, 10th Field Conference, 121-134.

Wenzel, B., & Joachimski, M.M. (1996). Carbon and oxygen isotopic composition of Silurian brachiopods (Gotland/Sweden)?: Palaeoceanographic implications. Palaeogeography, Palaeoclimatology, Palaeoecology, 122, 143-166.

Wenzel, B., Lecuyer, C., & Joachimski, M. (2000). Comparing oxygen isotope records of Silurian calcite and phosphate-$\delta^{18}O$ compositions of brachiopods and conodonts. Geochimica et Cosmochimica Acta, 64, 1859-1872.

West, A.J., Galy, A., & Bickle, M. (2005). Tectonic and climatic controls on silicate weathering. Earth and Planetary Science Letters, 235, 211-228.

Whalen, M.T., & Day, J.E. (2010). Cross-basin variations in magnetic susceptibility influenced by changing sea level, paleogeography, and paleoclimate: Upper Devonian, western Canada sedimentary basin. Journal of Sedimentary Research, 80, 1109-1127.

White, A.F., & Blum, A.E. (1995). Effects of climate on chemical weathering in watersheds. Geochimica et Cosmochimica Acta, 59, 1729-1747.

Wiberg, T.L., & Smith, G.A. (1994). Pennsylvanian glacio-eustasy recorded in a carbonate ramp succession, Ancestral Rocky Mountains, New Mexico. Canadian Society of Petroleum Geologists, 17, 545-556.

Williams, A., Mackay, S., & Cusack, M. (1992). Structure of the organo-phosphatic shell of the brachiopod Discina. Philosophical Transactions of the Royal Society of London, Biological Sciences, 337, 83-104.

Williams, J.Z., Bandstra, J.Z., Pollard, D., & Brantley, S.L. (2010). The temperature dependence of feldspar dissolution determined using a coupled weathering-climate model for Holocene-ages loess soils. Geoderma, 156, 11-19.

deWolde, J.R., Bintania, R., & Oerlemans, J. (1995). On thermal expansion over the last hundred years. Journal of Climate, 8, 2881-2891.

Yaalon, D. (1990). The relevance of soils and paleosols in interpreting past and ongoing climatic changes. Palaeogeography, Palaeoclimatology, Palaeoecology, 82, 63-64.

Ye, H., Royden, L., Burchfiel, C., & Schuepbacj, M. (1996). Late Paleozoic deformation of interior North America: the greater Ancestral Rocky Mountains. American Association of Petroleum Geologists Bulletin, 80, 1397-1432.

Yiming, G., Baohua, L., & Yi, W. (2001). Devonian Frasnian-Famennian transitional Milankovitch cycles and high-resolution stratigraphic correlation. Acta Geologica Sinica, 75, 354-363.

Zachos, J., Pagani, M., Sloan, L., Thomas, E., & Billups, K. (2001). Trends, rhythms, and
abberrations in global climate 65 Ma to present. Science, 292, 686–693.

Zamanzadeh, S.M., Amini, A., & Ghavidel-Syooki, M. (2009). Sequence stratigraphic controls on early-diagenetic carbonate cementation of shallow marine clastic sediments (the Devonian Zakeen Formation, southern Zagros, Iran). Geosciences Journal, 13, 31-57.

van Zeist, W. (1967). Late Quaternary vegetation history of western Iran. Review of Palaeobotany and Palynology, 2, 301-311.

Ziegler, A.M., Hulver, M.L., & Rowley, D.B. (1997). Permian World topography and climate *In* Martini, I.P. (ed). Late Glacial and Postglacial Environmental Changes: Quaternary Carboniferous-Permian, and Proterozoic. Oxford University Press, Oxford, U.K., 111-146.

Žigaité, Z., Joachimski, M.M, Lehnert, O., & Brazauskas, A. (2010). $\delta^{18}O$ composition of conodont apatite indicates climatic cooling during the Middle Pridoli. Palaeogeography, Palaeoclimatology, Palaeoecology, 294, 242-247.